Impaired thymic AIRE expression underlies autoantibodies against type I IFNs in humans with inborn errors of the alternative NF-kB pathway

Tom Le Voyer[1,2], Adrian Gervais[1,2], Jérémie Rosain[1,2], Audrey Parent[3], Axel Cederholm[4,5], Darawan Rinchai[6], Lucy Bizien[1,2], Gonca Hancioglu[7], Quentin Philippot[1,2], Mame Sokhna Gueye[1,2], Majistor Raj Luxman[1,2], Maglorius Renkilaraj[1,2], Masato Ogishi[6], Camille Soudée[1,2], Mélanie Migaud[1,2], Flore Rozenberg[8], Mana Momenilandi[1,2,9], Quentin Riller[10], Luisa Imberti[11], Ottavia Delmonte[12], Gabriele Müller[13], Bärbel Keller[13], Julio Orrego[14], William Alexander Gallego[14], Tamar Rubin[15], Melike Emiroglu[16], Nima Parvaneh[17], Daniel Eriksson[18,19,20], Maribel Aranda-Guillen[21], David I Berrios[3], Linda Vong[22,23], Connie H Katelaris[24], Peter Mustillo[25], Johannes Rädler[26], Jonathan Bohlen[1,2], Jale Bengi Celik[27], Camila Astudillo[28], Sarah Winter[29], Audrey Guichard[30], Vivien Béziat[1,2], Jacinta Bustamante[1,2,31], Qiang Pan-Hammarström[32], Yu Zhang[12,33], Lindsey B Rosen[12], Steve M Holland[12], Heather Kenney[33], Kaan Boztuğ[34], Nizar Mahlaoui[35,36], Sylvain Latour[29], Roshini Abraham[37], Vassilios Lougaris[38], Fabian Hauck[26], Anna Sediva[39], Faranaz Atschekzei[40], M Cecilia Poli[41], Mary A Slatter[42], Boaz Palterer[43], Michael D Keller[44], Alberto Pinzon-Charry[45,46], Anna Sullivan[45,46], Luke Droney[45,46], Daniel Suan[46,47], Nathalie Aladjidi[48], Miguel Hie[49], Estibaliz Lazaro[50], Jose Franco[14], Sevgi Keles[51], Marion Malphette[52], Marlene Pasquet[53], Maria Elena Maccari[13,54], Andrea Meinhardt[13,54], Aydan Ikinciogullari[55], Mohammad Shahrooei[9], Fatih Celmeli[56], Patrick Frosk[57], Christopher C Goodnow[58,59], Paul E Gray[60], Alexandre Belot[61], Hye Sun Kuehn[62], Sergio D Rosenzweig[62], Francesco Licciardi[63], Amélie Servettaz[64], Vincent Barlogis[65], Guillaume Le Guenno[66], Vera-Maria Herrmann[67], Taco Kuijpers[68], Grégoire Ducoux[69], Françoise Sarrot-Reynauld[70], Catharina Schuetz[71], Charlotte Cunningham-Rundles[72], Frédéric Rieux-Laucat[10], Stuart G Tangye[58,59], Cristina Sobacchi[73], Rainer Doffinger[74], Klaus Warnatz[13,75], Bodo Grimbacher[13,75], Claire Fieschi[52], Laureline Berteloot[76], Vanessa Bryant[77], Sophie Trouillet Assant[78], Luigi D Notarangelo[12,33], Helen Su[12,33], Benedicte Neven[36], Laurent Abel[1,2,6], Qian Zhang[1,2,6], Bertrand Boisson[1,2,6], Aurélie Cobat[1,2], Emmanuelle Jouanguy[1,2], Olle Kampe[79], Paul Bastard[1,2,6], Chaim Roifman[22,23], Nils Landegren[4,5], Mark S Anderson[3], Jean-Laurent Casanova[1,2,6,80], and Anne Puel[1,2]

[1]University of Paris Cité, Imagine Institute
[2]Laboratory of Human Genetics of Infectious Diseases, Necker Branch, INSERM UMR1163, Paris, France
[3]Diabetes Center, University of California
[4]Science for Life Laboratory, Uppsala University
[5]Cochin-Saint-Vincent de Paul Hospital, Division of Pediatric Allergy and Immunology, Ondokuz Mayıs University Faculty of Medicine, University of Paris
[6]St. Giles Laboratory of Human Genetics of Infectious Diseases, Rockefeller Branch, The

Rockefeller University, New York, NY, United States
[7]Division of Pediatric Allergy and Immunology, Ondokuz Mayıs University Faculty of Medicine, Samsun, Turkey
[8]Virology, Cochin-Saint-Vincent de Paul Hospital, University of Paris, Paris, France
[9]Specialized Immunology Laboratory of Dr. Shahrooei
[10]Institut Imagine, INSERM UMR1163, Laboratory of Immunogenetics of Pediatric Autoimmune Diseases, Université de Paris
[11]Diagnostic Department, ASST Spedali Civili di Brescia, CREA Laboratory
[12]Laboratory of Clinical Immunology and Microbiology, Division of Intramural Research, National Institute of Allergy and Infectious Diseases, National Institutes of Health, Bethesda, MD, United Stated
[13]Institute for Immunodeficiency, Center for Chronic Immunodeficiencies, Medical Center -University Hospital Freiburg, Faculty of Medicine, Albert-Ludwigs-University
[14]Primary Immunodeficiencies Group, Department of Microbiology and Parasitology, School of Medicine, University of Antioquia, Medellín, Colombia
[15]Division of Pediatric Clinical Immunology and Allergy, Department of Pediatrics and Child Health, University of Manitoba, Winnipeg, Canada
[16]Department of Pediatric Infectious Diseases, Faculty of Medicine, Selcuk University, Konya, Turkey
[17]Division of Allergy and Clinical Immunology, Department of Pediatrics, Tehran University of Medical Sciences, Tehran, Iran
[18]Department of Clinical Genetics, Uppsala University Hospital, Uppsala, Sweden
[19]Department of Immunology, Genetics and Pathology, Uppsala University and University Hospital, Section of Clinical Genetics, Uppsala, Sweden
[20]Center for Molecular Medicine, Department of Medicine (Solna), Karolinska Institutet, Stockholm 171 76, Sweden
[21]Centre for Molecular Medicine, Department of Medicine (Solna), Karolinska Institutet, Stockholm, Sweden
[22]Division of Immunology and Allergy, Department of Paediatrics, Hospital for Sick Children and University of Toronto, Toronto, ON, Canada
[23]The Canadian Centre for Primary Immunodeficiency and The Jeffrey Modell Research Laboratory for the Diagnosis of Primary Immunodeficiency, The Hospital for Sick Children, Toronto, ON, Canada
[24]Immunology and Allergy, University of Western Sydney and Campbelltown Hospital, NSW Australia
[25]Division of Allergy and Immuology, Nationwide Children's Hospital, The Ohio State University College of Medicine, Comumbus, OH, United States
[26]Division of Pediatric Immunology and Rheumatology, Department of Pediatrics, Dr. von Hauner Children's Hospital, University Hospital, Ludwig-Maximilians-Universität München, Munich, Germany
[27]Department of Anesthesiology and Reanimation, Selcuk University Faculty of Medicine, Konya, Turkey
[28]Department of Pediatrics, Facultad de Medicina Clinica Alemana Universidad del Desarrollo, Santiago, Chile

[29]Laboratory of Lymphocyte Activation and Susceptibility to EBV, Imagine - Institut des Maladies Génétiques-Inserm UMR 1163, 24, boulevard du Montparnasse, 75015 Paris
[30]Joint unit Hospices Civils de Lyon – BioMérieux, Lyon, France
[31]Study Center of Immunodeficiencies, Necker Hospital for Sick Children, Paris, France
[32]Department of Biosciences and Nutrition, Karolinska Institutet, 17177 Stockholm, Sweden
[33]NIAID Clinical Genomics Program, NIH, Laboratory of Clinical Immunology and Microbiology, Division of Intramural Research, NIAID, NIH, Bethesda, MD, United States
[34]CeMM Research Center for Molecular Medicine of the Austrian Academy of Sciences, Vienna, Austria; Department of Pediatrics and Adolescent Medicine, Medical University of Vienna, Vienna, Austria
[35]French National Reference Center for Primary Immunodeficiencies (CEREDIH), Necker-Enfants University Hospital, Assistance Publique-Hôpitaux de Paris (AP-HP), Paris, France
[36]Department of Pediatric Immunology, Hematology and Rheumatology, Necker-Enfants Malades Hospital, APHP, Paris, France
[37]Department of Pathology and Laboratory Medicine, Nationwide Children's Hospital, Columbus, OH, United States
[38]Department of Clinical and Experimental Sciences, Pediatrics Clinic and Institute for Molecular Medicine A. Nocivelli, University of Brescia ASST-Spedali Civili di Brescia, Brescia, Italy
[39]Department of Immunology, Second Faculty of Medicine Charles University and Motol University Hospital, Prague, Czech Republic
[40]Division of Rheumatology and Clinical Immunology, Hannover Medical University, Hannover, Germany
[41]Hospital de Niños Dr. Roberto del Río, Santiago Chile
[42]Children's Haemopoietic Stem Cell Transplant Unit, Great North Children's Hospital, Newcastle upon Tyne Hospital NHS Foundation Trust, Newcastle upon Tyne, United Kingdom
[43]Allergy and Clinical Immunology, Department of Experimental and Clinical Medicine, University of Florence, Florence, Italy
[44]Division of Allergy and Immunology, Children's National Medical Center, Washington, DC, United States
[45]Immunology and Allergy, Queensland Children's Hospital, Level 12, Queensland Children's Hospital, 501 Stanley Street, South Brisbane, QLD 4101, Australia
[46]Clinical Immunogenomics Research Consortium Australasia (CIRCA), Darlinghurst, NSW Australia
[47]Westmead Clinical School, University of Sydney
[48]Pediatric Oncology Hematology Unit, University Hospital, Plurithématique CIC (CICP), Centre d'Investigation Clinique (CIC) 1401, Bordeaux, France
[49]Internal Medicine Department, Pitié-Salpêtrière Hospital, Paris, France
[50]Department of Internal Medicine & Infectious Diseases, Bordeaux Hospital University, Bordeaux, France
[51]Necmettin Erbakan University, Meram Medical Faculty, Division of Pediatric Allergy and

Immunology, Konya, Turkey
[52]Clinical Immunology Department, Saint Louis Hospital, Paris, France
[53]Department of Pediatric Hematology, Toulouse University Hospital, Toulouse, France
[54]Division of Pediatric Hematology and Oncology, Department of Pediatrics and Adolescent Medicine, Medical Center-University of Freiburg, Faculty of Medicine, University of Freiburg, Freiburg, Germany
[55]Department of Pediatric Immunology and Allergy, Ankara University School of Medicine, Ankara, Turkey
[56]Department of Allergy and Immunology, University of Medical Science, Antalya Education and Research Hospital, Antalya, Turkey
[57]Department of Biochemistry and Medical Genetics, Rady Faculty of Health Sciences, University of Manitoba, Winnipeg, MB, Canada
[58]Garvan Institute of Medical Research, Darlinghurst 2010, NSW, Sydney, Australia
[59]School of Clinical Medicine, UNSW Medicine & Health, Darlinghurst 2010, NSW, Australia
[60]Immunology and Infectious Diseases, Sydney Children's hospital Randwick, Western Sydney university, Campbelltown NSW, Australia
[61]CNRS UMR 5308, ENS, UCBL, Lyon, France; National Referee Centre for Rheumatic, and Autoimmune and Systemic Diseases in Children (RAISE), Lyon, France; Lyon; Immunopathology Federation LIFE, Hospices Civils de Lyon, Lyon, France
[62]Immunology Service, Department of Laboratory Medicine, Clinical Center, National Institutes of Health, Bethesda, United States
[63]Department of Pediatrics and Public Health, Università degli Studi di Torino, Turin, Italy
[64]Internal Medicine, Clinical Immunology and Infectious Diseases Department, University Hospital Center, Reims, France
[65]CHU Marseille, Hôpital La Timone, Service d'Hémato-oncologie Pédiatrique, Assistance Publique-Hôpitaux de Marseille, Marseille, France
[66]Centre Hospitalier Universitaire Estaing, Clermont-Ferrand, France
[67]Institute of Human Genetics, University of Leipzig Medical Center, Leipzig, Germany
[68]Department of Pediatric Immunology, Rheumatology and Infectious Diseases, Emma Children's Hospital, Amsterdam University Medical Center, University of Amsterdam, Amsterdam, The Netherlands
[69]Department of Internal Medicine, Edouard Herriot Hospital, Lyon, France
[70]Department of Internal Medicine, Hôpital Michallon, CHU de Grenoble Alpes, Grenoble, France
[71]Department of Paediatrics, Universitätsklinikum Carl Gustav Carus, Technische Universität Dresden, Dresden, Germany
[72]Departments of Medicine and Pediatrics, Mount Sinai School of Medicine, New York, United States
[73]Humanitas Clinical and Research Institute, Rozzano, Italy; CNR-IRGB, Milan Unit, Milan, Italy
[74]Department of Clinical Biochemistry and Immunology, Addenbrooke's Hospital, Cambridge, United Kingdom
[75]Department of Rheumatology and Clinical Immunology, Medical Center – University of

Freiburg, Faculty of Medicine, University of Freiburg, Freiburg, Germany
[76]Pediatric Radiology Department, Assistance Publique-Hôpitaux de Paris (AP-HP), Necker Hospital for Sick Children, Paris, France
[77]Walter and Eliza Hall Institute, Melbourne, Parkville, Australia
[78]CIRI (Centre International de Recherche en Infectiologie), Université de Lyon, Université Claude Bernard Lyon 1, INSERM U1111, CNRS, UMR5308, ENS Lyon, Université Jean Monnet de Saint-Etienne, Lyon, France
[79]Department of Endocrinology, Metabolism and Diabetes, Karolinska University Hospital, Stockholm 171 76, Sweden
[80]Howard Hughes Medical Institute, New York, NY, United States

January 9, 2023

Abstract

Patients with inborn errors of the alternative NF-ϰB pathway have low thymic AIRE expression, leading to the development of auto-Abs neutralizing type I IFNs, and severe viral diseases.

Impaired thymic AIRE expression underlies autoantibodies against type I IFNs in humans with inborn errors of the alternative NF-κB pathway

Tom Le Voyer[1,2*], Adrian Gervais[1, 2&], Jérémie Rosain[1,2&], Audrey V. Parent[3&], Axel Cederholm[4&], Darawan Rinchai[5], Lucy Bizien[1,2], Gonca Hancioglu[6], Quentin Philippot[1, 2], Mame Sokhna Gueye[1, 2], Majistor Raj Luxman Maglorius Renkilaraj[1, 2], Masato Ogishi[5], Camille Soudée[1,2], Mélanie Migaud[1, 2], Flore Rozenberg[7], Mana Momenilandi[1,2,8], Quentin Riller[9], Luisa Imberti[10], Ottavia Delmonte[32], Gabriele Müller[11,12], Bärbel Keller[11,12], Julio Orrego[13], William Alexander Gallego[13], Tamar Rubin[14], Melike Emiroglu[15], Nima Parvaneh[16], Daniel Eriksson[17,18,19], Maribel Aranda-Guillen[20], David I. Berrios[3], Linda Vong[21,22], Connie H. Katelaris[23], Peter Mustillo[24], Johannes Rädler[25], Jonathan Bohlen[1,2], Jale Bengi Celik[26], Camila Astudillo[27], Sarah Winter[28], Canonical NF-κB consortium[†], COVID Human Genetic Effort[†], Audrey Guichard[29], Vivien Béziat[1,2,5], Jacinta Bustamante[1,2,5,30], Qiang Pan-Hammarström[31], Yu Zhang[32,33], Lindsey B. Rosen[32], Steve M. Holland[32], Heather Kenney[33], Kaan Boztuğ[34], Nizar Mahlaoui[35,36], Sylvain Latour[28], Roshini Abraham[37], Vassilios Lougaris[38], Fabian Hauck[25], Anna Sediva[39], Faranaz Atschekzei[40], M. Cecilia Poli[41], Mary A. Slatter[42], Boaz Palterer[43], Michael D. Keller[44], Alberto Pinzon-Charry[45,46], Anna Sullivan[45,46], Luke Droney[45,46], Daniel Suan[46,47], Nathalie Aladjidi[48], Miguel Hie[49], Estibaliz Lazaro[50], Jose Franco[12], Sevgi Keles[51], Marion Malphette[52], Marlene Pasquet[53], Maria Elena Maccari[11,54], Andrea Meinhardt[1,54], Aydan Ikinciogullari[55], Mohammad Shahrooei[8], Fatih Celmeli[56], Patrick Frosk[57], Christopher C. Goodnow[58,59,46], Paul E. Gray[60,46], Alexandre Belot[61], Hye Sun Kuehn[62], Sergio D. Rosenzweig[62], Francesco Licciardi[63], Amélie Servettaz[64], Vincent Barlogis[65], Guillaume Le Guenno[66], Vera-Maria Herrmann[67], Taco Kuijpers[68], Grégoire Ducoux[69], Françoise Sarrot-Reynauld[70], Catharina Schuetz[71], Charlotte Cunningham-Rundles[72], Frédéric Rieux-Laucat[9], Stuart G. Tangye[46,58,59], Cristina Sobacchi[73], Rainer Doffinger[74], Klaus Warnatz[11,12], Bodo Grimbacher[11,12], Claire Fieschi[52], Laureline Berteloot[75], Vanessa Bryant[76], Sophie Trouillet Assant[77], Luigi D. Notarangelo[32,33], Helen Su[32,33], Benedicte Neven[36], Laurent Abel[1,2,5], Qian Zhang[1,2,5], Bertrand Boisson[1,2,5], Aurélie Cobat[1,2,5], Emmanuelle Jouanguy[1,2,5], Olle Kampe[78,‡], Paul Bastard[1, 2,5,‡], Chaim Roifman[21,22,‡], Nils Landegren[4,18, ‡], Mark S. Anderson[3,79,§], Jean-Laurent Casanova[1,2,5,80,§,*] and Anne Puel[1, 2,5§*]

[1] Laboratory of Human Genetics of Infectious Diseases, Necker Branch, INSERM UMR1163, Paris, France.
[2] University of Paris Cité, Imagine Institute, Paris, France.
[3] Diabetes Center, University of California, San Francisco, San Francisco, United States.
[4] Science for Life Laboratory, Uppsala University, Uppsala 751 23, Sweden.
[5] St. Giles Laboratory of Human Genetics of Infectious Diseases, Rockefeller Branch, The Rockefeller University, New York, NY, United States.
[6] Division of Pediatric Allergy and Immunology, Ondokuz Mayıs University Faculty of Medicine, Samsun, Turkey.
[7] Virology, Cochin-Saint-Vincent de Paul Hospital, University of Paris, Paris, France.
[8] Specialized Immunology Laboratory of Dr. Shahrooei, Ahvaz, Iran.
[9] Laboratory of Immunogenetics of Pediatric Autoimmune Diseases, Université de Paris, Institut Imagine, INSERM UMR1163, Paris, France.
[10] CREA Laboratory, Diagnostic Department, ASST Spedali Civili di Brescia, Brescia, Italy.
[11] Institute for Immunodeficiency, Center for Chronic Immunodeficiencies, Medical Center – University Hospital Freiburg, Faculty of Medicine, Albert-Ludwigs-University, Freiburg, Germany.

[12] Department of Rheumatology and Clinical Immunology, Medical Center – University of Freiburg, Faculty of Medicine, University of Freiburg, Freiburg, Germany.
[13] Primary Immunodeficiencies Group, Department of Microbiology and Parasitology, School of Medicine, University of Antioquia, Medellín, Colombia.
[14] Division of Pediatric Clinical Immunology and Allergy, Department of Pediatrics and Child Health, University of Manitoba, Winnipeg, Canada.
[15] Department of Pediatric Infectious Diseases, Faculty of Medicine, Selcuk University, Konya, Turkey.
[16] Division of Allergy and Clinical Immunology, Department of Pediatrics, Tehran University of Medical Sciences, Tehran, Iran.
[17] Department of Clinical Genetics, Uppsala University Hospital, Uppsala, Sweden.
[18] Department of Immunology, Genetics and Pathology, Uppsala University and University Hospital, Section of Clinical Genetics, Uppsala, Sweden.
[19] Center for Molecular Medicine, Department of Medicine (Solna), Karolinska Institutet, Stockholm 171 76, Sweden.
[20] Centre for Molecular Medicine, Department of Medicine (Solna), Karolinska Institutet, Stockholm, Sweden.
[21] Division of Immunology and Allergy, Department of Paediatrics, Hospital for Sick Children and University of Toronto, Toronto, ON, Canada.
[22] The Canadian Centre for Primary Immunodeficiency and The Jeffrey Modell Research Laboratory for the Diagnosis of Primary Immunodeficiency, The Hospital for Sick Children, Toronto, ON, Canada.
[23] Immunology and Allergy, University of Western Sydney and Campbelltown Hospital, NSW Australia.
[24] Division of Allergy and Immuology, Nationwide Children's Hospital, The Ohio State University College of Medicine, Comumbus, OH, United States.
[25] Division of Pediatric Immunology and Rheumatology, Department of Pediatrics, Dr. von Hauner Children's Hospital, University Hospital, Ludwig-Maximilians-Universität München, Munich, Germany.
[26] Department of Anesthesiology and Reanimation, Selcuk University Faculty of Medicine, Konya, Turkey.
[27] Department of Pediatrics, Facultad de Medicina Clinica Alemana Universidad del Desarrollo, Santiago, Chile.
[28] Laboratory of Lymphocyte Activation and Susceptibility to EBV, Imagine - Institut des Maladies Génétiques-Inserm UMR 1163, 24, boulevard du Montparnasse, 75015 Paris.
[29] Joint unit Hospices Civils de Lyon – BioMérieux, Lyon, France.
[30] Study Center of Immunodeficiencies, Necker Hospital for Sick Children, Paris, France.
[31] Department of Biosciences and Nutrition, Karolinska Institutet, 17177 Stockholm, Sweden.
[32] Laboratory of Clinical Immunology and Microbiology, Division of Intramural Research, National Institute of Allergy and Infectious Diseases, National Institutes of Health, Bethesda, MD, United Stated.
[33] NIAID Clinical Genomics Program, NIH, Laboratory of Clinical Immunology and Microbiology, Division of Intramural Research, NIAID, NIH, Bethesda, MD, United States.
[34] CeMM Research Center for Molecular Medicine of the Austrian Academy of Sciences, Vienna, Austria; Department of Pediatrics and Adolescent Medicine, Medical University of Vienna, Vienna, Austria.
[35] French National Reference Center for Primary Immunodeficiencies (CEREDIH), Necker-Enfants University Hospital, Assistance Publique-Hôpitaux de Paris (AP-HP), Paris, France.
[36] Department of Pediatric Immunology, Hematology and Rheumatology, Necker-Enfants Malades Hospital, APHP, Paris, France.

[37] Department of Pathology and Laboratory Medicine, Nationwide Children's Hospital, Columbus, OH, United States.
[38] Department of Clinical and Experimental Sciences, Pediatrics Clinic and Institute for Molecular Medicine A. Nocivelli, University of Brescia ASST-Spedali Civili di Brescia, Brescia, Italy.
[39] Department of Immunology, Second Faculty of Medicine Charles University and Motol University Hospital, Prague, Czech Republic.
[40] Division of Rheumatology and Clinical Immunology, Hannover Medical University, Hannover, Germany.
[41] Hospital de Niños Dr. Roberto del Río, Santiago Chile
[42] Children's Haemopoietic Stem Cell Transplant Unit, Great North Children's Hospital, Newcastle upon Tyne Hospital NHS Foundation Trust, Newcastle upon Tyne, United Kingdom.
[43] Allergy and Clinical Immunology, Department of Experimental and Clinical Medicine, University of Florence, Florence, Italy.
[44] Division of Allergy and Immunology, Children's National Medical Center, Washington, DC, United States.
[45] Immunology and Allergy, Queensland Children's Hospital, Level 12, Queensland Children's Hospital, 501 Stanley Street, South Brisbane, QLD 4101, Australia.
[46] Clinical Immunogenomics Research Consortium Australasia (CIRCA), Darlinghurst, NSW Australia.
[47] Westmead Clinical School, University of Sydney.
[48] Pediatric Oncology Hematology Unit, University Hospital, Plurithématique CIC (CICP), Centre d'Investigation Clinique (CIC) 1401, Bordeaux, France.
[49] Internal Medicine Department, Pitié-Salpêtrière Hospital, Paris, France.
[50] Department of Internal Medicine & Infectious Diseases, Bordeaux Hospital University, Bordeaux, France.
[51] Necmettin Erbakan University, Meram Medical Faculty, Division of Pediatric Allergy and Immunology, Konya, Turkey.
[52] Clinical Immunology Department, Saint Louis Hospital, Paris, France.
[53] Department of Pediatric Hematology, Toulouse University Hospital, Toulouse, France.
[54] Division of Pediatric Hematology and Oncology, Department of Pediatrics and Adolescent Medicine, Medical Center-University of Freiburg, Faculty of Medicine, University of Freiburg, Freiburg, Germany.
[55] Department of Pediatric Immunology and Allergy, Ankara University School of Medicine, Ankara, Turkey.
[56] Department of Allergy and Immunology, University of Medical Science, Antalya Education and Research Hospital, Antalya, Turkey.
[57] Department of Biochemistry and Medical Genetics, Rady Faculty of Health Sciences, University of Manitoba, Winnipeg, MB, Canada.
[58] Garvan Institute of Medical Research, Darlinghurst 2010, NSW, Sydney, Australia.
[59] School of Clinical Medicine, UNSW Medicine & Health, Darlinghurst 2010, NSW, Australia.
[60] Immunology and Infectious Diseases, Sydney Children's hospital Randwick, Western Sydney university, Campbelltown NSW, Australia.
[61] CNRS UMR 5308, ENS, UCBL, Lyon, France; National Referee Centre for Rheumatic, and Autoimmune and Systemic Diseases in Children (RAISE), Lyon, France; Lyon; Immunopathology Federation LIFE, Hospices Civils de Lyon, Lyon, France.
[62] Immunology Service, Department of Laboratory Medicine, Clinical Center, National Institutes of Health, Bethesda, United States.
[63] Department of Pediatrics and Public Health, Università degli Studi di Torino, Turin, Italy.

[64] Internal Medicine, Clinical Immunology and Infectious Diseases Department, University Hospital Center, Reims, France.
[65] CHU Marseille, Hôpital La Timone, Service d'Hémato-oncologie Pédiatrique, Assistance Publique-Hôpitaux de Marseille, Marseille, France.
[66] Centre Hospitalier Universitaire Estaing, Clermont-Ferrand, France.
[67] Institute of Human Genetics, University of Leipzig Medical Center, Leipzig, Germany.
[68] Department of Pediatric Immunology, Rheumatology and Infectious Diseases, Emma Children's Hospital, Amsterdam University Medical Center, University of Amsterdam, Amsterdam, The Netherlands.
[69] Department of Internal Medicine, Edouard Herriot Hospital, Lyon, France.
[70] Department of Internal Medicine, Hôpital Michallon, CHU de Grenoble Alpes, Grenoble, France.
[71] Department of Paediatrics, Universitätsklinikum Carl Gustav Carus, Technische Universität Dresden, Dresden, Germany.
[72] Departments of Medicine and Pediatrics, Mount Sinai School of Medicine, New York, United States.
[73] Humanitas Clinical and Research Institute, Rozzano, Italy; CNR-IRGB, Milan Unit, Milan, Italy.
[74] Department of Clinical Biochemistry and Immunology, Addenbrooke's Hospital, Cambridge, United Kingdom.
[75] Pediatric Radiology Department, Assistance Publique-Hôpitaux de Paris (AP-HP), Necker Hospital for Sick Children, Paris, France.
[76] Walter and Eliza Hall Institute, Melbourne, Parkville, Australia.
[77] CIRI (Centre International de Recherche en Infectiologie), Université de Lyon, Université Claude Bernard Lyon 1, INSERM U1111, CNRS, UMR5308, ENS Lyon, Université Jean Monnet de Saint-Etienne, Lyon, France.
[78] Department of Endocrinology, Metabolism and Diabetes, Karolinska University Hospital, Stockholm 171 76, Sweden.
[79] Department of Medicine, University of California, San Francisco, San Francisco, United States.
[80] Howard Hughes Medical Institute, New York, NY, United States.

* correspondence (casanova@rockefeller.edu; anne.puel@inserm.fr; tom.le-voyer@institutimagine.org)

[&],[§] These authors contributed equally

[†] List of authors in appendix

Abstract

Patients with autoimmune polyendocrinopathy syndrome type 1 (APS-1) caused by autosomal recessive AIRE deficiency display autoantibodies (auto-Abs) neutralizing type I IFNs, conferring a predisposition to life-threatening COVID-19 pneumonia. We report that patients with autosomal recessive NIK or RelB deficiency, or a specific type of autosomal dominant (AD) NF-κB2 deficiency also display neutralizing auto-Abs against type I IFNs and are prone to life-threatening COVID-19 pneumonia. Among patients with AD NF-κB2 deficiency, these auto-Abs are found only in heterozygotes with variants that are both transcriptionally loss-of-function (p52 activity), due to impaired p100 processing into p52, and regulatory gain-of-function (IκBδ activity), due to accumulation of unprocessed p100, thus increasing the inhibitory IκBδ activity ($p52^{LOF}$/$IκBδ^{GOF}$). Conversely, neutralizing auto-Abs against type I IFNs are not found in individuals heterozygous for *NFKB2* variants causing either p100 and p52 haploinsufficiency ($p52^{LOF}$/$IκBδ^{LOF}$), or p52 gain-of-function ($p52^{GOF}$/$IκBδ^{LOF}$). Unlike patients with APS-1, patients with disorders of NIK, RelB, or NF-κB2 harbor very few other auto-Abs. Their thymuses are however abnormally structured, and their medullary thymic epithelial cells (mTECs) have defective AIRE expression. Human inborn errors of the alternative NF-κB pathway impair thymic AIRE expression in mTECs, thereby underlying the production of auto-Ab against type I IFNs and predisposition to viral diseases.

One-Sentence Summary: Patients with inborn errors of the alternative NF-κB pathway have low thymic AIRE expression, leading to the development of auto-Abs neutralizing type I IFNs, and severe viral diseases.

Introduction

Auto-antibodies (auto-Abs) neutralizing type I interferons (IFNs) were discovered in the early 1980s in patients treated with type I IFNs [1]. Shortly after this discovery, they were also detected in patients with systemic lupus erythematosus (SLE), thymoma, or myasthenia gravis [2–4]. These auto-Abs were widely thought to be clinically silent, with the notable exception of a 77-year-old woman with disseminated shingles reported in 1984 by Ion Gresser *et al.* [5]. Nearly 40 years later, we showed, in an international cohort (www.covidhge.com), that pre-existing neutralizing auto-Abs to type I IFNs underlie at least 15% of cases of life-threatening COVID-19 pneumonia [1,6–9], an observation that has since been replicated in various ways in at least 29 centers worldwide [1,8,10–36]. These auto-Abs also underlie about one third of cases in a small series of patients with severe adverse reactions to yellow fever YFV-17D live-attenuated viral vaccine [37]. More recently, they were found in about 5% of patients aged under 70 years of age with critical influenza pneumonia [38]. Consistent with the 1984 case report, they also confer predisposition to shingles in patients with COVID-19 pneumonia [14] or with impaired T cell development due to biallelic hypomorphic *RAG1* or *RAG2* variants [39]. Auto-Abs against type I IFNs underlie clinical phenocopies of inborn errors of type I IFN immunity, the same viral diseases have been reported in patients with autosomal recessive (AR) IFNAR1 or IFNAR2 deficiency [1,8]. Plasma or serum (diluted 1/10) from patients with these auto-Abs can neutralize low (100 pg/mL) or high (10 ng/mL) concentrations of all 13 subtypes of IFN-α and/or IFN-ω, and, more rarely, IFN-β (10 ng/mL), evidenced by impaired STAT1 activation or induction of a reporter gene [6,7], or the cell protective effect of IFN-α2 against SARS-CoV-2, YFV-17D, or influenza virus *in vitro* [6,37,38]. These auto-Abs also impair the induction of IFN-stimulated genes (ISGs) in peripheral blood mononuclear cells and nasal mucosae infected with SARS-CoV-2 *ex vivo* [6,40,41]. Finally, these auto-Abs are also present in the general population [6,9]. The prevalence of neutralizing auto-Abs against IFN-β (10 ng/mL) is about 0.2% across

age groups, whereas that of auto-Abs against IFN-α and/or IFN-ω is 0.3% (10 ng/mL) or 1% (100 pg/mL), in individuals under the age of 70 years old, rising to 4% (10 ng/mL) or 7% (100 pg/mL) over 70 years old, thereby contributing to the age-related increase in the risk of severe COVID-19 [6,9].

Remarkably, the production of auto-Abs against type I IFNs can be driven by monogenic inborn errors of immunity (IEI). Only a handful of IEI to date have been shown to underlie the production of such antibodies [1]. These IEI include 1) autoimmune polyendocrine syndrome type-1 (APS-1), also known as autoimmune polyendocrinopathy-candidiasis-ectodermal dystrophy (APECED), which is caused by germline biallelic deleterious variants of *AIRE*, 2) immunodysregulation polyendocrinopathy enteropathy X-linked (IPEX) syndrome, which is caused by deleterious hemizygous variants of *FOXP3*, and 3) combined immunodeficiency due to biallelic hypomorphic *RAG1* or *RAG2* variants [1]. Some patients with autosomal dominant (AD) APS-1 can also develop these auto-Abs. A common feature of these IEI is that they affect the thymic selection of T cells, in a T cell-intrinsic or -extrinsic manner. For example, AIRE deficiency impairs the expression of tissue-specific antigens (TSAs) in medullary thymic epithelial cells (mTECs), allowing the escape of autoreactive T cells, whereas FOXP3 deficiency impairs the development of thymic regulatory T cells (Tregs) [42,43]. Hypomorphic variants of *RAG1* or *RAG2* that are T cell-intrinsic have an impact on thymic architecture and the development of mTECs [44–46]. The disruption of self-tolerance in the thymus therefore seems to underlie the production of auto-Abs against type I IFNs. APS-1 patients present a wide range of auto-Abs against TSAs, but the production of these auto-Abs only partially accounts for the many endocrine susceptibility phenotypes of these patients [42]. APS-1 patients also frequently harbor neutralizing auto-Abs against IL-17A and/or IL-17F which underlie chronic mucocutaneous candidiasis (CMC), a disease seen in patients with inborn errors of IL-17A/F immunity [47]. Most, if not all (>95%) APS-1 patients also produce auto-Abs

against type I IFNs in early childhood [48–51]. These auto-Abs were thought to be silent when they were first discovered in APS-1 patients in 2006 [51,52]. However, it was discovered in 2021 that these antibodies render APS-1 patients highly vulnerable to critical COVID-19 pneumonia [23,25,53–56], or, more recently, to severe varicella [57].

In mice, expression of the *AIRE* gene in mTECs is controlled by the tumor necrosis factor receptor (TNFR)-family member RANK via the alternative (or non-canonical) NF-κB pathway [58–61]. Activation of this pathway is tightly controlled and depends on TRAF6 and the NF-κB-inducing kinase (NIK), IKKα, NF-κB2, and RelB, which operate with slower activation kinetics than the classical NF-κB pathway [62]. Once the alternative NF-κB pathway has been triggered by RANKL or other TNFR ligands such as CD40L, lymphotoxin α1β2 (Lt) or BAFF, NIK accumulates in the cytoplasm, activates IKKα, and phosphorylates the full-length NF-κB2 precursor p100 (amino-acids 1-900) on serine residues S866 and S870 located within the NIK-responsive sequence (NRS). This leads to p100 ubiquitinylation (K855) and processing by the 26S proteasome to generate the active form, p52 (aa 1-405), which preferentially dimerizes with RelB *in vivo* via its REL homology domain (RHD) [62]. This p52/RelB heterodimer migrates to the nucleus, where it induces transcription of target genes involved, notably, in lymphoid organ development, germinal center formation, B-cell survival, maturation, homeostasis, mTEC development, and osteoclastogenesis [62]. *In vitro*, p52 can also form homodimers and act as a transcriptional repressor of the NF-κB *cis*-regulatory element (κB sites) when present in excess [63,64]. Both p52 dependent transcriptional activity are later referred as p52 function. In resting cells, the processing inhibitory domain (PID) of p100 protects against the spontaneous processing and nuclear translocation of the p100 precursor. Unprocessed cytoplasmic p100 can form high molecular weight complexes by homo-multimerization (generating kappaBsomes) via its C-terminal IκB-like domain, thereby inhibiting the DNA-binding activity of almost all NF-κB subunits (this is referred to as IκBδ function) [65–67]. In the mouse thymus, RANK and the

alternative NF-κB pathway, thus, play a crucial role in mTECs by governing self-tolerance [58,60]. Moreover, cooperation between RANKL and CD40L is required for correct mouse mTEC development and for the concomitant expression of AIRE and TSA [60]. Furthermore deficiencies of mouse *Traf6, Ikkα, Nik,* or *RelB* all impair both mTEC development and AIRE expression in mTECs [60,68]. We therefore tested the hypothesis that human inborn errors of the alternative NF-κB pathway — including AD NF-κB2 disorders, and AR RelB, IKK-α and NIK deficiencies — can underlie the production of auto-Abs against type I IFNs, thereby predisposing patients to severe viral diseases, including COVID-19 pneumonia [69–73]. No patients with inherited TRAF6 deficiency have ever been identified. Whereas the three inborn errors of the alternative NF-κB pathway are AR (NIK, RelB, and IKKα) and biochemically partial or complete, the mode of inheritance and the biochemical nature of AD NF-κB2 disorders are less well known [74–77].

Results

A cohort of patients with inborn errors of the alternative NF-κB pathway

We investigated whether inborn errors of the alternative NF-κB pathway could underlie the presence of auto-Abs against type I IFNs, in an international cohort of 65 patients from 46 kindreds heterozygous for 26 different rare (MAF< 0.0001) non-synonymous *NFKB2* variants (**Fig. 1A-B and Table SI**). Most affected individuals had a predominant phenotype of antibody deficiency (PAD) (56/59, 94.9% of these patients) (**Fig. 1A-B and Table SI**). This cohort included 28 patients from 18 families with 12 *NFKB2* variants reported in previous studies (**Table SI**). The condition was familial in 42 patients from 24 kindreds, and sporadic in 19 patients (unknown in 4 patients) (**Fig. 1A and Table SI**). Consistent with AD inheritance, *NFKB2* is under strong negative selection, with a CoNeS score of -1.6 [78] and a high probability of being loss-of-function-intolerant (pLI of 1) (**Fig. 1C and S1C**). Nineteen variants (73%) clustered in a region corresponding to the C-terminal domain of the protein (CTD, aa 760-900) **(Fig. 2A)**. These variants comprised 13 predicted loss-of-function (pLOF) variants, and six missense variants, five of which were predicted to affect the NRS (aa 861-871). This region, which is crucial for NIK-mediated phosphorylation and the processing of p100 to generate p52, is under particularly strong purifying selection, with a low missense tolerance ratio (MTR) score (**Fig. S1B**). Fifty-three patients from 37 kindreds carried 18 heterozygous variants in the CTD (pLOF, *n*=36 from 27 kindreds or missense, *n*=17 patients from 10 kindreds), including 19 individuals from 13 kindreds with the recurrent R853* variant (**Fig. 1A, Table SI**). The recurrence of this variant probably reflects the existence of a mutational hotspot, as opposed to a founder effect, because this variant was previously detected in patients from nine different countries and was shown to have occurred *de novo* in six patients [79–84]. The other 12 patients were heterozygous for *NFKB2* variants in the Rel homology domain (RHD) (*n*=3 from 3 kindreds; pLOF, *n*=2 and missense, *n*=1), or the ankyrin repeat domain (ARD) (pLOF, *n*=6

patients from 3 kindreds, and missense, *n*=3 from 3) (**Fig. 2A**). The consequence of the c.104-1G>C/WT *NFKB2* variant of patient P62, predicted to disrupt an essential acceptor splicing site, was evaluated by TOPO TA cloning on cDNA from T-cell blasts. About half the transcripts were abnormally spliced, mostly by a skipping of exon 4, and were predicted to encode a truncated protein (A35Efs*10), confirming the detrimental effect of the c.104-1G>C variant on the splicing of the *NFKB2* mRNA (**Fig. S1D**). We also enrolled 14 patients with other inborn errors of the alternative NF-κB pathway (AR NIK (*n*=2) and AR RelB (*n*=8) deficiencies) or upstream receptors (AR BAFF (*n*=1) or XR-CD40L (*n*=3) deficiencies) (**Fig. S1A, E and Table SII**).

Luciferase reporter assay testing the p52-dependent transcriptional activity of the *NFKB2* alleles

NF-κB2 (the corresponding *NFKB2* gene encodes both p100 and its cleaved product, p52) is one of the five REL/NF-κB proteins. The active form, p52 can bind DNA, but, like NF-κB1 (p105/p50), and unlike RelA, RelB, and cRel, it lacks a transcriptional activation domain (TAD). Its transcriptional activation, thus, requires heterodimerization with another TAD-containing REL protein [65]. The p52 protein predominantly dimerizes with RelB *in vivo*, but an excess of p52 can lead to p52/p52 homodimerization occurring *in vitro,* potentially repressing the κB-site transcriptional activity of other dimers though a dosage effect [63,64] (**Fig. S2A**). Whereas 23 *NFKB2* variants have been reported in more than 80 patients with AD NF-κB2 disorders have been reported, but only five of the these variants have been tested functionally. The E418* and R635* variants resulted in spontaneous nuclear translocation, while the R853*, S866R and A867Cfs*19 variants prevented processing of p100 to p52 [85–87]. However, these assays did not distinguish the two functions (p52 and IκBδ) of proteins encoded by the *NFKB2* locus. We therefore developed an assay for evaluating the functional impact of *NFKB2* variants

by assessing κB luciferase activity 24 and 48 h after the cotransfection of HEK293T cells with plasmids encoding NIK, RelB, and/or NF-κB2/p100 (**Fig. S2A**). Transfection with NIK alone or together with RelB led to strong RelA-dependent κB transcriptional activity in HEK293T cells, 24 to 72 hours after transfection, as only a weak luciferase signal was detected in *RELA*-deficient HEK293T cells (**Fig. S2B**). With this assay, we were, therefore, able to assess the p52-dependent capacity of the NF-κB2 variants to bind the κB promoter and to prevent the transcriptional activity induced by endogenous RelA-containing dimers [63] (**Fig. S2A**). For the validation of this test, we generated plasmids encoding previously characterized biochemical NF-κB2 mutants (**Fig. S2C**), including a dimerization-defective NF-κB2 mutant (Y247A) shown to prevent heterodimerization with RelB or RelA and subsequent processing into p52 [67,88], and two processing-resistant NF-κB2 mutant (S866A and S870A) [67,89,90]. Cotransfection with WT *NFKB2* (p100) repressed the κB transcriptional activity induced by NIK and RelB, 24 h and 48 h post-transfection (**Fig. 2B and Fig. S2D**, black bars). By contrast, in the same conditions, the repression of κB transcriptional activity by Y247A, S866A or S870A was impaired, indicating that these variants were $p52^{LOF}$ relative to the WT NF-κB2 [89,91,92]. Mutants truncated within the ARD (p100 1-455 or p100 1-665), had an enhanced capacity to repress κB transcriptional activity because they lack their last ANK repeats in the ARD and their PID (aa 761-851), and were thus p52-gain-of-function ($p52^{GOF}$), 24 h and/or 48 h after transfection [89]. Biochemical mutants lacking the PID but with all their ankyrin (ANK) repeats intact (NF-κB2 1-776), and variants with mutations of the ubiquitinylation residue (K855R) displayed a partial impairment of repression capacity (**Fig. 2B,** colored bars).

NFKB2 variants can be LOF or GOF in terms of p52/p52 homodimer function

We used this assay to evaluate the impact of 25 *NFKB2* variants from our cohort of patients, and the 12 additional previously reported variants [93] (**Fig. 2C and S2D-E**). The three

RHD pLOF variants (c.104-1G>C/A35Efs*10, W270*, and K321Sfs*160 (referred to hereafter as K321Sfs)) were $p52^{LOF}$ (**Fig. 2C and S2D**). The E418* pLOF variant was $p52^{GOF}$, as previously reported [85], 24 h but not 48 h after transfection. The four ARD pLOF variants lacking the PID [94] (L531Cfs*5, Q539*, R611*, and R635*) were $p52^{GOF}$. All the CTD pLOF (*n*=16, from S762Afs*21 to Q871*) and missense variants located within the NRS (*n*=6, from D865G to S870N) were $p52^{LOF}$ (**Fig. 2C and S2D**). All seven additional missense variants (K321E, G369R, P491S, A567V, V661M, P681L, and V844A), reported in patients with PAD (probably due to another genetic lesion, referred to hereafter as 'idiopathic PAD'), localized outside of the NRS, were isomorphic in terms of p52 inhibitory function ($p52^{WT}$) at 24 h and 48 h after transfection (**Fig. S2E-F)**. Finally, we tested the 14 missense variants with a MAF > 10^{-4} reported in the heterozygous state in the gnomAD and BRAVO public databases (**Fig. S1C**). All these variants were $p52^{WT}$ at 24 h and 48 h after transfection (**Fig. S2E-F**). Overall, our findings show that the deleterious *NFKB2* variants found in patients with PAD can be GOF or LOF in terms of the repression of transcription activity by p52/p52 homodimers, with RHD pLOF variants and CTD pLOF or missense variants within the NRS being $p52^{LOF}$, pLOF variants impairing the ARD (E418* and pLOF variants located within the ARD) being $p52^{GOF}$, while other missense variants (K321E, G369R, P491S, A567V, V661M, P681L, and V844A and variants found in the public databases with a MAF > 10^{-4}) being $p52^{WT}$. We inferred from these data that the transcriptional activity of p52-RelB heterodimers may follow the same pattern.

The $p52^{LOF}$ variants of the CTD resist the NIK-dependent processing of p100

We then assessed the impact of *NFKB2* variants on p100 activation, by analyzing the phosphorylation of this protein at position S866 (P-p100) using an antibody recognizing the phosphorylated serine 866 [90], and its proteolytic cleavage to generate p52, following

cotransfection with NIK [89]. The Y247A, S866A and S870A mutants abolished p100 processing, but only the S866A mutant abolished p100 phosphorylation (**Fig. S2C**). The truncated $p52^{GOF}$ mutants displayed an abolition of p100 phosphorylation. After 48h of transfection, the $p52^{LOF}$ W270* and K321Sfs variants of the RHD, and the E418* and the other $p52^{GOF}$ variants of the ARD (L531Cfs*5, Q539*, R611*, and R635*) had produced a truncated protein, with no P-p100 or p52 production following cotransfection with NIK, contrasting with the results for the WT *NFKB2* cDNA (**Fig. 2D**) [85]. The 23 $p52^{LOF}$ variants of the CTD tested (the 17 pLOF and 6 missense variants of the NRS) presented an impairment (Q871* and S870N) or abolition (the other 21) of p100 phosphorylation, and all were resistant to p100 processing, with no p52 produced upon cotransfection with NIK (**Fig. 2D**). As expected, the 10 most frequent missense variants with a MAF>10^{-4} from public databases and shown above to be $p52^{WT}$ in terms of repressing transcriptional activity had normal P-p100 levels and p100 processing capacity (**Fig. S2G**). Overall, these findings suggest that the deleterious *NFKB2* alleles can be $p52^{LOF}$ due to an impairment of normal p52 expression, because the p52 mutant protein is truncated or because p52 generation is impaired by p100 processing-resistance. Alternatively, they may be $p52^{GOF}$, possibly due to constitutive p52 translocation and DNA-binding activity in the absence of a functional PID (**Summarized in Fig. S2H and Table SIII**).

The processing-resistant p100 variants have enhanced IκBδ inhibitory capacities for repressing RelA-dependent canonical NF-κB activation

We tested the hypothesis that monoallelic processing-resistant CTD variants may have IκBδ GOF activity ($p52^{LOF}$/$IκBδ^{GOF}$) because their C-terminal region cannot be degraded by NIK, unlike that of the WT protein or variants affecting in the RHD or ARD (predicted $IκBδ^{LOF}$). The transfection of HEK293T cells with plasmids encoding NIK plus WT-NF-κB2 (aa 1-900), $p52^{GOF}$ R611*, or the $p52^{LOF}$ processing-resistant variants (R853* or S866N) resulted in similar

levels of repression of κB transcriptional activity, suggesting that this test evaluates the two i*n vitro* repressive functions of NF-κB2 (p52-dependent, through p52/p52 homodimer DNA-binding, and IκBδ-dependent, through cytoplasmic retention of the REL-containing NF-κB complexes) (**Fig. S3A-B**). In these conditions, W270* was null, consistent with its lack of both p52 and IκBδ functions (**Fig. S3A**). We specifically evaluated the IκBδ capacity of the WT and mutant p100 proteins to inhibit RelA-dependent transcriptional activity, by cotransfecting cells with a plasmid encoding NIK together with a plasmid encoding only the C-terminal WT or mutant region of NF-κB2 (p100-Cter^{WT}, aa 405-900). The p100-Cter^{WT} protein had no transcriptional repression activity in this system, consistent with its sensitivity to proteasomal degradation upon cotransfection with NIK (IκBδ^{WT}) (**Fig. 3A**). As expected, the Cter^{R611*} (aa 405-611) protein did not repress κB transcriptional activity (IκBδ^{LOF}), confirming the specificity of this assay for evaluating NF-κB2 IκBδ function. By contrast, the Cter^{R853*} (aa 405-853) and Cter^{S866N} (aa 405-900) mutants, which were insensitive to proteasomal degradation upon cotransfection with NIK, repressed κB transcriptional activity strongly (IκBδ^{GOF}). For confirmation of the IκBδ^{GOF} activity of the R853* and S866N variants, we used the dimerization-defective and processing-resistant NF-κB2 mutant (Y247A) to create double mutants. Co-transfection of NIK with simple mutant (p100^{Y247A}), or even more, with p100$^{R853*/Y247A}$ or p100$^{S866N/Y247A}$ double mutant resulted in an enhanced capacity to repress κB transcriptional activity relative to transfection with NIK alone, or with p100$^{W270*/Y247A}$ or p100$^{R611*/Y247A}$ **(Fig. 3B).** Thus, processing-resistant CTD variants are IκBδ^{GOF} (p52^{LOF}/IκBδ^{GOF}) in terms of transcriptional repression in the RelA-dependent canonical NF-κB pathway following cotransfection with NIK, whereas W270* and R611* are IκBδ^{LOF} (p52^{LOF}/IκBδ^{LOF} and p52^{GOF}/IκBδ^{LOF}, respectively).

The processing-resistant IκBδ^{GOF} CTD NF-κB2 variants impair WT NF-κB2- and RelB-dependent alternative NF-κB activation

We then investigated whether the p52^{LOF}/IκBδ^{GOF} variants impaired the activation of WT NF-κB2 or RelB. Cotransfection with various amounts of the p52^{LOF}/IκBδ^{GOF} R853* or S866N and constant amounts of NIK and WT p100 revealed a dose-dependent inhibition of WT p100 phosphorylation and, to a lesser extent, of its processing to generate p52 (**Fig. 3C**). By contrast, increasing the amount of p52^{LOF}/IκBδ^{LOF} W270* cDNA had no effect on WT P-p100 levels or WT p100 processing (**Fig. 3C**). We then assessed the effects of the p52^{LOF}/IκBδ^{GOF} variants on RelB and p52 nuclear translocation, by confocal microscopy in transiently transfected HeLa cells. Transfection with the p52^{LOF}/IκBδ^{LOF} K321Sfs or p52^{GOF}/IκBδ^{LOF} R611*, with or without NIK, resulted in constitutive nuclear localization of the encoded protein, consistent with the absence of a nuclear export sequence (NES) [95] (**Fig. S3C**). Transfection of RelB, either alone or together with the IκBδ^{LOF} K321Sfs or R611*, led to the translocation of RelB to the nucleus (**Fig. 3D**, left panel). By contrast, transfection of RelB with WT p100, R853*, or S866N, in the absence of NIK, resulted in an absence of RelB translocation to the nucleus, consistent with the functional p100-IκBδ activity of these proteins (**Fig. 3D**, left panel). Addition of NIK to this system led to RelB translocation to the nucleus after cotransfection with WT-p100, but not with the IκBδ^{GOF} R853* or S866N proteins (**Fig. 3D**, right panel). Similar results were obtained with plasmids encoding the WT or mutant C-terminal domain of NF-κB2 (**Fig. S3D**). Overall, our findings suggest that the p52^{LOF}/IκBδ^{GOF} mutant alleles block activation of the alternative NF-κB pathway induced by NIK through their enhanced IκBδ function, by preventing the phosphorylation of WT-p100 and its processing into p52, and the nuclear translocation of RelB-containing dimers.

The p52^{LOF}/IκBδ^{GOF} variants impair p100 processing in heterozygous fibroblasts

We then investigated the consequences of the p52^{LOF}/IκBδ^{GOF} variants in stromal (primary and SV-40-immortalized fibroblasts) and hematopoietic (T-cell blasts and monocyte-derived dendritic cells (MDDCs) cells from patients following the activation of the alternative NF-κB pathway by Lt, TWEAK (fibroblasts), or CD40L (leukocytes) [62,96]. Cells heterozygous for the p52^{LOF}/IκBδ^{GOF} R853* allele produced a truncated protein, whereas cells heterozygous for the p52^{LOF}/IκBδ^{LOF} c.104-1G>C/A35Efs*10 or K321Sfs variant produced no mutant protein detectable with an antibody binding to the N-terminus of the protein (**Fig. 3E and Fig. S3E-G**). Primary fibroblasts from a healthy control stimulated with Lt for 48 h displayed p100 phosphorylation and processing to generate p52 (**Fig. 3E**). By contrast, primary fibroblasts from a patient heterozygous for the p52^{LOF}/IκBδ^{GOF} R853* presented an accumulation of the truncated p100 mutant protein after Lt stimulation, with lower levels of WT p100, P-p100 and p52 induction than WT cells or cells heterozygous for the p52^{LOF}/IκBδ^{LOF} K321Sfs (P-p100 in particular). Similarly, primary fibroblasts from a patient with AR complete NIK deficiency (NIK$^{-/-}$, homozygous for P565R [74]) presented an accumulation of unprocessed p100 following Lt stimulation, with an abolition of p100 phosphorylation, and no p52 production, consistent with the essential role NIK in p100 processing, whereas RelB-deficient fibroblasts (RelB$^{-/-}$, homozygous for Q73Tfs*152, *unpublished*) had low levels of P-p100 and p100 following stimulation with Lt, with a normal p100 processing capacity (**Fig. 3E**). An accumulation of the truncated p100 mutant protein and an impaired p100 processing into p52 were also observed in SV-40-transformed fibroblasts (from R853*/WT, *n*=1) after Lt stimulation, and in MDDCs (from R848Efs*38/WT (*n*=1) or R853*/WT (*n*=1) patients) 48 h after CD40L stimulation, relative to WT or K321Sfs/WT cells (**Fig. S3E and G**). Given the impairment of p100 processing and the accumulation of the mutant p100 upon stimulation of the non-canonical pathway, the p100/p52 ratio was higher in cells from patients heterozygous for a

p52^{LOF}/IκBδ^{GOF} variant (primary and SV-40-transformed fibroblasts and MDDCs) than in cells from healthy donors or the patient with K321Sfs/WT (**Fig. 3E and S3E and G)**.

The p52^{LOF}/IκBδ^{GOF} variants impair the translocation of p52- and RelB-containing dimers into the nucleus in heterozygous fibroblasts

We then evaluated the consequences of the p52^{LOF}/IκBδ^{GOF} variants in terms of RelB and p52 activation in cells from heterozygous patients. The activation of primary or SV-40-transformed control fibroblasts by incubation with TWEAK for 48 h induced the processing of p100 to generate p52, and the induction and translocation to the nucleus of RelB and p52 (**Fig. 3F and S3H-I**). Almost no RelB or p52 translocation to the nucleus was detected after TWEAK stimulation in primary fibroblasts from an R853*/WT patient (**Fig. 3F and S3I**). Similarly, no RelB or p52 was detected in the nucleus of primary fibroblasts from patients with AR complete NIK (NIK$^{-/-}$) or RelB deficiency (RelB$^{-/-}$) after TWEAK stimulation. By contrast, K321Sfs-heterozygous primary fibroblasts displayed almost normal RelB induction and nuclear translocation after Lt stimulation. Almost no RelB translocation was detected in SV-40-transformed fibroblasts from two unrelated R853*/WT patients or a NIK$^{-/-}$ patient, but was normal in these cells heterozygous for the K321Sfs *NFKB2* variant (**Fig. S3J**). Similar results were obtained in MDDCs from two healthy controls, and from patients heterozygous for the p52^{LOF}/IκBδ^{LOF} K321Sfs or the c.104-1G>T, or p52^{LOF}/IκBδ^{GOF} R853* variant, after stimulation with CD40L (**Fig. S3K**). Overall, these findings suggest that heterozygosity for a p52^{LOF} mutant allele can cause NF-κB2 deficiency by two different mechanisms: (1) p52/p100 haploinsufficiency for p52^{LOF}/IκBδ^{LOF} mutants, or (2) enhanced p100-IκBδ inhibitory function (p52^{LOF}/IκBδ^{GOF}) impairing phosphorylation of the WT p100 and its processing, and preventing the translocation of RelB-containing dimers to the nucleus after activation of the alternative NF-κB pathway.

Distinctive immunological phenotype of patients with p52^{LOF}/IκBδ^{GOF} variants

We assessed the immunological phenotype of patients with the three types of *NFKB2* alleles (p52^{LOF}/IκBδ^{LOF}, p52^{GOF}/IκBδ^{LOF}, and p52^{LOF}/IκBδ^{GOF}). Most patients with inborn errors of NF-κB2 (aged 1-75 years) had low serum concentrations of IgG, IgM and IgA, and few, if any circulating B cells (25/33 after the age of 15, 75%) (**Fig. S4A-B**). None of these patients were treated by B-cell depletion therapy. B-cell deficiency was also observed in the three patients with the R635* p52^{GOF}/IκBδ^{LOF} variant tested (aged 20, 47, and 75 years) and in the patient with the K321Sfs p52^{LOF}/IκBδ^{LOF} variant (aged 65 years) (**Fig. S4B**). We performed a deep immunological analysis in 12 patients with inborn errors of *NFKB2* (p52^{LOF}/IκBδ^{GOF}, n=10, and p52^{LOF}/IκBδ^{LOF}, n=2), by cytometry by time of flight (CyTOF) on fresh whole blood samples (**Fig. 4A**). Ten of the 12 patients tested had low circulating B-cell counts, with a low counts and proportions of switched memory B cells (**Fig. 4B and S4C**). FlowSOM-guided unsupervised clustering showed that p52^{LOF}/IκBδ^{GOF} mutants mostly affected the CD19^{+}CD27^{+} memory B-cell compartment, relative to healthy donors (HDs) and a patient with p52^{LOF}/IκBδ^{LOF} variants (*metaclusters* 03, 04, 05, 06 and 12, p<0.005) (**Fig. 4C and S4D**). The numbers of total lymphocytes, CD4^{+} and CD8^{+} T and γδ T cells were within the normal ranges with p52^{LOF}/IκBδ^{LOF} or p52^{LOF}/IκBδ^{GOF} variants (**Fig. S4E**). In analyses of T-cell subsets, patients with p52^{LOF}/IκBδ^{GOF} variants had more naïve CD4^{+} T cells than controls and patients with p52^{LOF}/IκBδ^{LOF} variants (**Fig. S4F**). Proportion of CD4^{+} recent emigrant thymic (RTE) cells, defined as CD4^{+}CD45RA^{-}CD31^{+}, was in the upper part of the normal range for age-matched controls in patients with p52^{LOF}/IκBδ^{GOF} variants, suggesting that thymic output was similar to or higher than that in patients with p52^{GOF}/IκBδ^{LOF} and p52^{LOF}/IκBδ^{LOF} variants [97] (**Fig. S4F**). The absolute numbers and proportions of CD4^{+}CD25^{+}CD127^{-} regulatory T cells (Tregs) were significantly lower in patients with p52^{LOF}/IκBδ^{GOF} variants than in age-matched

HDs, but their absolute number was comparable to the two patients with $p52^{LOF}/I\kappa B\delta^{LOF}$ variant (**Fig. 4D and Fig. S4G**). By contrast, four patients carrying the $p52^{GOF}/I\kappa B\delta^{LOF}$ R635* allele (reported in [85]) had normal proportions of Tregs (**Fig. S4G)**. Patients with $p52^{LOF}/I\kappa B\delta^{GOF}$ variants had significantly lower proportions of $CD4^+CD45RA^+CXCR5^+$ T follicular helper (Tfh) cells than patients with $p52^{LOF}/I\kappa B\delta^{LOF}$ variants and healthy controls, despite having normal memory $CD4^+$ T-cell counts (**Fig. 4E and S4H**). Patients with $p52^{LOF}/I\kappa B\delta^{GOF}$ variants had slightly low NK cell counts, with normal MAIT and iNKT cell counts (**Fig S4I**), and normal monocyte and dendritic cell counts (**Fig S4J**). Overall, patients heterozygous for a $p52^{LOF}/I\kappa B\delta^{GOF}$ variant had a distinctive immunological phenotype different from that of patients with $p52^{LOF}/I\kappa B\delta^{LOF}$ or $p52^{GOF}/I\kappa B\delta^{LOF}$variants, including a characteristic combination of low levels of memory B cells, cTfh cells, and Tregs.

Distinctive clinical phenotype including viral susceptibility in patients with $p52^{LOF}/I\kappa B\delta^{GOF}$ variants

We then assessed the clinical phenotype and infectious susceptibility associated with the three types of inborn errors of NF-κB2. PAD (association of hypogammaglobulinemia and recurrent bacterial respiratory tract infections [98]) was reported in most patients with $p52^{LOF}/I\kappa B\delta^{GOF}$ variants (*n*=49/51, 96%), and in more than half the patients with $p52^{LOF}/I\kappa B\delta^{LOF}$ (*n*=3/5) or $p52^{GOF}/I\kappa B\delta^{LOF}$ (*n*=4/6) variants (**Fig. 4F**). Auto-immune disease was reported in about a third of patients with $p52^{LOF}/I\kappa B\delta^{GOF}$ (*n*=21/51) or $p52^{LOF}/I\kappa B\delta^{LOF}$ (*n*=2/5) variants and in one patient with $p52^{GOF}/I\kappa B\delta^{LOF}$ (**Table SI**). By contrast, ectodermal dysplasia (sparse hair, eyebrows, or eyelashes, or nail dysplasia, with or without alopecia areata or totalis) and anterior pituitary hormone deficiencies were reported exclusively in patients carrying $p52^{LOF}/I\kappa B\delta^{GOF}$ variants, occurring in 29% of cases (*n*=15/51), each (**Fig. 4F**). Similarly, severe or recurrent viral diseases were mostly reported in patients carrying

p52^{LOF}/IκBδ^{GOF} variants (*n*=29/51, 56.9%) (**Fig. 4G**). This viral susceptibility could not be explained by immunosuppressive treatments (used in 7 patients with p52^{LOF}/IκBδ^{GOF} variant). The main viral disease reported was recurrent mucocutaneous HSV-1 lesions (n=20/51, 39%), with extensive skin lesions observed in two of the patients affected [99] (**Fig. 4G**). Six of the nine unvaccinated patients, and two patients with an unknown vaccination status, with p52^{LOF}/IκBδ^{GOF} variants developed hypoxemic COVID-19 pneumonia (NIH scale 5-8 out of 8) after being infected with SARS-CoV-2. Three of these patients, aged 17, 23, and 39 years, were admitted to intensive care with two individuals succumbing (aged 23 and 39) [69,70] (**Fig. 4H**). One patient was hospitalized for COVID-19 pneumonia without requiring oxygen supplementation (NIH scale 4). Six additional unvaccinated patients developed asymptomatic disease or mild symptoms (NIH scale 1-2) without pneumonia or hospitalization. These patients carried a p52^{LOF}/IκBδ^{GOF} (*n*=2, aged 7 and 22 years), p52^{GOF}/IκBδ^{LOF} (*n*=2, aged 20 and 49 years), or neutral (*n*=2, aged 30 and 31) NF-κB2 variant (**Fig. 4H**). COVID-19 severity was not associated with age or treatment (**Fig. 4I and Table SI**). Severe influenza pneumonia was reported in *n*=6/51 patients with p52^{LOF}/IκBδ^{GOF} variant (12%), four of whom required hospitalization and oxygen supplementation, including one patient with acute respiratory distress syndrome (ARDS) and encephalitis (**Fig. 4G**). Three patients suffered from recurrent (*n*=1) or severe (*n*=2) varicella. The two patients with severe varicella were both hospitalized, one with encephalitis and the other with severe skin disease requiring acyclovir. The other severe viral diseases observed are indicated in **Table SI**. None of the patients were vaccinated with yellow fever YFV-17D live-attenuated vaccine. All eight of the patients with inborn errors of NF-κB2 who died carried a p52^{LOF}/IκBδ^{GOF} variants. Six of these patients died from suspected or proven viral illnesses, including two from COVID-19. Together, these findings suggest that, unlike patients with the other two forms of inborn errors of NF-κB2, patients with p52^{LOF}/IκBδ^{GOF} variants present a distinctive syndrome, previously called DAVID syndrome

(immunodeficiency with hypogammaglobulinemia, plus central pituitary deficiency [79]), which is strongly associated with the risk of developing PAD and/or a severe viral disease. Conversely, p52/p100 haploinsufficiency and $p52^{GOF}$ may underlie humoral deficiency with variable clinical and immunological penetrance, whereas these conditions do not appear to underlie ectodermal, endocrine, or viral phenotypes [100]. The milder clinical phenotype associated with these forms may account for the smaller number of patients with such defects identified.

Auto-Abs against type I IFNs are exclusively associated with $p52^{LOF}$/IκBδ^{GOF} variants

We assessed the presence of auto-Abs against type I IFNs in the plasma of 65 patients heterozygous for a deleterious ($p52^{LOF}$/IκBδ^{LOF}, *n*=2; $p52^{GOF}$/IκBδ^{LOF}, *n*=6; $p52^{LOF}$/IκBδ^{GOF}, *n*=51) or neutral (idiopathic PAD, *n*=6) *NFKB2* variant. We detected high titers (absolute units, A.U. >50) of anti-IFN-α2 IgG in 29/50 (58%) patients with $p52^{LOF}$/IκBδ^{GOF} variants, 41/45 (91%) patients with APS-1, but none of those carrying $p52^{LOF}$/IκBδ^{LOF} or $p52^{GOF}$/IκBδ^{LOF} alleles, or with idiopathic PAD (**Fig. 5A**). In addition, patients with $p52^{LOF}$/IκBδ^{GOF} variants and auto-Abs against IFN-α2 also had detectable auto-Abs against most of the 13 IFN-α subtypes and IFN-ω, but not against IFN-β, IFN-κ, and IFN-ε, as evaluated with the HuProt array (**Fig. 5B**) and multiplex beads assay (**Fig. S5A**). We then assessed the neutralization capacity of the plasma in a luciferase interferon-stimulated response element (ISRE) reporter assay in the presence of high (10 ng/mL) or low (100 pg/mL) concentrations of IFN-α2, IFN-ω, or IFN-β (10 ng/mL) [6]. Overall, 33/51 (65%), 28/51 (55%) and 4/51 (8%) patients with $p52^{LOF}$/IκBδ^{GOF} variants neutralized high concentrations of IFN-α2, IFN-ω and IFN-β, respectively (**Fig. S5B-D**), and 37/51 (73%) and 39/51 (76%) neutralized low concentrations of IFN-α2 or IFN-ω, respectively (**Fig. 5C, D and S5E)**. For comparison, 41 (91%), 43 (96%), and 1 (2%) of the 45 APS-1 patients neutralized IFN-α, IFN-ω, and IFN-β, respectively, at a

concentration of 10 ng/mL (**Fig. S5B, C)**, and serum from all these patients neutralized IFN-α2 and/or IFN-ω at a concentration of 100 pg/mL (**Fig. S5C, D and S5F)**. By contrast, none of the plasma samples from any of the patients with $p52^{LOF}$/$I\kappa B\delta^{LOF}$ (*n*=2), $p52^{GOF}$/$I\kappa B\delta^{LOF}$ (*n*=6), or neutral *NFKB2* variants (*n*=6) neutralized IFN-α2, IFN-ω, or IFN-β (at 10 ng/mL or 100 pg/mL). The proportion of $p52^{LOF}$/$I\kappa B\delta^{GOF}$ patients carrying auto-Abs was higher among those carrying pLOF variants than among those carrying missense variants (**Fig. S5G**) but was independent of patients age at testing (*p*=0.6) or sex (**Fig. S5H**). Plasma samples from 80% (41/51) of the patients with a $p52^{LOF}$/$I\kappa B\delta^{GOF}$ variant neutralized IFN-α2 and/or IFN-ω, including two patients whose plasma neutralized only IFN-α2, four whose plasma neutralized only IFN-ω, and three whose plasma neutralized IFN-α2, IFN-ω and IFN-β (**Fig. S5E**). Overall, we found a strong association between *NFKB2* genotype ($p52^{LOF}$/$I\kappa B\delta^{GOF}$) and the presence of anti-type I IFN auto-Abs (**Fig. 5I**).

Neutralizing auto-Abs against type I IFNs in patients with NIK or RelB deficiency

We then investigated the presence of auto-Abs against type I IFNs in patients with other inborn errors of the alternative NF-κB pathway (AR complete NIK deficiency (*n*=2 from 2 kindreds [74] and unpublished); AR partial (*n*=4 from 2 kindreds) or complete (*n*=4 from 2 kindreds) RelB deficiency [74–76,101,102] and unpublished results), or the related TNFR (AR complete BAFFR deficiency (*n*=1 [101]); or XR partial CD40L deficiency (*n*=3 from 3 kindreds (unpublished)). No plasma from AR IKK-α deficient patients was available. Neutralizing auto-Abs against type I IFNs were detected in the two patients with complete AR NIK deficiency (both sampled after hematopoietic stem cell transplantation (HSCT)). In one of these patients, the detected auto-Abs neutralized IFN-α2 and IFN-ω at a concentration of 10 ng/mL, whereas, in the other, they neutralized IFN-α2 at 10 ng/mL and IFN-ω at 100 pg/mL (**Fig. 5F-H and S5J-L**). Auto-Abs neutralizing type I IFNs were also detected in patients with AR RelB

deficiency (*n*=5/8), including auto-Abs neutralizing IFN-α2 and IFN-ω at 10 ng/mL in two patients, and auto-Abs neutralizing IFN-α2 and/or IFN-ω at 100 pg/mL in three patients, all tested pre-HSCT (**Fig. 5F-H)**. By contrast, no neutralizing auto-Abs against type I IFNs were detected in patients with AR BAFFR or XL-CD40L deficiency, or in plasma from heterozygous relatives of patients with AR RelB deficiency (*n*=8) (**Fig. 5F-H and S5J-K**). Finally, we tested eight patients with AD NF-κB1 haploinsufficiency [103], and 29 additional patients with deleterious mutations of eight different canonical NF-κB pathway-related genes (*REL, RELA, IKBKB, IKBKG, NFKBIA, HOIL1, CARD11, MALT1*) [104]. All tested negative for neutralizing auto-Abs against type I IFNs (**Fig. S5M-N**). As HSCT procedures do not cure thymic stromal cells, we wondered whether neutralizing auto-Abs against type I IFNs could appear post-transplantation in the four patients without neutralizing auto-Abs before transplantation (AR cRel, *n*=1, and AR RelB, *n*=3). Neutralizing auto-Abs against type I IFNs were detected in two of the three patients with AR RelB deficiency (Q73Tfs*152 and Y397*) 6 and 2.5 years post-transplantation, whereas no such auto-Abs were detected in the patient with AR cRel deficiency for up to 13 months after HSCT (**Table SV**). They were also detected in the plasma from one patient with $p52^{LOF}$/$I\kappa B\delta^{GOF}$ variant post-transplant (P60). These results suggest that inborn errors of RelB, NIK, and NF-κB2 from the alternative NF-κB pathway underlie the development of neutralizing auto-Abs against type I IFNs, even after HSCT, whereas defects of the canonical NF-κB pathway do not. The alternative NF-κB pathway therefore appears to be essential to prevent the generation of auto-Abs against type I IFNs.

Narrow spectrum of auto-Abs in patients with inborn errors of the alternative NF-κB pathway

We then search for the presence of auto-Abs against other proteins using a panel of ~20,000 full-length human proteins (the Human Proteome Array, HuProt [105]) in patients with

inborn errors of the alternative NF-κB pathway with (*n*=15) or without (*n*=9) auto-Abs against type I IFNs ($p52^{LOF}$/$IκBδ^{GOF}$ (*n*=8 and 5), AR RelB (*n*=5 and 3) and AR NIK deficiency (*n*=2 with auto-Abs)), conditions not associated with these auto-Abs ($p52^{LOF}$/$IκBδ^{LOF}$ (*n*=1)) and healthy controls (*n*=22). The IFN-α subtypes and IFN-ω were among the autoantigens with the highest level of enrichment in the 13 patients with $p52^{LOF}$/$IκBδ^{GOF}$ tested relative to control plasma (log_2-fold change >1.8) (**Fig. 5J and S5O)**. This enrichment was specific to the IFN-α subtypes and IFN-ω, but not other type I IFNs (IFN-β, IFN-κ, or IFN-ε) or type III IFNs (**Fig. 5J**). In contrast to type I IFNs, most other enriched antigens in patients with $p52^{LOF}$/$IκBδ^{GOF}$, identified by HuProt, were not detected by multiplex bead assay (**Fig. S5A,O**). In addition, most of the auto-Abs directed against TSA or cytokines (including IL-17A, IL-17F, IL-22 and type III IFNs) previously reported in patients with APS-1 were not detected in plasma from patients with inborn errors of NF-κB2, NIK and RelB by HuProt or beads assay [105–107] (**Fig. S5Q-S**). No pituitary, skin, or other tissue-specific autoantigens were detected with this assay. This unbiased approach showed that auto-Abs neutralizing the 13 IFN-α subtypes and IFN-ω were the principal disease-associated auto-Abs in patients with inborn errors of the alternative NF-κB pathway.

Incomplete penetrance for the development of neutralizing auto-Abs against type I IFNs in patients carrying a $p52^{LOF}$/$IκBδ^{GOF}$ variant

For 10 of the 51 (20%) patients carrying $p52^{LOF}$/$IκBδ^{GOF}$ variants, no auto-Abs against IFN-α2 or IFN-ω at 100 pg/mL, or against IFN-β (at 10 ng/mL) were detected. Plasma from these patients did not neutralize any of the 13 IFN-α subtypes at 1 ng/mL, contrasting with the findings for other patients with $p52^{LOF}$/$IκBδ^{GOF}$ variants, AR RelB, or AR NIK deficiency, whose plasma neutralized IFN-α2 at a concentration of 10 ng/mL (**Fig. S5T**). None of them reported a severe or recurrent viral disease. Most of the patients who lacked neutralizing auto-

Abs against type I IFNs carried the A867V variant (*n*=7/10). They were from two countries (French, *n*=2 kindreds; Australian, *n*=2 kindreds) and were aged 11 to 51 years at testing. Three other patients carrying the same A867V variant had neutralizing auto-Abs against type I IFNs, with the auto-Abs from two of these patients neutralizing only IFN-ω at 100 pg/mL. Two additional unrelated patients carrying the recurrent R853* $p52^{LOF}$/$I\kappa B\delta^{GOF}$ variants (of the 18 patients with R853*), aged 17 and 61 years at testing, and one with the K855Sfs*7 variant (aged 47 years) did not have detectable neutralizing auto-Abs against type I IFNs. None of these patients received immunosuppressive treatment. Age or sex ratio was not statistically different in patients with a $p52^{LOF}$/$I\kappa B\delta^{GOF}$ variants with or without neutralizing auto-Abs to type I IFNs (ratio F/M 1.2 (23/18) and 1 (5/5), respectively). These findings suggest that the penetrance of type I IFN auto-Abs in $p52^{LOF}$/$I\kappa B\delta^{GOF}$ variant carriers is high (~80%), but not complete by the age of 61 years, especially in patients heterozygous for the A867V variant.

Susceptibility to severe viral diseases and COVID-19 is strongly associated with neutralizing auto-Abs against type I IFNs

We then hypothesized that the viral susceptibility reported in the patients with inborn errors of the alternative NF-κB pathway, including COVID-19, might be at least partly explained by the presence of neutralizing auto-Abs against type I IFNs. All the patients (*n*=29) with $p52^{LOF}$/$I\kappa B\delta^{GOF}$ variants and severe viral infections had neutralizing auto-Abs against type I IFNs, including all those with severe form of COVID-19, influenza, VZV, or recurrent HSV-1 disease (**Fig. 6A**). Furthermore, at least one episode of severe or recurrent viral disease was reported in 29 of the 41 (71%) $p52^{LOF}$/$I\kappa B\delta^{GOF}$ patients with neutralizing auto-Abs against type I IFNs, but not in those without such antibodies. Other than for viral, there were no strong clinical or immunological differences between $p52^{LOF}$/$I\kappa B\delta^{GOF}$ patients with and without neutralizing auto-Abs against type I IFNs (**Fig. 6B-C**). Two of the eight patients with AR RelB

deficiency developed a severe viral disease (varicella pneumonia *n*=2 and PML, *n*=1), and both had auto-Abs neutralizing IFN-α and IFN-ω (**Table SII**). All seven patients with $p52^{LOF}$/$IκBδ^{GOF}$ variants who developed COVID-19 pneumonia during the pre-vaccination period had neutralizing auto-Abs against both IFN-α2 and IFN-ω, and suffered critical (*n*=4), severe (*n*=2), or moderate (*n*=1) COVID-19 pneumonia (**Fig. 4H and Table SIV**). Plasma samples collected from two of these patients before SARS-CoV-2 infection neutralized IFN-α2 and IFN-ω at a concentration of 10 ng/mL. These samples were collected up to 16 years before COVID-19, demonstrating that these neutralizing auto-Abs were present before infection and were not, therefore, triggered by SARS-CoV-2 infection (**Fig. S6A)**. Two other patients were infected without developing pneumonia or requiring hospitalization: one 22-year-old patient with auto-Abs neutralizing only IFN-ω at the lowest dose of 100 pg/mL (P5, S762Afs*21/WT) and one seven-year-old patients with auto-Abs neutralizing both IFN-α2 and IFN-ω at a concentration of 10 ng/mL (P38, G869Vfs*18/WT) (**Fig. 6D-E).** The four infected patients without auto-Abs against type I IFNs received ambulatory care and did not develop pneumonia. They are heterozygous for neutral (A567 and V661M) variants or for the Q539* $p52^{GOF}$/$IκBδ^{LOF}$ variant (*n*=2) (**Fig. 6D-E and S6B).** In addition, 8 patients with a $p52^{LOF}$/$IκBδ^{GOF}$ variant and pre-existing auto-Abs against type I IFN encountered SARS-CoV-2 following vaccination (corresponding to the omicron period, from October 2021 to February 2022) (**Fig. S6C)**. They received anti-SARS-CoV-2 monoclonal antibodies infusion (*n*=4, with sotrovimab (*n*=3), tixagevimab/cilgavimab (*n*=1)) or remdesivir (*n*=1) and/or recombinant IFN-ß (*n*=2) in addition to their IVIg supplementation (*n*=8). All these patients reported asymptomatic to moderate (NIH scale 1-4) COVID-19 without pneumonia (**Fig. S6D and Table SIV)**. P3 who developed a critical COVID-19 during the first wave of SARS-CoV-2 pandemic developed an ambulatory disease (NIH score 2) after vaccination and therapeutic infusion of sotrovimab. The two patients with a $p52^{LOF}$/$IκBδ^{LOF}$ (P43 and P62) and three with

a $p52^{GOF}$/IκBδ^{LOF} variant (P39, P40 and P41) without auto-Abs against type I IFNs had ambulatory disease. Overall, these results indicate that auto-Abs against type I IFNs are clinically significant, underlying severe forms of COVID-19 pneumonia and, probably, other severe viral diseases, including influenza pneumonia and severe varicella.

IFN-β-dependent ISG induction *in vivo* in patients with auto-Abs against IFN-α and/or IFN-ω

Neutralizing auto-Abs against type I IFNs have been shown to impair the induction of ISGs in PBMCs and nasal mucosa during COVID-19 [6,40,41]. We monitored the disease caused by infection with the B.1.529 variant (omicron) of SARS-CoV2 in two patients (P27 and P28) carrying the R853Afs*30/WT $p52^{LOF}$/IκBδ^{GOF} variant. Prior to the infection, both patients had received three injections of Pfizer-BioNTech mRNA vaccine, one of whom (P28) subsequently developed detectable IgG directed against the spike protein (anti-S). Both patients received recombinant IFN-β (as their auto-Abs did not neutralize IFN-β at 10 ng/mL) and anti-spike mAb (sotrovimab in P27 and tixagevimab/cilgavimab in P28) within the first four days after symptom onset. Both experienced a mild form of COVID-19 without pneumonia or a need for oxygen supplementation. We performed longitudinal assessments, from day 2 to day 27, of SARS-CoV-2 viral load and type I IFN response, by determining IFN score (quantifying four type I/III IFN-dependent ISGs by NanoString [41]) on whole blood and nasal swabs, and by performing RNA-seq on whole blood (**Fig. S6E**). Within the first few days of symptoms, infection with the SARS-CoV2 B.1.529 variant led to a high IFN score for whole blood and the upper respiratory tract in individuals with mild COVID-19 without auto-Abs against type I IFN (**Fig. 6F-G** and [41]**)**. By contrast, P27, whose plasma neutralized high concentrations of all 13 IFN-α subtypes plus IFN-ω, and P28, whose plasma neutralized high concentrations of all 13 IFN-α subtypes but not IFN-ω, had negative or weakly positive blood and nasal IFN scores,

respectively, despite having a nasal SARS-CoV-2 viral load similar to that in the individuals without auto-Abs (**Fig. 6F, G and S6F**). The neutralizing activity of the auto-Abs of P27 against IFN-α2 and IFN-ω was also demonstrated in the respiratory tract (**Fig. S6G**). The injection of recombinant IFN-β from day 4 after the onset of the symptoms led to a high nasal and whole-blood IFN score, which increased to the levels observed in individuals with mild COVID-19 and no auto-Abs against type I IFNs (**Fig. 6G**). RNA-seq on whole-blood samples from the two patients showed an impaired induction of ISGs four days after symptom onset relative to two age-matched controls with mild COVID-19 but comparable SARS-CoV-2 viral loads (**Fig. 6H and S6I)**. Three to four days after IFN-β and anti-spike mAb infusion, the ISG module scores increased, with the expression of these genes becoming undetectable by day 13 post-treatment, once viral replication was controlled (**Fig. 6H and Fig. S6I)**. Thus, auto-Abs against IFN-α and IFN-ω can block type I IFN signaling *in vivo* in the blood and upper respiratory tract, and ISG induction can be rescued by exogenous IFN-β treatment, which might have contributed to the favorable clinical outcome in these patients.

Impaired mTEC development and AIRE thymic expression in patients with p52^{LOF}/IκBδ^{GOF} variants and AR RelB deficiency

In mice, mTEC development and AIRE expression are dependent on the alternative NF-κB pathway, via NIK and RelB [58–60]. Consequently, *Relb*- and *Nik*-deficient mice, and mice heterozygous for a p52^{LOF}/IκBδ^{GOF} variant display thymic hypoplasia with weak medullary thymic formation, impaired mTEC AIRE expression, and tolerance breakdown [60,108–111]. In human fetal thymuses, *NFKB2* and *RELB* transcripts are highly abundant in AIRE^{+} mTECs [112]. However, the impact on AIRE expression of deleterious variants affecting the alternative NK-κB pathway remains unknown. We hypothesized that patients with inborn errors of NIK, RelB, or NF-κB2 develop auto-Abs against type I IFNs due to insufficient AIRE expression in the

thymus. We first analyzed the thymic volume of patients with $p52^{LOF}$/IκBδ^{GOF} variants (*n*=9) aged 4 to 16 years, by comparing the CT-scans of these patients with those of age-matched controls with conditions unrelated to immunity. Patients with $p52^{LOF}$/IκBδ^{GOF} variants had a smaller global thymic volume than the controls (**Fig. 7A**). We then analyzed a thymic biopsy specimen from a patient of with complete AR RelB deficiency (mutation Y397*/ Y397*, P2 from ref [75], aged 1 year-old) and a patient with a $p52^{LOF}$/IκBδ^{GOF} variant (P850Sfs*36/WT from [113], aged 27). An immunofluorescence analysis of thymic tissue sections from the patient with AR RelB deficiency showed a small dysplastic organ with a disorganized cortico-medullary architecture, atrophic medulla area and undetectable AIRE expression (**Fig. 7B)**. In addition, keratin 10 (K10) positive post-AIRE mTECs and Hassall's corpuscles were not detected in the patient's tissues (**Fig. 7B**). An analysis of the thymus from the patient with the $p52^{LOF}$/IκBδ^{GOF} variant revealed the presence of disorganized keratin 5 (K5)- and keratin 8 (K8)-positive thymic epithelium, and a lack of AIRE-expressing and $K10^{+}$ post-AIRE cells relative to an aged-matched control thymus (**Fig. 7B**). Overall, these findings suggest that inborn errors of the human alternative NF-κB pathway underlie the production of auto-Abs against type I IFN due to the impairment of AIRE expression in mTECs.

Discussion

We found that human inborn errors of the alternative NF-κB pathway (AR NIK, AR RelB, or AD $p52^{LOF}$/IκBδ^{GOF} NF-κB2 disorders) define a new group of IEI underlying the development of auto-Abs neutralizing type I IFNs. The presence of these auto-Abs is remarkably consistent with the cellular phenotype found in the patients' fibroblasts, culminating in defective p52/RelB activity, which may be secondary to the impaired processing of p100 to generate p52 (either through processing-resistance for $p52^{LOF}$/IκBδ^{GOF} variants or an absence of NIK controlling this process), or to a quantitative or qualitative RelB deficiency

(either enhanced p100-IκBδ inhibitory capacity against RelB or a mutant RelB protein). In marked contrast, no anti-type I IFN neutralizing auto-Abs were found in patients heterozygous for p100-IκBδ LOF variants ($p52^{LOF}$/$IκBδ^{LOF}$ causing p100 and p52 haploinsufficiency, or $p52^{GOF}$/$IκBδ^{LOF}$ causing p52-GOF), or in patients with inborn errors of the canonical NF-κB pathway. This suggests that the correct processing of p100 is a key checkpoint for p52/RelB-dependent activation of the alternative NF-κB pathway required to prevent the development of auto-Abs against type I IFNs.

The alternative NF-κB pathway is essential for the control of AIRE expression in mouse mTECs [60,110,114,115]. Indeed, *Nik*-, *Ikka*-, or *Relb*-deficient mice, and mice heterozygous for a p100 processing-resistant variant present an absence of thymic AIRE expression [60,110,114,115]. Furthermore, deletion of the essential enhancer element (CNS1) containing two NF-κB binding sites upstream from the *Aire* coding locus phenocopies *Aire* deficiency [116,117]. In human thymuses, *NFKB2* and *RELB* are selectively upregulated in mature AIRE-expressing mTECs expressing [118,119]. We detected no AIRE expression in human thymuses lacking RelB or heterozygous for a $p52^{LOF}$/$IκBδ^{GOF}$ variant. These data suggest that, similar to the mouse model, the alternative human NF-κB pathway is essential for AIRE expression in the thymus through its role in ensuring correct p52/RelB activation. The remarkable association between the presence of auto-Abs against type I IFNs in patients with human inborn errors of NIK, RelB, and NF-κB2 and impaired p52/RelB activity suggests that intact p52/RelB activation is essential to prevent the breakdown of thymic central tolerance toward type I IFNs in humans. An absence of AIRE expression has also been reported in patients with germline (AR AIRE or RAG1/2 [44–46]) or somatic (mTEC neoplasia [120]) conditions and auto-Abs against type I IFNs, further suggesting that AIRE-dependent thymic central tolerance prevents the development of these auto-Abs [48–50]. Finally, as RANK-RANKL and CD40-CD40L have been shown to control AIRE expression in mice, evaluating the roles of these receptor-ligand crosstalk in mTEC

development and AIRE expression via the alternative NF-κB pathway in humans, is therefore, warranted.

It is surprising that AIRE deficiency in patients with inborn errors of the alternative NF-κB pathway led to a breakdown of central tolerance almost exclusively restricted to the 13 IFN-α subtypes and IFN-ω. This situation contrasts with the immunological and clinical manifestations of APS-1 patients, which only partially overlap those of patients with inborn errors of the NF-κB pathway, in whom adrenal insufficiency and hypoparathyroidism, two of the main endocrine features reported in APS-1 patients, or the associated auto-Abs targeting TSA, were not reported [49,50,106]. Ectodermal dysplasia, reported in patients with $p52^{LOF}$/$I\kappa B\delta^{GOF}$ variants or AR IKK-α deficiency, also seems to differ to some extent from that in APS-1 patients, with little or no enamel dysplasia, but a higher frequency of alopecia, nail dysplasia, and hypotrichosis [77,121]. These clinical and immunological differences may be explained by residual AIRE expression or function in a lineage-specific mTEC population. The clinical manifestations in patients with $p52^{LOF}$/$I\kappa B\delta^{GOF}$ variants also differ from those in patients with the other two forms of AD inborn errors of NF-κB2, probably due to the higher levels of IκBδ activity of the mutant. They define a unique syndrome including neutralizing auto-Abs against type I IFNs, central pituitary deficiency, and mild ectodermal dysplasia, expanding the previously proposed DAVID syndrome ("immunodeficiency with hypogammaglobulinemia, plus central pituitary deficiency") as "deficit of anterior pituitary, auto-Abs against type I IFNs, viral susceptibility, immunodeficiency, and ectodermal dysplasia" [79].

Our findings confirm the detrimental consequences of the presence of neutralizing auto-Abs against type I IFNs for viral susceptibility [6,7,37,53]. Despite their high risk of developing life-threatening COVID-19 pneumonia, unvaccinated patients with inborn errors of the alternative NF-κB pathway displayed a high but incomplete penetrance of hypoxemic COVID-19 pneumonia (6/9, 67%), as reported in patients with APS-1 or SLE (21 of 33, 64%, and 4 of 7,

57% respectively) [24,48–50,53]. Additional protective or risk factors may be required to influence the clinical outcome of COVID-19 in these patients. Thus, it may not be a fortuitous coincidence that the two patients who developed mild SARS-CoV-2 infection despite the presence of neutralizing auto-Abs were young (seven years old, with auto-Abs neutralizing IFN-α and IFN-ω at 10 ng/mL), or had auto-Abs neutralizing only low concentrations of a single type I IFN (only IFN-ω at 100 pg/mL), two factors associated with a lower risk of developing severe COVID-19 [6,8]. Auto-Abs against type I IFNs seem to results in viral susceptibility extending beyond COVID-19, with a higher risk of developing severe herpesvirus diseases, such as chickenpox, early-onset shingles, and non-mucosal HSV-1 infection, as observed in patients with APS-1 or SLE [24,57]. Consistently, $p52^{LOF}$/$I\kappa B\delta^{GOF}$ patients had a higher risk of severe forms of varicella and recurrent shingles. Furthermore, consistent with the presence of neutralizing auto-Abs against type I IFNs in almost 5% of individuals with critical influenza pneumonia studied [38], we found that 15% of the patients with $p52^{LOF}$/$I\kappa B\delta^{GOF}$ variants developed severe influenza pneumonia, mostly at a young age, suggesting that auto-Abs against type I IFNs may also underlie severe forms of influenza pneumonia in children and probably also in APS-1 patients.

Our findings also suggest that a reinforcement of prophylactic or therapeutic interventions can improve the clinical outcome of viral diseases in patients with auto-Abs against type I IFNs. Thus, favorable outcomes of SARS-CoV2 infection were observed in all patients with $p52^{LOF}$/$I\kappa B\delta^{GOF}$ variants with pre-existing auto-Abs against type I IFNs managed by vaccination, together with prophylactic or therapeutic neutralizing anti-SARS-CoV-2 monoclonal antibodies, IVIg supplementation, and/or recombinant IFN-β, as reported in patients with inborn errors of type I IFN immunity [122]. Yellow fever and other live-attenuated viral vaccines should be avoided [37,123]. Importantly, as these auto-Abs are probably caused by a thymic stromal defect, patients with inborn errors of the NF-κB pathway who undergo HSCT

may remain at high risk of severe viral disease due to the persistence of defective NF-κB signaling in their mutated host thymic epithelial cells. Collectively, these results suggest that the human alternative NF-κB pathway controls AIRE expression in mTECs and that human inborn errors of this pathway thereby underlie the development of neutralizing auto-Abs against type I IFNs and the resulting predisposition to viral infection. They also confirm that at least some individuals develop auto-Abs against type I IFNs because of an underlying IEI. The occurrence of critical COVID-19 in these patients is, therefore, due to an autoimmune phenocopy of IEI of type I IFN immunity. This finding suggests that other genetic etiologies remain to be discovered in the 0.3 to 2% of individuals under 65 years of age who carry such auto-Abs. The observation that genetic etiologies of *AIRE* in *cis* or in *trans* that disrupt central T-cell tolerance underlie these auto-Abs suggests that as yet undiscovered genetic etiologies may also affect this process. The genetic study of patients with auto-Abs against type I IFNs may reveal new molecular components in this or other processes. What triggers the rise in auto-Ab levels against type I IFNs after the age of 65 years is another related question potentially related to thymic involution.

Materials and methods

Subjects and samples

We enrolled 65 patients with rare variants of *NFKB2* though an international collaborative study. All the enrolled subjects provided written informed consent and were collected through protocols conforming to local ethics requirements. Ethics approval was obtained from the Comitato Etico Provinciale (NP 4000 – Studio CORONAlab). Clinical and immunological data were collected with a standardized questionnaire, together with at least one plasma sample. The plasma samples from the patient P1 were obtained through the NCT03394053, NCT03610802 protocols.

Outcome measures and definitions

The severity of COVID-19 was defined according to the NIH Ordinal Scale, as previously reported [7,124]. The NIH scale is an eight-point ordinal scale ranging from ambulatory (1 = no limitations of activities, 2 = limitation in activity), to hospitalized (3 = not requiring supplemental oxygen), moderate (4 = not requiring supplemental oxygen but requiring ongoing medical care (related to Covid-19 or to other medical conditions), severe (5 = requiring any supplemental oxygen) or critical (6 = requiring noninvasive ventilation or use of high-flow oxygen devices; 7 = receiving invasive mechanical ventilation or extracorporeal membrane oxygenation (ECMO); and 8 = death).

Detection of anti-cytokine autoantibodies

Gyros

Cytokines, recombinant human (rh)IFN-α2 (Milteny Biotec, ref. number 130-108-984) or rhIFN-ω (Merck, ref. number SRP3061) were first biotinylated with EZ-Link Sulfo-NHS-LC-

Biotin (Thermo Fisher Scientific, cat. number A39257), according to the manufacturer's instructions, with a biotin-to-protein molar ratio of 1:12. The detection reagent contained a secondary antibody (Alexa Fluor 647 goat anti-human IgG (Thermo Fisher Scientific, ref. number A21445) diluted in Rexip F (Gyros Protein Technologies, ref. number P0004825; 1/500 dilution of the 2 mg/mL stock to yield a final concentration of 4 µg/mL). PBS-T 0.01% buffer and Gyros Wash buffer (Gyros Protein Technologies, ref. number P0020087) were prepared according to the manufacturer's instructions. Plasma or serum samples were then diluted 1/100 in PBS-T 0.01% and tested with Bioaffy 1000 CD (Gyros Protein Technologies, ref. number P0004253), and Gyrolab X-Pand (Gyros Protein Technologies, ref. number P0020520). Cleaning cycles were performed in 20% ethanol.

Plasmids and mutagenesis

The NFKB2/p100, RELB and MAP3K14 plasmids were obtained from Origen with a C-terminal DDK tag. The κB reporter construct (κB-luc), pGL4.32[luc2P/NF-κB-RE/Hygro] and pRL-SV40 vectors were obtained from Li et al. [103]. Site-directed mutagenesis was performed as previously described [103].

Cell culture and transfection

HEK293T cells (American Type Culture Collection) were maintained in DMEM (Gibco) supplemented with 10% FBS (Gibco). Transient transfection was performed with X-tremeGENE™ 9 DNA Transfection Reagent (Merck), in accordance with the manufacturer's instructions.

Functional evaluation of *NFKB2* variants

Luciferase reporter assays

The luciferase reporter assay was performed as previously described [103]. WT HEK293T cells were transfected with a reporter plasmid (96-well plate), the pRL-SV40 vector (10 ng/well), WT *MAP3K15*, WT *RELB*, and a WT or mutant p100 in the presence of X-tremeGENE™ 9 DNA Transfection Reagent (Merck). After incubation for 24 to 48 h, cells were harvested, and luciferase activity was measured with the Dual-Glo Luciferase Assay System (Promega). We considered a deleterious variant to be LOF if its luciferase activity was equivalent to that of the EV, hypomorphic if this activity was more than half that of the WT allele and gain-of-function (GOF) if this activity was less than half that of the WT.

Western blot

Whole-cell lysates from HEK293T, MDDC, T-cell blasts, primary or SV-40-transformed fibroblasts were prepared in RIPA buffer (50 mM Tris-HCl, pH 7.5, 150 mM NaCl, 1% Nonidet P40, 0.5% sodium deoxycholate, and 0.1% SDS) supplemented with Complete Protease Inhibitor Cocktail (Roche). Proteins were separated by electrophoresis in 10% PROTEAN TGX Precast Protein Gels (Bio-Rad), and transferred onto Immobilon-P polyvinylidene fluoride membrane (Millipore). All blots were incubated overnight with primary antibodies and developed with the Pierce ECL Western Blotting Substrate (Thermo Fisher Scientific). The antibodies used in this study included antibodies against p100/p52 (4882; Cell Signaling Technology), p105/p50 (N terminus; 3035; Cell Signaling Technology), p65 (sc-372; Santa Cruz Biotechnology), RelB (sc-48366; Santa Cruz Biotechnology), c-Rel (sc-6955; Santa Cruz Biotechnology), and the following secondary antibodies: Amersham ECL mouse IgG, HRP-linked whole antibody (from sheep; NA931; GE Healthcare Life Sciences) and Amersham ECL rabbit IgG, HRP-linked whole antibody (from donkey; NA934; GE Healthcare Life Sciences).

Confocal microscopy

HeLa cells were plated on chambered coverslips (#80826, iBidi) and were left untransfected or were transiently transfected with the a plasmid encoding p100, RelB and/or NIK and/or an empty pCMV6 vector for 48 hours. Primary or SV-40 fibroblasts were plated on chamber coverslips and left stimulated or not with Lt 100 ng/mL for 48 hours. The cells were fixed in 4% formaldehyde in phosphate-buffered saline (PBS), pH 7.4. Cells were incubated overnight at 4°C with anti-p100/p52 (4882; Cell Signaling Technology), or RelB (sc-48366; Santa Cruz Biotechnology) primary antibodies. The cells were washed three times with PBS 1X and stained by incubation with secondary antibodies for 1 h at room temperature (goat anti-mouse IgG Alexa Fluor 488 (#A-11029); goat anti-rabbit IgG Alexa Fluor 633 (#A-11037)) and before mounting in Prolong-gold and visualization by confocal microscopy (×63 or x40 oil immersion lens).

Functional evaluation of anti-cytokine autoantibodies

Luciferase reporter assays

The blocking activity of anti-IFN-α2 and anti-IFN-ω auto-Abs was determined with a reporter luciferase assay. Briefly, HEK293T cells were transfected with a plasmid containing the firefly luciferase gene under the control of the human *ISRE* promoter in the pGL4.45 backbone, and a plasmid constitutively expressing *Renilla* luciferase for normalization (pRL-SV40). Cells were transfected in the presence of the X-tremeGene 9 transfection reagent (Sigma Aldrich, ref. number 6365779001) for 24 hours. Cells in Dulbecco's modified Eagle medium (DMEM, Thermo Fisher Scientific) supplemented with 2% fetal calf serum (FCS) and 10% healthy control or patient serum/plasma were either left unstimulated or were stimulated with IFN-α2 (Milteny Biotec, ref. number 130-108-984) or IFN-ω (Merck, ref. number SRP3061) at 10 ng/mL or 100 pg/mL, or with IFN-β (Miltenyi Biotech, ref. number: 130-107-888) at 10 ng/mL, or 1 ng/mL, or with one of the 13 IFN-α subtypes for 16 hours at 37°C. Each sample was tested

once for each cytokine and dose. Finally, cells were lysed for 20 minutes at room temperature and luciferase levels were measured with the Dual-Luciferase® Reporter 1000 assay system (Promega, ref. number E1980), according to the manufacturer's protocol. Luminescence intensity was measured with a VICTOR X Multilabel Plate Reader (PerkinElmer Life Sciences, USA). Firefly luciferase activity values were normalized against *Renilla* luciferase activity values. These values were then normalized against the plasma used in non-stimulated condition. Samples were considered to be neutralizing if the indication of the luciferase activity, normalized the non-stimulated constitution, was below 5.

Protein microarray

Protein microarrays (HuProt™ from CDI laboratories) were incubated in 5 ml blocking buffer, consisting of phosphate-buffered saline (PBS) supplemented with 2% bovine serum albumin and 0.05 % Tween 20, for 90 min. The arrays were then incubated overnight in 5 mL of blocking buffer per array with serum from a blood donor or patient diluted 1:2000. Each array was then washed five times, for five minutes each, with 5 mL PBST (PBS + 0.05 % Tween 20). Alexa Fluor 647 goat anti-human IgG (Thermo Fisher Scientific Cat# A-21445, RRID:AB_2535862) and Dylight® 550 goat anti-GST (Columbia Biosciences Corporation Cat# D9-1310) were diluted in blocking buffer (1:2000 and 1:10 000 respectively) and each array was incubated in 5 mL of the resulting mixture for 90 minutes. Five washes were then conducted as previously described. Incubations and washes were performed on an orbital shaker, with aluminum foil to block out the light during the steps following the addition of fluorescent antibodies. Finally, each array was immersed in deionized water three times and centrifuged for approximately 30 seconds for drying. The arrays were scanned later the same day with an Innoscan 1100AL Fluorescence scanner (Innopsys) operating Mapix software and the resulting images were analyzed with Jan18-22_Huprot_v4.0_Gal and either GenePix Pro

5.1.0.19 or GenePix Pro 7. Data were normalized to compensate for signal intensity variation between experiments. Data from additional healthy controls from separate protein array experiments were included as described below.Signal intensities were extracted from the scanned image with GenePix Pro 5.1.0.19 or GenePix Pro 7, with subtraction of the local background:

$$Signal_{Protein} =$$

$$\text{median}(Spot\ Pixel\ Intensity_{635}) - (Background\ Pixel\ Intensity_{635})$$

Each protein was printed as duplicate spots. The resulting signal for one sample is defined as:

$$Signal_{Sample} = \max \begin{cases} Signal_{Protein}\ duplicate\ 1 \\ Signal_{Protein}\ duplicate\ 2 \end{cases}$$

We checked for spurious results, by screening duplicates for large differences:

$$Maximum\ duplicate\ discordance\ _{Protein} =$$

$$\max \begin{cases} Signal_{Sample\ 1}\ duplicate\ 1 - Signal_{Sample\ 1}\ duplicate\ 2 \\ Signal_{Sample\ 2}\ duplicate\ 1 - Signal_{Sample\ 2}\ duplicate\ 2 \\ \dots \\ Signal_{Sample\ n}\ duplicate\ 1 - Signal_{Sample\ n}\ duplicate\ 2 \end{cases}$$

The mean signal intensity was calculated across case and control samples separately:

$$\mu_{SignalCases} = \sum_{i=1}^{n_{Cases}} Signal_{Sample}\ in\ cases$$

$$\mu_{SignalControls} = \sum_{i=1}^{n_{Controls}} Signal_{Sample}\ in\ controls$$

The difference between cases and controls was estimated as follows:

$$\log_2(\text{Fold change}) = \log_2 \frac{\mu_{SignalCases}}{\mu_{SignalControls}}$$

where μ is the mean signal.

Detection of auto-Abs against cytokines by multiplex beads-array

The method for detection of human IgG in serum using magnetic beads have been previously described [doi: 10.1007/s10875-021-01151-y] with the few exceptions that are specified in the brief description that follows. AnteoTech Activation Kit for Multiplex Microspheres (Cat# A-LMPAKMM-10) was applied in accordance with the protocol of the manufacturer, including the optional blocking, to couple Magnetic beads (MagPlex®, Luminex Corp.) to the following commercial proteins (using 1,5 * 10^6 beads and 3 micrograms of each respective protein – one micrograms less in the cases of DSG1 and OR4K13) : CYP21A2, ADH7, ALOX15, alpha 2 macroglobulin like, CASK, Desmocolin 2, DPYSL5, Desmoglein-3, KLHL31, KLHL40, KLHL41, Laminin gamma 1, LRRC32, PADI3, PKP1, PNMA5, RARS2, SERPINB3, SERPINB4, SFN, TFAP2B, TGM1, TGM3, TMPRSS11D, TROVE2, UGP2, UNC45B, ZNF300, IFNA2, IFNA1, IFNA7, IFNA14, IFNB1, IFNE, IFNW1, IL23, Antithrombin III, Factor V, Protein S, SARS-CoV-2 Nucleocapsid, SARS-CoV-2 S protein spike, SARS-CoV-2 S protein RBD, Desmoglein-1, IFNA5, IL1F6, Prothrombin, IL22, OR4K13, IFNA6, IL1RN, JUP, IL28a, IFNA10, IFNA8, SPCS2, IL28b, IFNA16, IFNG, ADH5, IL29, IFNA17, IFNK, anti-IgG, IL6, IFNA2, IFNL4, EBNA1, ADAMS13, IFNA21, IL17A, RBM38, CXCL4, IFNA4, IL17F, ATP4A, ISG15, IFNG, IFNW1, IL17F, IL22, ApoH GM-CSF, MUSK, TNF-alpha, Protein C, IL12. Samples were diluted 1:25 in PBS prior to 1:10 dilution in Assay buffer (0,05 PBST, 3% BSA, 5% Milk). Stock of magnetic beads were sonicated for 1 minute before distribution and then mixed with storage buffer from the activation kit. Diluted samples were centrifuged 1 min at 3000 rpm, and 45 microliters of each was subsequently incubated 2 hours with 5 microliters from the stock bead solution on a shaker at 650 rpm protected from light at room temperature. Beads were then washed (3xPBS-T 0.05%) after a 2000 rpm pulse and resuspended in 50 microliters of 0.2% PFA per well followed by careful vortex. After 10 minutes of incubation at room temperature and 2000 rpm pulse, beads were washed (3xPBS-T

0.05%) and incubated with secondary antibody (Invitrogen, H10104 lot#2384336) 30 minutes at room temperature. Finally, the above washing routine was repeated and beads were dispensed in PBS-T 0.05% before the analysis.

Microbiological investigations

The normalized viral load was determined for each sample, by determining the viral load for 1 million cells in the nasopharyngeal swabs by RT-qPCR with the SARS-CoV-2 R-gene kit (bioMérieux, Marcy l'Etoile, France). Briefly, nucleic acids were extracted from 0.2 mL NPS with NUCLISENS easyMAG and amplification was performed with a Bio-rad CFX96 instrument. Viral load was determined with four internally developed quantification standards (QS) targeting the SARS-CoV-2 N gene: QS1 to QS4, at $1x10^5$, $1x10^4$, $1x10^3$, and $1x10^2$ copies/µL, respectively, of a SARS-CoV-2 DNA standard. These QS were controlled and quantified with a Nanodrop spectrophotometer (Thermo Fisher Scientific, MA, USA) and Applied Biosystems QuantStudio 3D Digital PCR. In parallel, NPS were tested with the CELL Control R-GENE kit (amplification of the HPRT1 housekeeping gene, bioMérieux), which contains two quantification standards, QS1 and QS2, at 10^4 copies/µL (50,000 cells/PCR in our conditions) and 10^3 copies/µL (5,000 cells/PCR) of DNA standard, respectively, to normalize the viral load according to the amount of sample. Normalized viral load was calculated as [Log_{10} cp/10^6 cells] $= Log10\,[\frac{Number\ of\ SARS-CoV-2\ copies}{Number\ of\ cells} \times 10^6\ cells]$. Potential co-infections were investigated with the BioFire Respiratory 2.1 plus Panel (RP2.1plus) detecting 23 respiratory pathogens, including SARS-CoV-2 (bioMérieux, Lyon, France).

Blood and nasal IFN score by Nanostring

Total RNA from whole blood was extracted from blood in PAXgene tubes with the Maxwell16 LEV simplyRNA Blood kit (Promega), according to the manufacturer's instructions. Blood IFN score was determined with Nanostring technology, as previously described [125]. For nasal IFN score, we tested 100 µL nasal pharyngeal swab samples with the IFN prototype as previously described [41]. The first prototype of the IFN pouch encompasses four ISGs (IFNα-inducible protein 27, IFI44L, IFN-induced protein with tetratricopeptide repeats 1, radical S-adenosyl methionine domain containing 2) and three housekeeping genes (hypoxanthine phosphoribosyltransferase 1, peptidylprolyl isomerase B, and 2,4-dienoyl-CoA reductase 1) for signal normalization. In brief, the pouches were hydrated with the hydration solution supplied with the kit. The PAXgene blood or nasal pharyngeal swab samples were mixed with 800 µL of the sample buffer provided with the kit and injected directly into the pouch and run on FilmArray 2.0 and FilmArray Torch instruments (BioFire Diagnostics). Results were delivered within one hour. Using a research version of the instrument, real-time quantification cycle values and post-amplification melt peaks were determined for each assay. The normalized expression values for each assay were then calculated with the internal reference genes. The nasal pharyngeal ISG score was calculated by the same method as for PAXgene samples, as previously described (Pescarmona et al., 2019).

Cytometry by Time of Flight

Whole-blood mass cytometry was performed with two different panels. The panels used were custom-produced, and their contents are shown in **Table SVI.** Labeled cells were frozen at -80°C after overnight dead-cell staining, and acquisition was performed on a Helios machine (Fluidigm). All the samples were processed within 48 hours of sampling. Data analysis was performed with OMIQ software.

Immunostaining of human thymic sections

Tissue was fixed in 4% paraformaldehyde (Thermo Fisher Scientific), washed with PBS, and embedded in paraffin. Antigen retrieval was performed on rehydrated tissue, by boiling sections in Citra antigen retrieval solution (Biogenex). Sections were blocked by incubation for 30 min at room temperature in CAS-Block (Thermo Fisher Scientific) plus 0.2% Triton X-100 (Sigma-Aldrich), followed by incubation overnight at 4°C with primary antibodies. Sections were washed with PBS-Tween 0.1% and stained with a biotinylated secondary antibody for 1 h at room temperature for AIRE visualization. When necessary, secondary antibody staining was performed at room temperature for 1 h. Sections were washed with PBS-Tween 0.1% and mounted in ProLong Diamond Antifade mounting solution (Thermo Fisher Scientific). Images were acquired on an Apotome microscope (Zeiss). The antibodies used were KRT8-Alexa647, Rb (clone EP1628Y) – Abcam ab192468, 1:300; KRT5 Alexa488, Rb (clone EP1601Y) – Abcam ab193894, 1:300; AIRE, rat – eBioscience 14-9534-82, 1:50 and pan-ketatin, Rb – Abcam ab9377, 1 :200.

RNA extraction and sequencing and analysis

Total RNA was isolated from whole blood as previously described [125]. RNA-sequencing was performed with Illumina Novaseq S2 instruments (2x100) and a read depth of 70 M. Single samples were sequenced across two lanes, and the resulting FASTQ files were merged by sample. All FASTQ files passed quality control and the sequences were aligned with the GRCh38 reference genome, with STAR (2.6.1d). BAM files were converted to a raw count expression matrix with featurecount. Raw count data were normalized with DEseq2. The ensemble IDs targeting multiple genes were collapsed (average), and a final data matrix gene was generated for single gene set enrichment analysis with the BloodGen3Module gene set [PMID: 34282143, 33624743]. Statistical analysis were conducted with a predefined gene set.

Specifically, we employed a fixed repertoire of 382 blood transcriptional modules that were thoroughly annotated and characterized functionally, as described in detail in recent publications [PMID: 34282143, 33624743]. Briefly, this repertoire of transcriptional modules ("BloodGen3") was identified based on co-expression, as measured in a collection of reference blood transcriptome datasets encompassing 16 pathological or physiological states and 985 individual transcriptome profiles. Sets of co-expressed transcripts were derived from a large weighted coclustering network in which edges represented the number of times a pair of genes coclustered in the 16 reference datasets (with a weight of 1 to 16). We calculated an interferon module enrichment score for individual samples, by performing single-sample gene set enrichment analysis (ssGSEA) (GSVA package (60)), with the six interferon-response modules of the BloodGen3 module aggregate A28 as input. The enrichment scores of individual samples were used for heatmap visualization.

Thymus CT scan

We performed a retrospective assessment of the thymus for those patients for whom a chest CT-scan was available. For patients with several scans, we selected the first scan or the scan on which the thymus was largest. Most of the patients' scans were performed without contrast injection, and the thymic margins were assessed by multiplanar reconstruction. The thymus was measured in three planes: thickness and width in the axial plane through the aortic arch, greatest height in a coronal or sagittal oblique plane. We established a control group matched for age (+/- one month) and sex. Three controls were selected per patient. The control group was randomly selected from scans performed at our center for polytrauma, excluding severe head trauma with coma or neurologic disorders and thoracic trauma (so as not to alter mediastinal anatomic reports).

Statistical methods

Statistical analyses were performed with GraphPad Prism 9.3.1. Mann-Whitney was performed. In the relevant figures, n.s. indicates not significant, ***$p < 0.001$; **$p < 0.01$; and *$p < 0.05$.

References

1. Puel, A., Bastard, P., Bustamante, J. & Casanova, J.-L. Human autoantibodies underlying infectious diseases. *J. Exp. Med.* **219**, e20211387 (2022).
2. Shiono, H. *et al.* Spontaneous production of anti-IFN-α and anti-IL-12 autoantibodies by thymoma cells from myasthenia gravis patients suggests autoimmunization in the tumor. *Int. Immunol.* **15**, 903–913 (2003).
3. Meager, A., Vincent, A., Newsom-Davis, J. & Willcox, N. Spontaneous neutralising antibodies to interferon-a and interleukin-12 in thymoma-associated autoimmune disease. *The Lancet* **350**, 1596–1597 (1997).
4. Panem, S., Check, I. J., Henriksen, D. & Vilcek, J. Antibodies to alpha-interferon in a patient with systemic lupus erythematosus. *J. Immunol. Baltim. Md 1950* **129**, 1–3 (1982).
5. Pozzetto, B., Mogensen, K. E., Tovey, M. G. & Gresser, I. Characteristics of Autoantibodies to Human Interferon in a Patient with Varicella-Zoster Disease. *J. Infect. Dis.* **150**, 707–713 (1984).
6. Bastard, P. *et al.* Autoantibodies neutralizing type I IFNs are present in ~4% of uninfected individuals over 70 years old and account for ~20% of COVID-19 deaths. *Sci. Immunol.* (2021) doi:10.1126/sciimmunol.abl4340.
7. Bastard, P. *et al.* Auto-antibodies against type I IFNs in patients with life-threatening COVID-19. *Science* (2020) doi:10.1126/science.abd4585.
8. Zhang, Q., Bastard, P., COVID Human Genetic Effort, Cobat, A. & Casanova, J.-L. Human genetic and immunological determinants of critical COVID-19 pneumonia. *Nature* **603**, 587–598 (2022).
9. Manry, J. *et al.* The risk of COVID-19 death is much greater and age dependent with type I IFN autoantibodies. *Proc. Natl. Acad. Sci.* **119**, e2200413119 (2022).
10. Schidlowski, L. *et al.* Diagnosis of APS-1 in Two Siblings Following Life-Threatening COVID-19 Pneumonia. *J. Clin. Immunol.* (2022) doi:10.1007/s10875-022-01245-1.
11. Abers, M. S. *et al.* Neutralizing type-I interferon autoantibodies are associated with delayed viral clearance and intensive care unit admission in patients with COVID-19. *Immunol. Cell Biol.* **99**, 917–921 (2021).
12. Acosta-Ampudia, Y. *et al.* COVID-19 convalescent plasma composition and immunological effects in severe patients. *J. Autoimmun.* **118**, 102598 (2021).
13. Akbil, B. *et al.* Early and rapid identification of COVID-19 patients with neutralizing type I-interferon auto-antibodies by an easily implementable algorithm. 2021.11.12.21266249 Preprint at https://doi.org/10.1101/2021.11.12.21266249 (2021).
14. Busnadiego, I. *et al.* Critically ill COVID-19 patients with neutralizing autoantibodies against type I interferons have increased risk of herpesvirus disease. *PLOS Biol.* **20**, e3001709 (2022).
15. Carapito, R. *et al.* Identification of driver genes for critical forms of COVID-19 in a deeply phenotyped young patient cohort. *Sci. Transl. Med.* **14**, eabj7521 (2021).
16. Chang, S. E. *et al.* New-onset IgG autoantibodies in hospitalized patients with COVID-19. *Nat. Commun.* **12**, 5417 (2021).
17. Chauvineau-Grenier, A. *et al.* Autoantibodies Neutralizing Type I Interferons in 20% of COVID-19 Deaths in a French Hospital. *J. Clin. Immunol.* **42**, 459–470 (2022).
18. Eto, S. *et al.* Neutralizing Type I Interferon Autoantibodies in Japanese Patients With Severe COVID-19. *Res. Sq.* rs.3.rs-1430985 (2022) doi:10.21203/rs.3.rs-1430985/v1.
19. Frasca, F. *et al.* Anti-IFN-α/-ω neutralizing antibodies from COVID-19 patients correlate with downregulation of IFN response and laboratory biomarkers of disease severity. *Eur. J. Immunol.* **n/a**, (2022).

20. Goncalves, D. *et al.* Antibodies against type I interferon: detection and association with severe clinical outcome in COVID-19 patients. *Clin. Transl. Immunol.* **10**, (2021).
21. Koning, R. *et al.* Autoantibodies against type I interferons are associated with multi-organ failure in COVID-19 patients. *Intensive Care Med.* **47**, 704–706 (2021).
22. Lamacchia, G. *et al.* Clinical and Immunological Features of SARS-CoV-2 Breakthrough Infections in Vaccinated Individuals Requiring Hospitalization. *J. Clin. Immunol.* (2022) doi:10.1007/s10875-022-01325-2.
23. Lemarquis, A. *et al.* Severe COVID-19 in an APS1 patient with interferon autoantibodies treated with plasmapheresis. *J. Allergy Clin. Immunol.* **148**, 96–98 (2021).
24. Mathian, A. *et al.* Lower disease activity but higher risk of severe COVID-19 and herpes zoster in patients with systemic lupus erythematosus with pre-existing autoantibodies neutralising IFN-α. *Ann. Rheum. Dis.* (2022) doi:10.1136/ard-2022-222549.
25. Meisel, C. *et al.* Mild COVID-19 despite autoantibodies against type I IFNs in autoimmune polyendocrine syndrome type 1. *J. Clin. Invest.* **131**, (2021).
26. Petrikov, S. S. *et al.* Anti-interferon alpha autoantibodies and their significance in COVID-19. *Russ. J. Infect. Immun.* **12**, 279–287 (2022).
27. Raadsen, M. P. *et al.* Interferon-α2 Auto-antibodies in Convalescent Plasma Therapy for COVID-19. *J. Clin. Immunol.* **42**, 232–239 (2022).
28. Savvateeva, E. *et al.* Microarray-Based Detection of Antibodies against SARS-CoV-2 Proteins, Common Respiratory Viruses and Type I Interferons. *Viruses* **13**, 2553 (2021).
29. Simula, E. R. *et al.* Increased Presence of Antibodies against Type I Interferons and Human Endogenous Retrovirus W in Intensive Care Unit COVID-19 Patients. *Microbiol. Spectr.* **0**, e01280-22 (2022).
30. Solanich, X. *et al.* Pre-existing Autoantibodies Neutralizing High Concentrations of Type I Interferons in Almost 10% of COVID-19 Patients Admitted to Intensive Care in Barcelona. *J. Clin. Immunol.* **41**, 1733–1744 (2021).
31. Soltani-Zangbar, M. S. *et al.* A comprehensive evaluation of the immune system response and type-I Interferon signaling pathway in hospitalized COVID-19 patients. *Cell Commun. Signal.* **20**, 106 (2022).
32. Troya, J. *et al.* Neutralizing Autoantibodies to Type I IFNs in >10% of Patients with Severe COVID-19 Pneumonia Hospitalized in Madrid, Spain. *J. Clin. Immunol.* **41**, 914–922 (2021).
33. Vazquez, S. E. *et al.* Neutralizing Autoantibodies to Type I Interferons in COVID-19 Convalescent Donor Plasma. *J. Clin. Immunol.* **41**, 1169–1171 (2021).
34. Wang, E. Y. *et al.* Diverse functional autoantibodies in patients with COVID-19. *Nature* **595**, 283–288 (2021).
35. Ziegler, C. G. K. *et al.* Impaired local intrinsic immunity to SARS-CoV-2 infection in severe COVID-19. *Cell* **184**, 4713-4733.e22 (2021).
36. Credle, J. J. *et al.* Unbiased discovery of autoantibodies associated with severe COVID-19 via genome-scale self-assembled DNA-barcoded protein libraries. *Nat. Biomed. Eng.* **6**, 992–1003 (2022).
37. Bastard, P. *et al.* Auto-antibodies to type I IFNs can underlie adverse reactions to yellow fever live attenuated vaccine. *J. Exp. Med.* **218**, e20202486 (2021).
38. Zhang, Q. *et al.* Autoantibodies against type I IFNs in patients with critical influenza pneumonia. *J. Exp. Med.* **219**, e20220514 (2022).
39. Walter, J. E. *et al.* Broad-spectrum antibodies against self-antigens and cytokines in RAG deficiency. *J. Clin. Invest.* **125**, 4135–4148 (2015).
40. van der Wijst, M. G. P. *et al.* Type I interferon autoantibodies are associated with systemic immune alterations in patients with COVID-19. *Sci. Transl. Med.* **13**, eabh2624 (2021).

41. Lopez, J. *et al.* Early nasal type I IFN immunity against SARS-CoV-2 is compromised in patients with autoantibodies against type I IFNs. *J. Exp. Med.* **218**, e20211211 (2021).
42. Cheng, M. & Anderson, M. S. Thymic tolerance as a key brake on autoimmunity. *Nat. Immunol.* **19**, 659–664 (2018).
43. Anderson, M. S. *et al.* Projection of an immunological self shadow within the thymus by the aire protein. *Science* **298**, 1395–1401 (2002).
44. Cavadini, P. *et al.* AIRE deficiency in thymus of 2 patients with Omenn syndrome. *J. Clin. Invest.* **115**, 728–732 (2005).
45. Poliani, P. L. *et al.* Early defects in human T-cell development severely affect distribution and maturation of thymic stromal cells: possible implications for the pathophysiology of Omenn syndrome. *Blood* **114**, 105–108 (2009).
46. De Ravin, S. S. *et al.* Hypomorphic Rag mutations can cause destructive midline granulomatous disease. *Blood* **116**, 1263–1271 (2010).
47. Puel, A. Human inborn errors of immunity underlying superficial or invasive candidiasis. *Hum. Genet.* **139**, 1011–1022 (2020).
48. Kisand, K. *et al.* Chronic mucocutaneous candidiasis in APECED or thymoma patients correlates with autoimmunity to Th17-associated cytokines. *J. Exp. Med.* **207**, 299–308 (2010).
49. Puel, A. *et al.* Autoantibodies against IL-17A, IL-17F, and IL-22 in patients with chronic mucocutaneous candidiasis and autoimmune polyendocrine syndrome type I. *J. Exp. Med.* **207**, 291–297 (2010).
50. Meyer, S. *et al.* AIRE-Deficient Patients Harbor Unique High-Affinity Disease-Ameliorating Autoantibodies. *Cell* **166**, 582–595 (2016).
51. Meager, A. *et al.* Anti-interferon autoantibodies in autoimmune polyendocrinopathy syndrome type 1. *PLoS Med.* **3**, e289 (2006).
52. Levin, M. Anti-Interferon Auto-Antibodies in Autoimmune Polyendocrinopathy Syndrome Type 1. *PLOS Med.* **3**, e292 (2006).
53. Bastard, P. *et al.* Preexisting autoantibodies to type I IFNs underlie critical COVID-19 pneumonia in patients with APS-1. *J. Exp. Med.* **218**, e20210554 (2021).
54. Beccuti, G. *et al.* A COVID-19 pneumonia case report of autoimmune polyendocrine syndrome type 1 in Lombardy, Italy: letter to the editor. *J. Endocrinol. Invest.* **43**, 1175–1177 (2020).
55. Carpino, A. *et al.* Autoimmune Polyendocrinopathy–Candidiasis–Ectodermal Dystrophy in Two Siblings: Same Mutations but Very Different Phenotypes. *Genes* **12**, 169 (2021).
56. Ferré, E. M. N. *et al.* SARS-CoV-2 Spike Protein-Directed Monoclonal Antibodies May Ameliorate COVID-19 Complications in APECED Patients. *Front. Immunol.* **12**, 720205 (2021).
57. Hetemäki, I. *et al.* Patients with autoimmune polyendocrine syndrome type 1 have an increased susceptibility to severe herpesvirus infections. *Clin. Immunol.* **231**, 108851 (2021).
58. Rossi, S. W. *et al.* RANK signals from CD4+3− inducer cells regulate development of Aire-expressing epithelial cells in the thymic medulla. *J. Exp. Med.* **204**, 1267–1272 (2007).
59. White, A. J. *et al.* Sequential phases in the development of Aire-expressing medullary thymic epithelial cells involve distinct cellular input. *Eur. J. Immunol.* **38**, 942–947 (2008).
60. Akiyama, T. *et al.* The Tumor Necrosis Factor Family Receptors RANK and CD40 Cooperatively Establish the Thymic Medullary Microenvironment and Self-Tolerance. *Immunity* **29**, 423–437 (2008).
61. Khan, I. S. *et al.* Enhancement of an anti-tumor immune response by transient blockade of central T cell tolerance. *J. Exp. Med.* **211**, 761–768 (2014).
62. Sun, S.-C. The non-canonical NF-κB pathway in immunity and inflammation. *Nat.*

Rev. Immunol. **17**, 545–558 (2017).
63. Chang, C.-C., Zhang, J., Lombardi, L., Neri, A. & Dalla-Favera, R. Rearranged NFKB-2 Genes in Lymphoid Neoplasms Code for Constitutively Active Nuclear Transactivators. *MOL CELL BIOL* **15**, 8 (1995).
64. Chang, C. C., Zhang, J., Lombardi, L., Neri, A. & Dalla-Favera, R. Mechanism of expression and role in transcriptional control of the proto-oncogene NFKB-2/LYT-10. *Oncogene* **9**, 923–933 (1994).
65. Ghosh, G. & Wang, V. Y.-F. Origin of the Functional Distinctiveness of NF-κB/p52. *Front. Cell Dev. Biol.* **9**, (2021).
66. Basak, S. *et al.* A Fourth IκB Protein within the NF-κB Signaling Module. *Cell* **128**, 369–381 (2007).
67. Fusco, A. J. *et al.* The NF-κB subunit RelB controls p100 processing by competing with the kinases NIK and IKK1 for binding to p100. *Sci. Signal.* **9**, ra96 (2016).
68. Hogquist, K. A., Baldwin, T. A. & Jameson, S. C. Central tolerance: learning self-control in the thymus. *Nat. Rev. Immunol.* **5**, 772–782 (2005).
69. Meyts, I. *et al.* Coronavirus disease 2019 in patients with inborn errors of immunity: An international study. *J. Allergy Clin. Immunol.* **147**, 520–531 (2021).
70. Abraham, R. S. *et al.* Severe SARS-CoV-2 disease in the context of a NF-κB2 loss-of-function pathogenic variant. *J. Allergy Clin. Immunol.* (2020) doi:10.1016/j.jaci.2020.09.020.
71. Parsons, K. *et al.* Severe Facial Herpes Vegetans and Viremia in NFKB2-Deficient Common Variable Immunodeficiency. *Front. Pediatr.* **7**, (2019).
72. Maccari, M.-E. *et al.* Severe Toxoplasma gondii infection in a member of a NFKB2-deficient family with T and B cell dysfunction. *Clin. Immunol.* **183**, 273–277 (2017).
73. Ramakrishnan, K. A. *et al.* Anticytokine autoantibodies in a patient with a heterozygous NFKB2 mutation. *J. Allergy Clin. Immunol.* **141**, 1479-1482.e6 (2018).
74. Willmann, K. L. *et al.* Biallelic loss-of-function mutation in NIK causes a primary immunodeficiency with multifaceted aberrant lymphoid immunity. *Nat. Commun.* **5**, 5360 (2014).
75. Sharfe, N. *et al.* The effects of RelB deficiency on lymphocyte development and function. *J. Autoimmun.* **65**, 90–100 (2015).
76. Merico, D., Sharfe, N., Hu, P., Herbrick, J.-A. & Roifman, C. M. RelB deficiency causes combined immunodeficiency. *LymphoSign J.* **2**, 147–155 (2015).
77. Bainter, W. *et al.* Combined immunodeficiency with autoimmunity caused by a homozygous missense mutation in inhibitor of nuclear factor κB kinase alpha (IKKα). *Sci. Immunol.* **6**, eabf6723 (2021).
78. Rapaport, F. *et al.* Negative selection on human genes underlying inborn errors depends on disease outcome and both the mode and mechanism of inheritance. *Proc. Natl. Acad. Sci.* **118**, (2021).
79. Brue, T. *et al.* Mutations in NFKB2and potential genetic heterogeneity in patients with DAVID syndrome, having variable endocrine and immune deficiencies. *BMC Med. Genet.* **15**, 139 (2014).
80. Lougaris, V. *et al.* Defective natural killer-cell cytotoxic activity in NFKB2-mutated CVID-like disease. *J. Allergy Clin. Immunol.* **135**, 1641–1643 (2015).
81. Okamura, K. *et al.* Neutrophilic dermatosis associated with an NFKB2 mutation. *Clin. Exp. Dermatol.* **44**, 350–352 (2019).
82. Nogueira, M. *et al.* Symptomatic hypoglycemia in a child with common variable immunodeficiency: Deficient anterior pituitary with variable immune deficiency (DAVID) syndrome. *Clin. Pediatr. Endocrinol.* **29**, 111–113 (2020).
83. Luo, M. Z. *et al.* [De novo NFκB2 gene mutation associated common variable immunodeficiency]. *Zhonghua Er Ke Za Zhi Chin. J. Pediatr.* **56**, 628–632 (2018).

84. Nagai, M., Imai, Y. & Yamanishi, K. Psoriasiform dermatitis associated with common variable immunodeficiency 10 due to an Arg853* mutation in the NFKB2 gene. *J. Dermatol.* **46**, e24–e26 (2019).
85. Kuehn, H. S. *et al.* Novel nonsense gain-of-function NFKB2 mutations associated with a combined immunodeficiency phenotype. *Blood* **130**, 1553–1564 (2017).
86. Lee, C. E. *et al.* Autosomal-dominant B-cell deficiency with alopecia due to a mutation in NFKB2 that results in nonprocessable p100. *Blood* **124**, 2964–2972 (2014).
87. Lindsley, A. W. *et al.* Combined Immune Deficiency in a Patient with a Novel NFKB2 Mutation. *J. Clin. Immunol.* **34**, 910–915 (2014).
88. Betts, J. C. & Nabel, G. J. Differential regulation of NF-kappaB2(p100) processing and control by amino-terminal sequences. *Mol. Cell. Biol.* **16**, 6363–6371 (1996).
89. Xiao, G., Harhaj, E. W. & Sun, S.-C. NF-κB-Inducing Kinase Regulates the Processing of NF-κB2 p100. *Mol. Cell* **7**, 401–409 (2001).
90. Liang, C., Zhang, M. & Sun, S.-C. β-TrCP binding and processing of NF-κB2/p100 involve its phosphorylation at serines 866 and 870. *Cell. Signal.* **18**, 1309–1317 (2006).
91. Derudder, E. *et al.* Identification and characterization of p100HB, a new mutant form of p100/NF-κB2. *Biochem. Biophys. Res. Commun.* **308**, 744–749 (2003).
92. Qing, G., Qu, Z. & Xiao, G. Regulation of NF-κB2 p100 Processing by Its cis-Acting Domain *. *J. Biol. Chem.* **280**, 18–27 (2005).
93. Klemann, C. *et al.* Clinical and Immunological Phenotype of Patients With Primary Immunodeficiency Due to Damaging Mutations in NFKB2. *Front. Immunol.* **10**, (2019).
94. Qing, G., Qu, Z. & Xiao, G. Endoproteolytic processing of C-terminally truncated NF-κB2 precursors at κB-containing promoters. *Proc. Natl. Acad. Sci.* **104**, 5324–5329 (2007).
95. Solan, N. J., Miyoshi, H., Carmona, E. M., Bren, G. D. & Paya, C. V. RelB Cellular Regulation and Transcriptional Activity Are Regulated by p100*. *J. Biol. Chem.* **277**, 1405–1418 (2002).
96. Saitoh, T. *et al.* TWEAK Induces NF-κB2 p100 Processing and Long Lasting NF-κB Activation*. *J. Biol. Chem.* **278**, 36005–36012 (2003).
97. Piscianz, E. *et al.* Familial hypogammaglobulinemia with high RTE and naïve T lymphocytes. *Inflamm. Res.* **68**, 901–904 (2019).
98. Tangye, S. G. *et al.* Human Inborn Errors of Immunity: 2022 Update on the Classification from the International Union of Immunological Societies Expert Committee. *J. Clin. Immunol.* (2022) doi:10.1007/s10875-022-01289-3.
99. Bienias, M. *et al.* More severe than CVID: Combined immunodeficiency due to a novel NFKB2 mutation. *Pediatr. Allergy Immunol.* **n/a**,.
100. Tuijnenburg, P. *et al.* Pathogenic NFKB2 variant in the ankyrin repeat domain (R635X) causes a variable antibody deficiency. *Clin. Immunol.* **203**, 23–27 (2019).
101. Warnatz, K. *et al.* B-cell activating factor receptor deficiency is associated with an adult-onset antibody deficiency syndrome in humans. *Proc. Natl. Acad. Sci.* **106**, 13945–13950 (2009).
102. Sharfe, N. *et al.* NFκB pathway dysregulation due to reduced RelB expression leads to severe autoimmune disorders and declining immunity. *J. Autoimmun.* 102946 (2022) doi:10.1016/j.jaut.2022.102946.
103. Li, J. *et al.* Biochemically deleterious human NFKB1 variants underlie an autosomal dominant form of common variable immunodeficiency. *J. Exp. Med.* **218**, e20210566 (2021).
104. Zhang, Q., Lenardo, M. J. & Baltimore, D. 30 Years of NF-κB: A Blossoming of Relevance to Human Pathobiology. *Cell* **168**, 37–57 (2017).
105. Landegren, N. *et al.* Proteome-wide survey of the autoimmune target repertoire in autoimmune polyendocrine syndrome type 1. *Sci. Rep.* **6**, 20104 (2016).
106. Vazquez, S. E. *et al.* Identification of novel, clinically correlated autoantigens in the

monogenic autoimmune syndrome APS1 by proteome-wide PhIP-Seq. *eLife* **9**, e55053 (2020).
107. Wang, E. Y. *et al.* High-throughput identification of autoantibodies that target the human exoproteome. *Cell Rep. Methods* **2**, 100172 (2022).
108. Burkly, L. *et al.* Expression of relB is required for the development of thymic medulla and dendritic cells. *Nature* **373**, 531–536 (1995).
109. Weih, F. *et al.* Multiorgan inflammation and hematopoietic abnormalities in mice with a targeted disruption of RelB, a member of the NF-κB/Rel family. *Cell* **80**, 331–340 (1995).
110. Wirasinha, R. C. *et al.* Nfkb2 variants reveal a p100-degradation threshold that defines autoimmune susceptibility. *J. Exp. Med.* **218**, (2021).
111. Tucker, E. *et al.* A Novel Mutation in the Nfkb2 Gene Generates an NF-κB2 "Super Repressor". *J. Immunol.* **179**, 7514–7522 (2007).
112. Bautista, J. L. *et al.* Single-cell transcriptional profiling of human thymic stroma uncovers novel cellular heterogeneity in the thymic medulla. *Nat. Commun.* **12**, 1096 (2021).
113. Slade, C. A. *et al.* Fatal Enteroviral Encephalitis in a Patient with Common Variable Immunodeficiency Harbouring a Novel Mutation in NFKB2. *J. Clin. Immunol.* **39**, 324–335 (2019).
114. Kinoshita, D. *et al.* Essential Role of IκB Kinase α in Thymic Organogenesis Required for the Establishment of Self-Tolerance. *J. Immunol.* **176**, 3995–4002 (2006).
115. Kajiura, F. *et al.* NF-κB-Inducing Kinase Establishes Self-Tolerance in a Thymic Stroma-Dependent Manner. *J. Immunol.* **172**, 2067–2075 (2004).
116. Haljasorg, U. *et al.* A highly conserved NF-κB-responsive enhancer is critical for thymic expression of Aire in mice. *Eur. J. Immunol.* **45**, 3246–3256 (2015).
117. LaFlam, T. N. *et al.* Identification of a novel cis-regulatory element essential for immune tolerance. *J. Exp. Med.* **212**, 1993–2002 (2015).
118. Wells, K. L. *et al.* Combined transient ablation and single-cell RNA-sequencing reveals the development of medullary thymic epithelial cells. *eLife* **9**, e60188 (2020).
119. Onder, L. *et al.* Alternative NF-κB signaling regulates mTEC differentiation from podoplanin-expressing precursors in the cortico-medullary junction. *Eur. J. Immunol.* **45**, 2218–2231 (2015).
120. Ströbel, P. *et al.* Deficiency of the autoimmune regulator AIRE in thymomas is insufficient to elicit autoimmune polyendocrinopathy syndrome type 1 (APS-1). *J. Pathol.* **211**, 563–571 (2007).
121. Cadieux-Dion, M. *et al.* Novel heterozygous pathogenic variants in CHUK in a patient with AEC-like phenotype, immune deficiencies and 1q21.1 microdeletion syndrome: a case report. *BMC Med. Genet.* **19**, 41 (2018).
122. Lévy, R. *et al.* Monoclonal antibody-mediated neutralization of SARS-CoV-2 in an IRF9-deficient child. *Proc. Natl. Acad. Sci.* **118**, e2114390118 (2021).
123. Casanova, J.-L., Zhang, Q., Bastard, P. & Jouanguy, E. In memoriam: Stephen J Seligman, MD. *J. Clin. Immunol.* (2022) doi:10.1007/s10875-021-01204-2.
124. Zhang, Q. *et al.* Inborn errors of type I IFN immunity in patients with life-threatening COVID-19. *Science* (2020) doi:10.1126/science.abd4570.
125. Pescarmona, R. *et al.* Comparison of RT-qPCR and Nanostring in the measurement of blood interferon response for the diagnosis of type I interferonopathies. *Cytokine* **113**, 446–452 (2019).

Acknowledgments

We warmly thank the patients and their families for participating in the study. We thank the members of the Laboratory of Human Genetics of Infectious Diseases for fruitful discussions. We thank Yelena Nemirovskaya, Dana Liu, Mark Woollett, Lazaro Lorenzo-Diaz, Christine Rivalain, Maya Charabieh and Tatiana Kochetkov for administrative and technical assistance. We thank Damien Chaussabel for assistance with RNA-seq analysis. We thank the National Facility for Autoimmunity and Serology Profiling at SciLifeLab for excellent technical support. LDN and HCS are supported by the Division of Intramural Research, National Institute of Allergy and Infectious Diseases, National Institutes of Health, Bethesda, MD, USA.

Funding

The Laboratory of Human Genetics of Infectious Diseases is supported by the Howard Hughes Medical Institute, the Rockefeller University, the St. Giles Foundation, the National Institutes of Health (NIH) (R01AI088364 , R01AI127564-06 and R01AI163029), the National Center for Advancing Translational Sciences (NCATS), NIH Clinical and Translational Science Award (CTSA) program (UL1 TR001866), the Fisher Center for Alzheimer's Research Foundation, the Meyer Foundation, the JBP Foundation, the French National Research Agency (ANR) under the "Investments for the Future" program (ANR-10-IAHU-01), the Integrative Biology of Emerging Infectious Diseases Laboratory of Excellence (ANR-10-LABX-62-IBEID), the French Foundation for Medical Research (FRM) (EQU201903007798), the FRM and ANR GENCOVID project, the ANRS-COV05, ANR GENVIR (ANR-20-CE93-003) and ANR AABIFNCOV (ANR-20-CO11-0001) projects, the ANR-RHU program (ANR-21-RHUS-08-COVIFERON), the European Union's Horizon 2020 research and innovation program under grant agreement No. 824110 (EASI-genomics), the HORIZON-HLTH-2021-DISEASE-04 program under grant agreement 01057100 (UNDINE), the Square Foundation, Grandir - Fonds de solidarité pour l'enfance, the Fondation du Souffle, the SCOR Corporate

Foundation for Science, the French Ministry of Higher Education, Research, and Innovation (MESRI-COVID-19), Institut National de la Santé et de la Recherche Médicale (INSERM) and the University of Paris Cité. J.R. was supported by the INSERM PhD program (poste d'accueil INSERM). J.R. and T.L.V. are supported by the Bettencourt-Schueller Foundation and the MD-PhD program of Imagine Institute. Q.P was supported by the Assistance Publique Hôpitaux de Paris (Année Recherche) and the MD-PhD program of INSERM (Ecole de l'INSERM Liliane Bettencourt). M.O. was supported by the David Rockefeller Graduate Program, the Funai Foundation for Information Technology (FFIT), the Honjo International Scholarship Foundation (HISF), the New York Hideyo Noguchi Memorial Society (HNMS), and the National Cancer Institute (NCI) F99 Award (F99CA274708). Nils Landegren is funded by The Swedish Research Council and the Göran Gustafsson Foundation. Bärbel Keller is funded by Bundesministerium für Bildung und Forschung; GAIN 01GM1910A. Qiang Pan Hamarström is supported by the Swedish Research Council, and the Knut and Alice Wallenberg Foundation (KAW). Fabian Hauck was funded by the Else Kröner-Fresenius Stiftung (EKFS, 2017_A110), and the German Federal Ministry of Education and Research (BMBF, 01GM1910C). J.-L.C. is an inventor on patent application PCT/US2021/042741, filed July 22, 2021, submitted by The Rockefeller University that covers diagnosis of susceptibility to, and treatment of, viral disease and viral vaccines, including Covid-19 and vaccine-associated diseases.

Author contributions

T.L.V., A.Pu., M.S.A. and J.-L.C. conceived the research, designed the experiments, interpreted the data, and wrote the manuscript. J.Ro., A.Ger., S.G, L.B., G.H., Q.P., M.O., J.B., participated in experiments on IFN neutralization assay and/or overexpression assay experiments. A.Pa. and M.S.A., performed thymic section staining and analysis. A.C., D.E., O.K., M.A-G., and N.L. performed HuProt microarray and multiplex beads-assay experiment and helped for the

data analysis. F.R. performed viral serological tests. D. R. analyzed the RNA-seq data. V.Be. helps with the CyTOF data analysis. L.B. performed the thymic volume analysis from CT scan. S.T.A and A.Ger., performed the IFN score on nasal swabs. M.Mom, M.R.L.M.R., Q.R., L.I., O.D., G.M., B.K., J.O., W.A.G., T.R., M.E., N.P., D.I.B., L.V., C.H.K., P.M., J.Ra., J.B.C., C.A., S.W., Q.P.H., K.B., N.M., S.L., R.A., V.L., F.H., L.U., O.D., L.B.R., S.M.H., H.K., Y.Z., H.S., L.N., An.S., F.A., M.C.P., M.A.S., B.P., M.D.K., A.P.-C., A.S., L.D., D.S., N.A., M.H., E.L., J.F., S.K., M.Mal., M.P., M.E.M., A.M., A.I., M.S., F.C., P.F., C.C.G., P.E.G., A.B., H.S.K., S.R., F.R., Am.S., V.Ba., G.L.G., V.M.H., T.K., G.D., F.S.-R., C.Sch., C.C.R., F.R.L., S.G.T., C.Sob., R.D., K.W., B.G., C.F., V.Br., L.D.N., H.S., B.N. Q.Z., B.B, P.B., E.J., recruited patients and coordinated the clinical study protocol and sample collection. L.A., and A.C. performed statistics studies. J-.L.C, and A.Pu. supervised experiments or analyses. All authors discussed, reviewed the manuscript, and approved its submission

Competing interests

A.Gui. is a Biomerieux employee. The other co-authors decaled no competing interests.

Supplementary tables:

Supplementary table I. Demographical and clinical characteristics of 65 patients with heterozygous *NFKB2* variants.

Supplementary table II. Demographical and clinical characteristics of the patients with inborn errors of NIK, RelB, CD40L, BAFFR.

Supplementary table III. In silico prediction and functional consequences of the NFKB2 variants from the patients included or reported in the literature.

Supplementary table IV. Characteristics of SARS-CoV-2 infection in patients with inborn errors of NF-κB2.

Supplementary table V: Hematopoietic stem cell transplantation in patients with inborn errors of the alternative NF-κB regarding their auto-Abs against type I IFNs status.

Figure legends

Fig 1. Pedigrees of the 65 patients with heterozygous *NFKB2* variants. (A) Pedigrees of the patients carrying heterozygous rare variant of *NFKB2*. Generations are indicated by Roman numerals (I–II), and each symptomatic carrier included in the study, represented by a black symbol, is indicated as P followed by an Arabic numeral (P1–P65). The relatives with a grey symbol represent symptomatic carriers but without material available for this study. A vertical bar, within a white or a grey symbol, indicates an asymptomatic carrier included or not included (because of no available material), respectively in the study; an arrow indicates the index case; a black diagonal line indicates a deceased individual. "E?" indicates individuals of unknown genotype. (**B**) CADD-MAF (combined annotation dependent depletion-minor allele frequency) graph of the rare or private *NFKB2* variants (*n*=26) from the 65 patients recruited. The red and white dots represent pLOF and missense heterozygous *NFKB2* variants, respectively. The dashed line represents the mutation significance (MSC) cutoff threshold of 33 for *NFKB2*. **(C)** CoNeS score of the *NFKB2* gene.

Fig. 2. **Functional testing of the *NFKB2* alleles by overexpression and assessments of p52-dependent transcriptional activity and NIK-dependent p100 processing. (A)** Schematic diagram of the protein (p100) encoded by the *NFKB2* gene with the previously reported variants (*n*=12) and variants included in this study (*n*=25). The p52 subunit spans amino acids 1~405. The C-terminal domain (CTD) spans amino acids 760-900. The RHD domain is shown in purple, the ARD in blue, the CTD, including the PID and the NRS in brown. The *NFKB2* variants that are LOF for the p52/p52 repression of κB transcriptional activity and located in the RHD domain (p52-LOF RHD) are shown in orange, the p52-GOF mutations in the ARD are shown in blue, and the p52-LOF mutants in the CTD (p52-LOF CTD) are shown in red.

Neutral *NFKB2* variants are shown in black. The variants shown in bold correspond to those of patients recruited in this study. **(B)** Relative luciferase activity (RLA) of HEK293T cells transfected with a κB reporter luciferase construct (κB-luc), in the presence or absence of plasmids encoding NIK, RelB, and/or p100/NF-κB2 WT, testing the biochemical p100/NF-κB2 biochemical mutants reported in the literature, normalized to the WT p100/NF-κB2. A deleterious mutant was considered p52-LOF if its luciferase activity was similar to that following cotransfection with the EV, *RELB* and *NIK*, and p52-GOF if this activity was less than half that following cotransfection with *RELB, NIK* and WT *NFKB2* **(C)** RLA of HEK293T cells transfected with a κB-luc testing the *NFKB2* variants from the patients included in this study and the other variants previously reported. A deleterious mutant was considered p52-LOF if its luciferase activity was similar to that following cotransfection with the EV, *RELB* and *NIK*, and p52-GOF if this activity was less than half that following cotransfection with *RELB, NIK* and WT *NFKB2* **(D)** Western blot of HEK293T cells transfected for 48 h in the presence or absence of plasmids encoding NIK and WT or mutant p100/NF-κB2, showing phosphorylated Y866-p100 (P-p100) levels, and p100 and p52 detected with an N-terminal antibody directed against NF-κB2 (p52). All experiments were performed at least three times, independently. The luciferase assay data shown are the means of at least three independent experiments.

Fig 3. The $p52^{LOF}$/IκBδ^{GOF} mutants have enhanced p100-IκBδ activity when overexpressed or when expressed endogenously in heterozygous patients' cells. (A) Relative luciferase activity (RLA), representing the p100/NF-κB2-dependent capacity to repress κB transcriptional activity for luciferase in the presence or absence of plasmids encoding NIK and increasing doses of a plasmid encoding the C-terminal part of p100/NF-κB2 (Cter, aa 405-900) from WT p100/NF-κB2 ($Cter^{WT}$), LOF-Cter ($Cter^{R611*}$), or GOF-Cter ($Cter^{R853*}$ and $Cter^{S866N}$) mutants,

48 h after transfection. Results are expressed as a percentage of the κB-luc RLA after transfection with NIK alone (left panel); the kinetic effect of NIK transfection alone or together with a plasmid encoding the various Cter constructs, represented by κB-luc transcriptional repression, from 24 to 72 h after transfection, is shown on the right panel. **(B)** Kinetics of transfection with NIK alone or together with a plasmid encoding the dimer-deficient Y247A simple ($p100^{Y247A}$) or double mutants ($p100^{/Y247A/W270*}$, $p100^{Y247A/R611*}$, $p100^{Y247A/S866N}$, or $p100^{Y247A/R853*}$), in terms of the capacity for κB transcriptional repression of luciferase activity from 24 to 72 h after transfection. Results are expressed as a percentage of the κB RLA after transfection with NIK alone. (**C**) Western blot of HEK293T cells cotransfected with a plasmid encoding NIK, together with various doses of a plasmid encoding the WT or the $p52^{LOF}$/$IκBδ^{LOF}$ W270* or the $p52^{LOF}$/$IκBδ^{GOF}$ R853* or S866N *NFKB2* variants, together with a constant dose of an empty vector (left panel) or of WT-*NFKB2* (right panel). **(D)** Subcellular localization of the WT or the K321Sfs, R611*, R853*, and S866N p100/NF-κB2 variants used for cotransfection with RelB, with or without NIK, as determined by confocal microscopy on HeLa cells. Nuclei were stained with DAPI; p100 and RelB were detected with antibodies recognizing their N-terminal domain. **(E)** Western blot of P-p100, NF-κB2 (p100/p52), NF-κB1 (p105/p50), RelB, and RelA in primary fibroblast from one healthy control, a patient with the $p52^{LOF}$/$IκBδ^{GOF}$ R853*/WT variant, a patient with the $p52^{LOF}$/$IκBδ^{LOF}$ K321Sfs/WT variant, a patient with AR complete (Q73Tfs*152/Q73Tfs*152) RelB or (P565R/P565R) NIK deficiency, with or without stimulation with LT-α1β2 (Lt) for 48 h, and a recapitulative graph depicting total p100/p52 intensity ratio is shown. The bars and error bars represent the mean of two different experiments and the standard deviation, respectively. (**F**) Confocal microscopy showing the subcellular distribution of RelB in primary fibroblasts from two healthy controls (HC1, HC2), patients with the a $p52^{LOF}$/$IκBδ^{LOF}$ K321Sfs/WT or a $p52^{LOF}$/$IκBδ^{GOF}$ R853*/WT NF-κB2/p100 variant, and patients with AR complete RelB (Q72Tfs*152/Q72Tfs*152) or NIK

(P565R/P565R) deficiency, with and without stimulation with 100 ng/mL of TWEAK for 48h. At least two independent experiments were performed. The luciferase assay data shown are the mean values from at least three independent experiments.

Fig. 4. Distinctive immunological and clinical phenotype of patients with p52^{LOF}/IκBδ^{GOF} variants. (A) tSNE analysis on concatenated whole-blood samples from 10 patients with p52^{LOF}/IκBδ^{GOF} variants, or 10 age-matched healthy controls, by CyTOF. tSNE analysis from the patients with p52^{LOF}/IκBδ^{LOF} are not represented as CyTOF was performed in only two patients. **(B)** Cell counts and proportions of total B and B-cell subsets determined by CyTOF in healthy controls, patients with a p52^{LOF}/IκBδ^{GOF} variant and auto-Abs against type I IFNs (*n*=10, red dots), patients with p52^{LOF}/IκBδ^{LOF} variants (*n*=2, K321Sfs/WT and c.104-1G>C/WT, orange dots). (**C**) UMAP-based unsupervised clustering analysis on CD19^{+} B cells from a concatenated group of 10 patients with p52^{LOF}/IκBδ^{GOF} variants and 31 age-matched controls, with a heatmap showing the mean levels of the surface markers included in the clustering defining 21 distinct *metaclusters*, the CD27 marker expression and the metacluster distribution in HC or in the patients with p52^{LOF}/IκBδ^{GOF} variants **(D-E)** Contour plots and proportions of Tregs (**D**) and of Tfh cells (**E**) in patients with a p52^{LOF}/IκBδ^{GOF} variant with (*n*=9, red circle) or without (*n*=1, red square) auto-Abs against type I IFN, relative to aged-matched controls (*n*=27) and two patients with a p52^{LOF}/IκBδ^{LOF} variant (K321Sfs/WT and c.104-1G>C/WT) without auto-Abs against type I IFNs (orange circle). (**F**) Proportion of patients with p52^{LOF}/IκBδ^{GOF} (*n*=51), p52^{GOF}/IκBδ^{LOF} (*n*=6) or p52^{LOF}/IκBδ^{LOF} (*n*=5, with 2 reported in this study and 3 previously reported i*n* [85]) NF-κB2 variants presenting clinical manifestations. (**G**) Proportion of patients with severe/recurrent or non-severe viral diseases among the 51 patients with p52^{LOF}/IκBδ^{GOF} NF-κB2 variants. (**H**) COVID-19 severity scale for unvaccinated patients with a p52^{LOF}/IκBδ^{GOF} (red), p52^{GOF}/IκBδ^{LOF} (blue), or neutral NF-κB2

(gray circle) variant. (**I**) Age at the COVID-19 episode in unvaccinated patients with a $p52^{LOF}$/IκBδ^{GOF} (red), $p52^{GOF}$/IκBδ^{LOF} (blue), or neutral NF-κB2 (gray circle) variant, as a function of COVID-19 severity.

Fig. 5. Neutralizing auto-Abs against type I IFNs detected in patients heterozygous for $p52^{LOF}$/IκBδ^{GOF} variants and patients with inborn errors of RelB or NIK. (A) Detection of IgG auto-Abs against IFN-α2 by Gyros in patients with AD inborn errors of NF-κB2 with $p52^{LOF}$/IκBδ^{LOF} (*n*=2), $p52^{GOF}$/IκBδ^{LOF} (*n*=6) or $p52^{LOF}$/IκBδ^{GOF} (*n*=50) variant and in six patients with idiopathic primary antibody deficiency (PAD) carrying a neutral *NFKB2* variant and in patients with APS-1 (*n*=45). Positive controls (C+, *n*=10) correspond to individuals previously identified with IgG auto-Abs against IFN-α2, healthy controls (HC, *n*=66) correspond to individuals previously identified without IgG auto-Abs against IFN-α2. **(B)** Detection by protein microarray analysis of the 17 type I IFNs including the 13 IFN-α, IFN-β, IFN-ε, IFN-κ, and IFN-ω in patients with $p52^{LOF}$/IκBδ^{GOF} variants (*n*=13), $p52^{LOF}$/IκBδ^{LOF} (*n*=1) or AR APS-1 (*n*=4) and auto-Abs against type I IFNs. Values are normalized against the mean fluorescence of plasma from controls (*n*=22). **(C-E)** Luciferase-based neutralization assay to detect auto-Abs neutralizing 100 pg/mL IFN-α2 (**C**), IFN-ω (**D**), or 10 ng/mL IFN-β (**E**), in individuals previously identified with neutralizing anti-IFN-I auto-Abs (C+, *n*=10), healthy controls (HC, *n*=66), patients with inborn errors of NF-κB2, including six patients with $p52^{GOF}$/IκBδ^{LOF} variants, two patients with a $p52^{LOF}$/IκBδ^{LOF} variant, 51 patient with a $p52^{LOF}$/IκBδ^{GOF} variant, six patients with idiopathic PAD carrying a neutral variant of *NFKB2*, and 45 APS-1 patients. Plasma samples were diluted 1:10 in all tests. HEK293T cells were transfected with the dual luciferase system with IFN-sensitive response elements (ISRE) before treatment with type I IFNs with or without patient plasma, and relative luciferase activity (RLA) was calculated by normalizing firefly luciferase activity against *Renilla* luciferase activity,

before normalization against non-stimulated conditions. An induction factor of less than five related to non-stimulated condition was considered to correspond to neutralizing activity (dashed line). (**F-H**) Luciferase-based neutralization assay to detect auto-Abs neutralizing 100 pg/mL IFN-α2 (**F**), IFN-ω (**G**) or 10 ng/mL IFN-β (**H**) in patients with inborn errors of BAFFR (*n*=1), XL-CD40L (*n*=3), AR NIK deficiency (*n*=2), AR RelB deficiency (*n*=8) and in healthy relatives heterozygous for a null or hypomorphic *RELB* allele (*n*=8). (**I**) Correlation between the p52 transcriptional activity assessed in the κB luciferase assay (y-axis) and the neutralizing status of auto-Abs against IFN-α2 at 100 pg/mL by the ISRE luciferase assay (x-axis) in patients with inborn errors of NF-κB2. (**J**) Protein microarray showing the distribution of auto-Ab reactivity against 20,000 human proteins in plasma samples from patients carrying a $p52^{LOF}$/$IκBδ^{GOF}$ variant (*n*=13, with detectable (*n*=8) or undetectable (*n*=5) auto-Abs against type I IFNs) and one patient with the $p52^{LOF}$/$IκBδ^{LOF}$ K321Sfs variant without auto-Abs against type I IFNs. Data are represented as the fold change relative to 22 plasma samples from healthy donors. Reds dots represent type I IFNs and yellow dots represent type III IFNs. Data for all Gyros, HuProt and neutralization assay experiments are presented as the mean for at least two technical replicates.

Fig. 6. Susceptibility to COVID-19 and other severe viral diseases is strongly associated with the presence of neutralizing auto-Abs against type I IFNs. (**A**) Proportion of patients with a $p52^{LOF}$/$IκBδ^{GOF}$ variant and manifestations of viral diseases as a function of their anti-type I IFN auto-Ab status. (**B**) Clinical and immunological manifestations in patients with a $p52^{LOF}$/$IκBδ^{GOF}$ variant, as a function of anti-type I IFN auto-Ab status. **(C)** Chord diagram plot of the main clinical and immunological manifestations of patients with inborn errors of NF-κB2. **(D)** Anti-IFN-α2 IgG detection by Gyros in individuals previously identified with neutralizing anti-IFN-I auto-Abs (C+, *n*=10), healthy controls (HC, n=7), patients with a

p52^{LOF}/IκBδ^{GOF} (*n*=9), p52^{GOF}/IκBδ^{LOF} (n=2) or neutral variant (*n*=2) and COVID-19, as a function of disease severity. (**E**) Heatmap showing the type I IFN neutralization profile of the nine patients with p52^{LOF}/IκBδ^{GOF} variants and two with a p52^{GOF}/IκBδ^{LOF} variant during COVID-19, according to disease severity and clinical presentation during infection. The red squares indicate a complete neutralization capacity of the plasma for ISRE induction in the luciferase reporter assay system (induction <5 relative to non-stimulated (NS) conditions), and the white squares indicate a total absence of neutralizing auto-Ab detection in the ISRE-luciferase assay. **(F)** IFN score and viral load in nasal swabs during the course of COVID-19 in two patients with a p52^{LOF}/IκBδ^{GOF} variant (P27 in blue and P28 in pink). **(G)** IFN score and viral load in whole blood (left panel) or nasal swabs (rights panels) during the course of COVID-19 in P27 and P28 (blue and pink dots, respectively), or *n*=36 individuals infected with SARS-CoV-2 and presenting only mild disease (gray dots). The vertical arrows indicate the times of recombinant IFN-β injection and the arrowheads indicate the infusion of monoclonal antibody against SARS-CoV-2 spike. (**H**) ISG score induction by IFN module analysis during the course of COVID-19 in P27 and P28 before and after recombinant FN-β treatment and two age-matched controls (HC1 and HC2) infected with SARS-CoV-2, regarding the presence or not of auto-Abs against type I IFNs and their nasal SARS-CoV-2 viral load.

Fig. 7. Impaired mTEC development and AIRE thymic expression in a patient with a p52^{LOF}/IκBδ^{GOF} variant and a patient with AR RelB deficiency. (**A**) Estimation of thymus volume in patients with a p52^{LOF}/IκBδ^{GOF} variant without (red squares) or with (red circles) auto-Abs against type I IFNs, across ages, relative to aged-matched controls aged from 3 to 16 years. (**B**) Immunofluorescence staining of thymic tissue from age-matched controls and patients with a p52^{LOF}/IκBδ^{GOF} variant or AR complete RelB deficiency. The thymic epithelium is stained with K5 (green) or K8 (red). Hassall's corpuscles in control tissue are marked "HC".

The scale bars correspond to 100 μm or 50 μm, as indicated. AIRE-expressing cells (green) and Hassall's corpuscles were found in the controls but not in patient tissues, as shown at higher magnification in the inset.

Supplementary Materials

Supplementary Fig. 1. Population genetics and constraint metrics of the *NFKB2* gene. (A) Representation of the alternative NF-κB pathway and the patients included. (**B**) Genomic constrained coding regions across *NFKB2* as estimated by the missense tolerance ratio (MTR) score evaluating region-specific intolerance to missense variants. A score < 1.0 indicates a lower-than-expected ratio of missense to synonymous variants in the gnomAD v2.0 dataset for the 21-bp window surrounding an amino-acid residue. The horizontal dashed lines represent the 5^{th} (red), 25^{th} (orange), 50^{th} (black) percentile most missense-depleted regions for *NFKB2*. The NIK-responsive sequence (NRS, amino acid 861-871, gray area), which includes all the deleterious *NFKB2* missense variants in the CTD and the two critical phosphorylation sites at S866 and S870, is within the 5th percentile for the most missense-depleted regions for *NFKB2.* The lower graph shows the distribution of the heterozygous *NFKB2* variants reported in gnomAD 2.1.1 and from the patients reported in this study, by location within the protein and CADD score. (**C**) CADD-MAF graph of the *NFKB2* variants reported in the public databases gnomAD v2.2.1 and BRAVO/TOPMed. The red and gray dots represent heterozygous pLOF and heterozygous in-frame (missense and indel) variants, respectively. The green dots represent homozygous missense variants. The horizontal dashed line represents the mutation significance (MSC) cutoff threshold of 33 for *NFKB2.* The vertical dashed line represents the MAF 10^{-4}. (**D**) Electropherograms showing the c.104-1G>C/WT essential splice-site mutation of P62 and a healthy control (left) and the proportion of transcripts identified by sequencing 100 colonies from TOPO cloning with cDNA from PCR products amplifying a region from exon 2 to 7 in P62 or a healthy control. **(E)** Pedigrees and mutations of patients with inborn errors of RelB, NIK, BAFFR and CD40L. The relatives with a grey symbol represent symptomatic carriers but without material available for this study. A dot within a white symbol indicates an

asymptomatic carrier; an arrow indicates the index case; a black diagonal line indicates a deceased individual. “E?” indicates individuals of unknown genotype.

Supplementary Fig. 2. Functional testing of *NFKB2* variants. (A) Schematic representation of the alternative NF-κB pathway and the function of the p52/RelB and p52/p52 heterodimers (left panel); a graphical overview of the luciferase assay to test the p52 function of the *NFKB2* variants (middle panel); and a schematic representation of the functional consequence of the WT, $p52^{GOF}$ or $p52^{LOF}$ variants by the luciferase assay. (**B**) Relative luciferase activity (RLA) of WT or RelA-deficient HEK293T cells transfected with a κB reporter construct (κB-luc) in the presence or absence of plasmids encoding NIK with or without RelB for 24, 48 or 72 h. Results represent RLA normalized according to the value for EV conditions. **(C)** Western blot of HEK293T cells transfected for 24 h (left panel) or 48 h (right panel) in the presence or absence of plasmids encoding NIK and WT or the previously reported biochemical p100 mutant. **(D)** Luciferase assay testing the NF-κB2/p100 biochemical mutants (left) or deleterious variants from patients (right), 24 h after transfection. (**E-F**) RLA of HEK293T cells transfected with a κB reporter construct (κB-luc) in the presence or absence of plasmids encoding NIK, RelB and WT NF-κB2/p100 or seven NF-κB2/p100 missense variants of patients included in this study (*n*=5 variants) or previously reported (*n*=2), or the 14 missense variants reported in the public databases at a MAF $>10^{-4}$, after 24 h (**E**) or 48 h **(F)** of transfection. **(G)** Western blot of HEK293T cells transfected in the presence or absence of plasmids encoding NIK and NF-κB2/p100 WT or containing the missense variants reported in the public databases at a MAF $>10^{-4}$. (**H**) Graphical illustration of allele testing in the NIK-RELB-NF-κB2 triple cotransfection assay.

Supplementary Fig. 3. The processing-resistant *NFKB2* mutants have enhanced p100-IκBδ activity when overexpressed and in heterozygous patients’ cells. (**A**) Functional

testing of the capacity of the NF-κB2/p100 WT, W270*, R611*, or R853* or A867V mutants for κB transcriptional repression of luciferase activity in the presence or absence of plasmids encoding NIK, and increasing doses of WT or mutant NF-κB2/p100, 48 h after transfection. Results are expressed as a percentage of the κB RLA after transfection with NIK alone. **(B)** Kinetic effect of the transfection of NIK alone or together with a plasmid encoding WT or mutant NF-κB2/p100 for κB transcriptional repression of luciferase from 24 to 72 h after transfection. Results are expressed as percentage of the κB RLU after transfection with NIK alone. (**C**) Subcellular localization of NF-κB2 in HeLa cells transfected with NF-κB2/p100 WT or the variants. **(D)** Subcellular localization of RelB after cotransfection with plasmids encoding the C-terminal part (Cter, aa 405-900) from WT ($Cter^{WT}$), LOF-Cter ($Cter^{R611*}$), or GOF-Cter ($Cter^{R853*}$ and $Cter^{S866N}$) p100/NF-κB2 mutants, with or without NIK, 24 h after the transfection of HeLa cells. **(E)** Western blot of MDDC total cell extracts from controls (HC1, HC2, HC3, HC11) or two patients carrying $p52^{LOF}$/$IκBδ^{GOF}$ (R848Efs*38/WT and R853*) variants, a patient with $p52^{LOF}$/$IκBδ^{LOF}$ carrying the K321Sfs/WT variant, and a patient with XL-CD40 deficiency (c.409+2T>C/ c.409+2T>C), with and without stimulation with CD40L for 48 h, and a recapitulative graph depicting total p100/p52 intensity ratio is shown. The bars and error bars represent the mean of two different experiments and the standard deviation, respectively. (**F**) Western blot of T-cell blast total cell extracts from two healthy controls (HC1, HC2), or two patients with the K321Sfs $p52^{LOF}$/$IκBδ^{LOF}$ or c.104-1G>C/WT variants. **(G)** Western blot of P-p100, p100, p52, RelB and NIK expression in total cells extracts of SV-40-transformed fibroblasts from two healthy controls, patients with the $p52^{LOF}$/$IκBδ^{GOF}$ R853*/WT variant, complete NEMO deficiency ($NEMO^{-/Y}$) or AR complete NIK deficiency ($NIK^{-/-}$), with or without stimulation with Lt, or TNF for 48 h, and a recapitulative graph depicting total p100/p52 intensity ratio is shown. The bars and error bars represent the mean of 2 different experiments and the standard deviation, respectively. (**H**) Western blot showing p100

processing into p52 and RelB induction in total cell extracts of SV-40-transformed fibroblasts from a healthy control or a patient with AR complete NIK deficiency ($NIK^{-/-}$). **(I)** Confocal microscopy showing the subcellular distribution of p52 in primary fibroblasts from two healthy controls (HC), patients with the $p52^{LOF}$/$IκBδ^{LOF}$ K321Sfs*/WT or the $p52^{LOF}$/$IκBδ^{GOF}$ R853*/WT NF-κB2/p100 variants, AR complete RelB deficiency ($RelB^{-/-}$, Q73Tfs*152/Q73Tfs*152), or AR complete NIK deficiency ($NIK^{-/-}$, P565R/P565R) with and without stimulation with 100 ng/mL TWEAK for 48 h, using an antibody recognizing the N-terminal of p100. **(J)** Confocal microscopy showing the subcellular distribution of RelB in SV-40-transformed fibroblasts from two healthy controls (HC), patients with the $p52^{LOF}$/$IκBδ^{LOF}$ K321Sfs*/WT or the $p52^{LOF}$/$IκBδ^{GOF}$ R853*/WT NF-κB2/p100 variants, AR complete RelB deficiency ($RelB^{-/-}$, Q73Tfs*152/Q73Tfs*152), AR complete NIK deficiency ($NIK^{-/-}$, P565R/P565R), complete NEMO deficiency ($NEMO^{-/Y}$), with and without stimulation with 100 ng/mL TWEAK for 48 h. (**K**) Confocal microscopy showing the subcellular distributions of p100/p52 (left panel), and RelB (right panel) in MDDCs from two healthy controls, two patients with $p52^{LOF}$/$IκBδ^{LOF}$ (K321Sfs*/WT and c.104-1G>C/WT), and a patient with $p52^{LOF}$/$IκBδ^{GOF}$ R853*/WT NF-κB2/p100 variants, stimulated with CD40L for 48 h.

Supplementary Fig. 4. Immunological investigation of patients with inborn errors of NF-κB2. (A) Immunoglobulin IgG, IgM, and IgA levels (g/L) in patients with inborn errors of NF-κB2. **(B)** B-cell count across ages in patients with $p52^{LOF}$/$IκBδ^{GOF}$ variants with (*n*=35, red dots) or without (*n*=8, red square) auto-Abs against type I IFNs, patients with $p52^{GOF}$/$IκBδ^{LOF}$ (*n*=3 blue dots) or neutral (PAD, gray dots) NF-κB2 variants. Normal B-cell count for age corresponds to the gray area. **(C)** Proportion of B cells in healthy controls (*n*=15), patients with a $p52^{LOF}$/$IκBδ^{GOF}$ variant (*n*=10, red dots), patients with $p52^{LOF}$/$IκBδ^{LOF}$ variants (*n*=2, K321Sfs/WT and c.104-1G>C/WT, orange dots). **(D)** Proportions and absolute values of B-cell

subsets identified in the 21 metaclusters, and representation of the CD27, CD21, CD38 and CD24 markers on UMAP in healthy controls (*n*=22), patients with a $p52^{LOF}$/$IκBδ^{GOF}$ variant (*n*=10, red dots), patients with $p52^{LOF}$/$IκBδ^{LOF}$ variants (*n*=1, K321Sfs/WT, orange dots). (**E-J**) Counts of lymphocytes and T-cell subsets (**E**); proportions and counts of CD8 and CD4 T-cell subsets (**F**); counts of Tregs (**G**), counts of memory $CD4^+$ T cells, counts and proportions of cTFh and cTFh subsets (**H**); counts and proportions of NK cells and NK cell subsets, counts of MAIT and iNKT cells(**I**); proportions and counts of monocytes and dendritic cells in patients with inborn errors of NF-κB2 and age-matched controls (**J**). (**K**) Gating strategy for CyTOF immunophenotyping. CD4+ RTE, Treg and Tfh phenotyping in the 4 patients with the E418*/WT (*n*=1) or R635*/WT (*n*=3) $p52^{GOF}$/$IκBδ^{LOF}$ variant (blue dots, from [85]) and their age-matched controls (black dots from the same panel) were performed by FACS.

Supplementary Fig. 5. Neutralizing auto-Abs against type I IFNs in patients with inborn errors of the alternative NF-κB pathway (A) Detection of auto-Abs against type I IFNs by multiplex bead array in patients with $p52^{LOF}$/$IκBδ^{GOF}$ variants (*n*=51 patients), $p52^{LOF}$/$IκBδ^{LOF}$ variant (*n*=1 patient), AR RelB (*n*=8 patients) or AR NIK (*n*=2 patient) deficiency, idiopathic PAD (*n*=5 patient), or APS-1 (*n*=1 patients), and healthy controls (HC, *n*=106). (**B-C**) Luciferase-based neutralization assay for detecting auto-Abs neutralizing 10 ng/mL IFN-α2 (**B**) or IFN-ω (**C**) in patients with inborn errors of NF-κB2 and APS-1 patients. Positive controls (C+, *n*=10) correspond to individuals previously identified with IgG auto-Abs against IFN-α2, healthy controls (HC, *n*=66) correspond to individuals previously identified without IgG auto-Abs against IFN-α2. **(D)** Correlation between the detection of auto-Abs against IFN-α2 by Gyros (x-axis) and results for the ISRE luciferase-based neutralization assay (y-axis) after stimulation with 100 pg/mL IFN-α2. The dotted line represents the cutoffs for detection (value >50) or neutralization (induction <5). **(E-F)** Proportion of patients with neutralizing

auto-Abs against type I IFNs at 10 ng/mL and 100 pg/mL for patients with a $p52^{LOF}$/$I\kappa B\delta^{GOF}$ variant (**E**), and APS-1 patients (**F**). (**G**) Proportion of patients with neutralizing auto-Abs against IFN-α and/or IFN-ω among patients carrying a missense or pLOF $p52^{LOF}$/$I\kappa B\delta^{GOF}$ variant. (**H**) Age distribution of patients with a $p52^{LOF}$/$I\kappa B\delta^{GOF}$ variant, AR RelB or NIK deficiency, or APS-1 according to the presence or absence of neutralizing auto-Abs against type I IFNs in their plasma. (**I**) Correlation between p52 transcriptional activity assessed in luciferase assays and auto-Abs neutralizing 100 pg/mL IFN-ω status in patients with inborn errors of the NF-κB pathway. (**J**) Detection of IgG auto-Abs against IFN-α2 by Gyros in patients with inborn errors of the alternative NF-κB signaling. (**K**) Luciferase-based neutralization assay for detecting auto-Abs neutralizing 10 ng/mL IFN-α2 or IFN-ω in patients with inborn errors of the alternative NF-κB signaling pathway. **(L)** Proportion of patients with auto-Abs neutralizing type I IFNs at 10 ng/mL and 100 pg/mL in patients with AR RelB deficiency. (**M-N**) Luciferase-based neutralization assay for detecting auto-Abs neutralizing 100 pg/mL IFN-α2 (**M**) or IFN-ω (**N**) in patients with inborn errors of the canonical NF-κB pathway. DN means dominant-negative RelA deficiency (unpublished) (**O**) Heat map of the autoantigens with the highest levels of enrichment in patients with a $p52^{LOF}$/$I\kappa B\delta^{GOF}$ variant (n=13, including 8 with and 5 without neutralizing auto-Abs against type I IFNs), AR RelB (n=8), AR NIK (n=2) deficiency, or with APS-1 (n=4) relative to 22 healthy controls (HC) by Protein microarray. Results are shown as the mean fluorescence of two replicates with a $\log_2$ fold-change >1.8 in patients with the 14 patients with inborn errors of NF-κB2 tested as compared to HC. (**P**) Detection of auto-Abs against ATP4A, RBM38, TROVE2 or KLHL31 by multiplex beads array. (**Q**) Heat map representing the autoantigens classically detected in APS-1 patients, as detected with the Protein microarray on plasma samples from patients with inborn errors of the alternative NF-κB pathway and 22 healthy controls. Results are shown as a $\log_2$ fold-change in luminescence in patients with inborn errors of NF-κB2 relative to healthy controls (**R**) Protein

microarray auto-Ab distribution in patients with a $p52^{LOF}$/IκB$δ^{GOF}$ variant relative to healthy controls. Green dots indicate auto-Abs classically found in APS-1 patients. (**S**) Detection of IgG auto-Abs against IL17A, IL17F, or IL-22 by multiplex beads-array. (**T**) Luciferase-based neutralization assay for detecting auto-Abs neutralizing the 13 IFN-α subtypes and IFN- ω at a concentration of 1 ng/mL in patients with a $p52^{LOF}$/IκB$δ^{GOF}$ variant (*n*=17), a $p52^{LOF}$/IκB$δ^{LOF}$ variant (*n*=1) or APS-1 (*n*=1), and plasma from healthy donors (*n*=3) (left panels) and patients with inborn errors of RelB (*n*=2), NIK (*n*=2) or BAFFR (*n*=1), and plasma from healthy donors (*n*=3) or APS-1 (*n*=1) (right panel). The neutralization capacity of the corresponding plasma samples against IFN-α2 or IFN-ω at concentrations of 10 ng/mL and 100 pg/mL is shown as gray (neutralizing) or white (non-neutralizing) squares.

Supplementary Fig. 6. Auto-Abs against type I IFNs prevent ISG induction in blood and the upper respiratory tract during COVID-19, a defect that can be rescued by exogenous IFN-β treatment. (**A**) Changes in the titers of auto-Abs against IFN-a2, as measured by Gyros, with age in patients with a $p52^{LOF}$/IκB$δ^{GOF}$ variant and COVID-19. Red arrows indicate the onset of SARS-CoV-2 infection. (**B**) Correlation between age and COVID-19 severity in patients with inborn errors of NF-κB2. The light red square represents a patient neutralizing only IFN-ω at 100 pg/mL. (**C**) Post-vaccinal anti-S Ig levels in patients with a $p52^{LOF}$/IκB$δ^{GOF}$ variant who encountered SARS-CoV-2. (**D**) COVID severity and age correlation in patients with a $p52^{LOF}$/IκB$δ^{GOF}$ (n=8), $p52^{LOF}$/IκB$δ^{LOF}$ (*n*=2), or $p52^{GOF}$/IκB$δ^{LOF}$ (*n*=3) variant previously vaccinated who were infected by SARS-CoV-2 (period October 2021 to February 2022). **(E)** Overview of the longitudinal investigation of COVID-19 episodes in two patients with a $p52^{LOF}$/IκB$δ^{GOF}$ variant. **(F)** Heatmap showing the neutralization profile in the two patients during COVID-19. (**G**) Neutralization capacity of the nasal swab from patients with a $p52^{LOF}$/IκB$δ^{GOF}$ variant and COVID-19 (*n*=2), and individuals infected with the omicron

variant but without detectable neutralizing auto-Abs against type I IFNs. (**H**) Longitudinal follow-up of the anti-S and anti-N IgG in P27 and P28 during the course of COVID-19, before and after treatment by the infusion of an anti-S monoclonal Ab (mAb, gray arrow). **(I)** IFN module M.10.1 and M.8.3 enrichment score of individual samples during the course of COVID-19 in P27 and P28 or in two age-matched controls infected with SARS-CoV-2 before and after the treatment of P27 and P28 with IFN-β (left panel) and RNA-seq comparison of gene expression between day 0, day 3, day 5, day 12 and day 13 or day 27 in the P27 and P28.

Figure 1

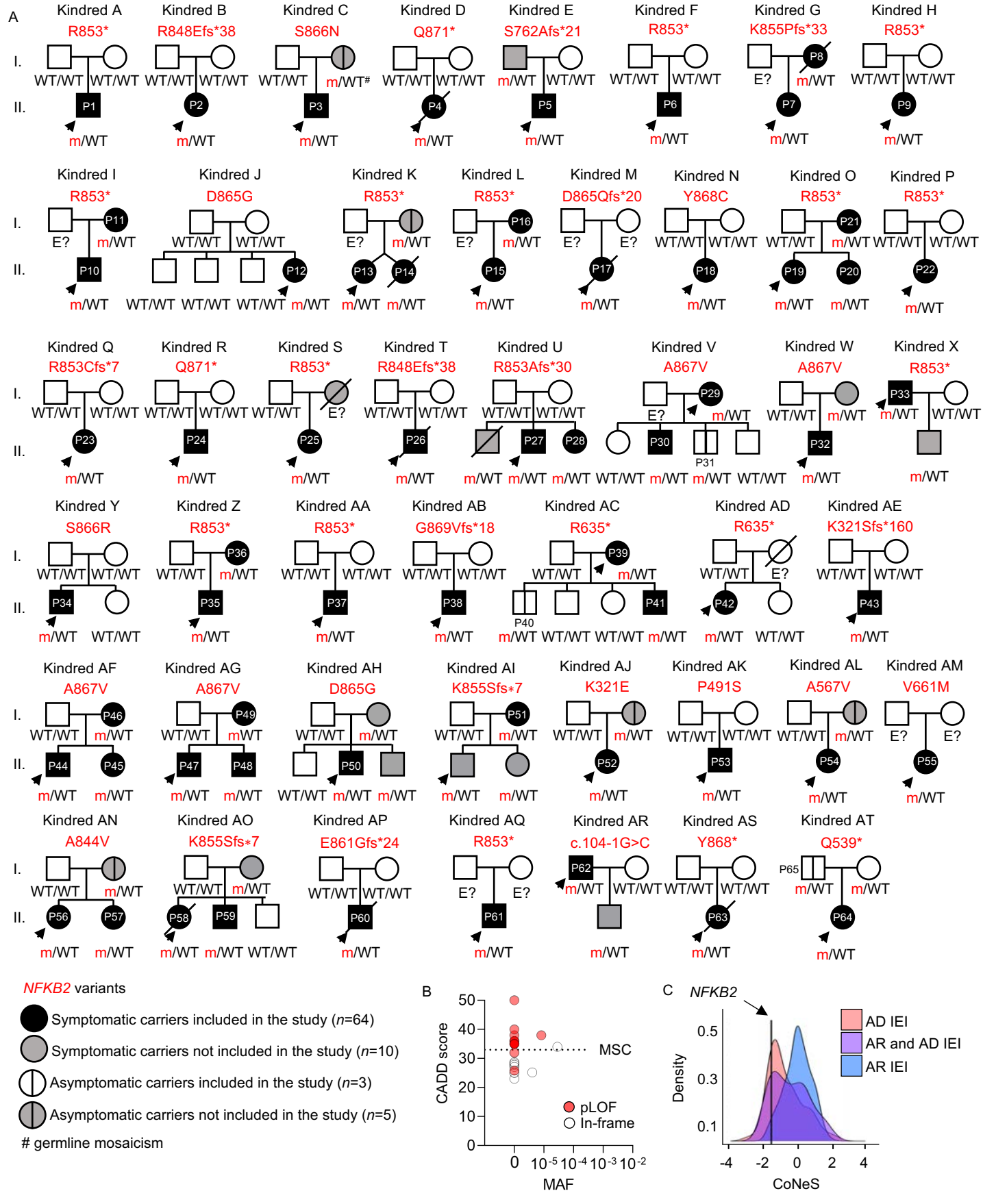
A
Kindred A
R853*
Kindred B
R848Efs*38
Kindred C
S866N
Kindred D
Q871*
Kindred E
S762Afs*21
Kindred F
R853*
Kindred G
K855Pfs*33
Kindred H
R853*
Kindred I
R853*
Kindred J
D865G
Kindred K
R853*
Kindred L
R853*
Kindred M
D865Qfs*20
Kindred N
Y868C
Kindred O
R853*
Kindred P
R853*
Kindred Q
R853Cfs*7
Kindred R
Q871*
Kindred S
R853*
Kindred T
R848Efs*38
Kindred U
R853Afs*30
Kindred V
A867V
Kindred W
A867V
Kindred X
R853*
Kindred Y
S866R
Kindred Z
R853*
Kindred AA
R853*
Kindred AB
G869Vfs*18
Kindred AC
R635*
Kindred AD
R635*
Kindred AE
K321Sfs*160
Kindred AF
A867V
Kindred AG
A867V
Kindred AH
D865G
Kindred AI
K855Sfs*7
Kindred AJ
K321E
Kindred AK
P491S
Kindred AL
A567V
Kindred AM
V661M
Kindred AN
A844V
Kindred AO
K855Sfs*7
Kindred AP
E861Gfs*24
Kindred AQ
R853*
Kindred AR
c.104-1G>C
Kindred AS
Y868*
Kindred AT
Q539*
NFKB2 variants
Symptomatic carriers included in the study (n=64)
Symptomatic carriers not included in the study (n=10)
Asymptomatic carriers included in the study (n=3)
Asymptomatic carriers not included in the study (n=5)
germline mosaicism
B
CADD score
MAF
MSC
pLOF
In-frame
C
NFKB2
Density
CoNeS
AD IEI
AR and AD IEI
AR IEI

Figure 2

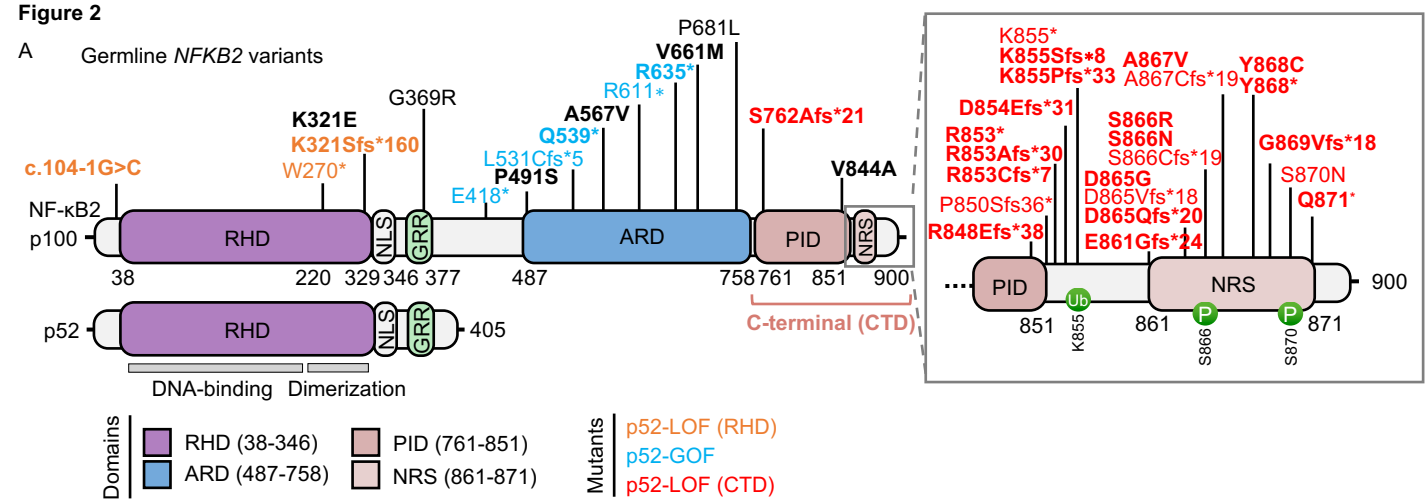
A
Germline NFKB2 variants
c.104-1G>C
K321E
K321Sfs*160
W270*
G369R
E418*
L531Cfs*5
P491S
A567V
Q539*
P681L
V661M
R635*
R611*
S762Afs*21
V844A
NF-κB2
p100
RHD
NLS
GRR
ARD
PID
NRS
38
220
329
346
377
487
758
761
851
900
p52
405
DNA-binding
Dimerization
C-terminal (CTD)
K855*
K855Sfs*8
K855Pfs*33
A867V
A867Cfs*19
Y868C
Y868*
D854Efs*31
S866R
S866N
S866Cfs*19
G869Vfs*18
R853*
R853Afs*30
R853Cfs*7
D865G
D865Vfs*18
S870N
Q871*
P850Sfs36*
D865Qfs*20
R848Efs*38
E861Gfs*24
Ub
K855
P
S866
S870
861
871
Domains
RHD (38-346)
ARD (487-758)
PID (761-851)
NRS (861-871)
Mutants
p52-LOF (RHD)
p52-GOF
p52-LOF (CTD)

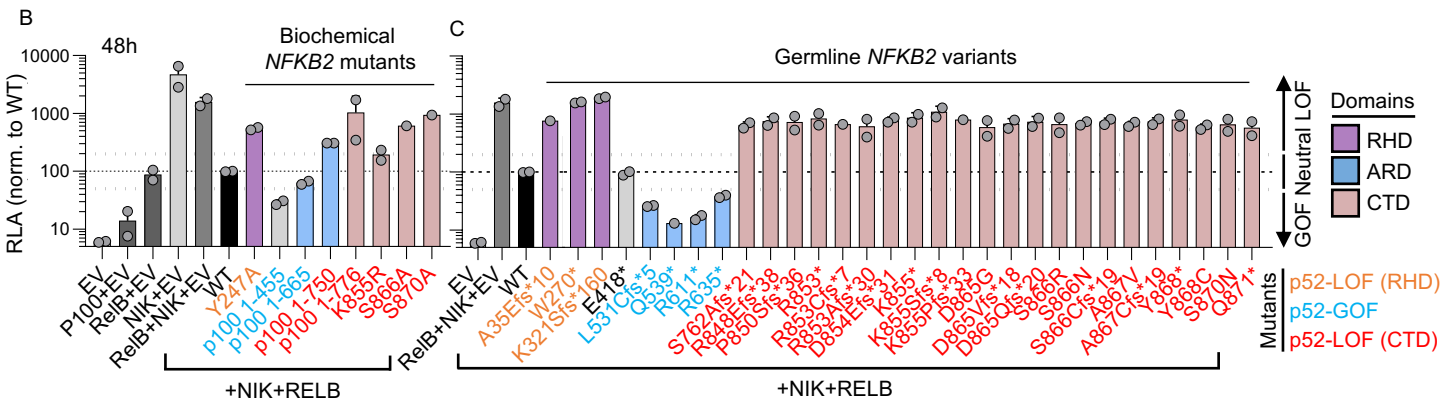
B
48h
Biochemical NFKB2 mutants
RLA (norm. to WT)
10000
1000
100
10
EV
P100+EV
RelB+EV
NIK+EV
RelB+NIK+EV
WT
Y247A
p100 1-455
p100 1-665
p100 1-750
p100 1-776
K855R
S866A
S870A
+NIK+RELB
C
Germline NFKB2 variants
GOF
Neutral
LOF
Domains
RHD
ARD
CTD
EV
RelB+NIK+EV
WT
A35Efs*10
W270*
K321Sfs*160
E418*
L531Cfs*5
Q539*
R611*
R635*
S762Afs*21
R848Efs*38
P850Sfs*36
R853*
R853Cfs*7
R853Afs*30
D854Efs*31
K855*
K855Sfs*8
K855Pfs*33
D865G
D865Vfs*18
D865Qfs*20
S866R
S866N
S866Cfs*19
A867V
A867Cfs*19
Y868*
Y868C
S870N
Q871*
+NIK+RELB
Mutants
p52-LOF (RHD)
p52-GOF
p52-LOF (CTD)

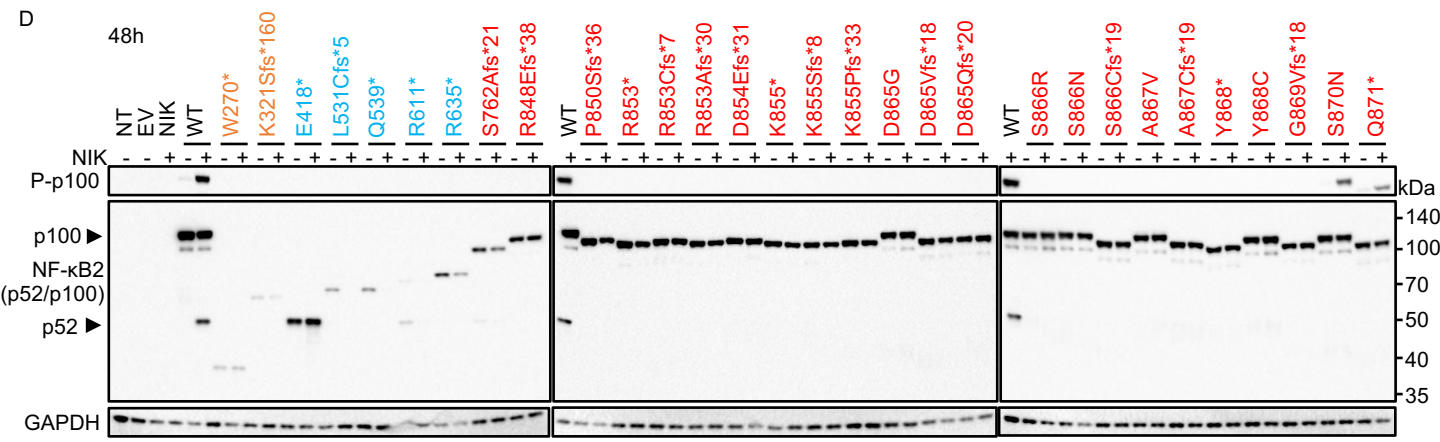
D
48h
NT
EV
NIK
WT
W270*
K321Sfs*160
E418*
L531Cfs*5
Q539*
R611*
R635*
S762Afs*21
R848Efs*38
P850Sfs*36
R853*
R853Cfs*7
R853Afs*30
D854Efs*31
K855*
K855Sfs*8
K855Pfs*33
D865G
D865Vfs*18
D865Qfs*20
S866R
S866N
S866Cfs*19
A867V
A867Cfs*19
Y868*
Y868C
G869Vfs*18
S870N
Q871*
NIK
P-p100
p100 ▶
NF-κB2
(p52/p100)
p52 ▶
GAPDH
kDa
140
100
70
50
40
35

Figure 3

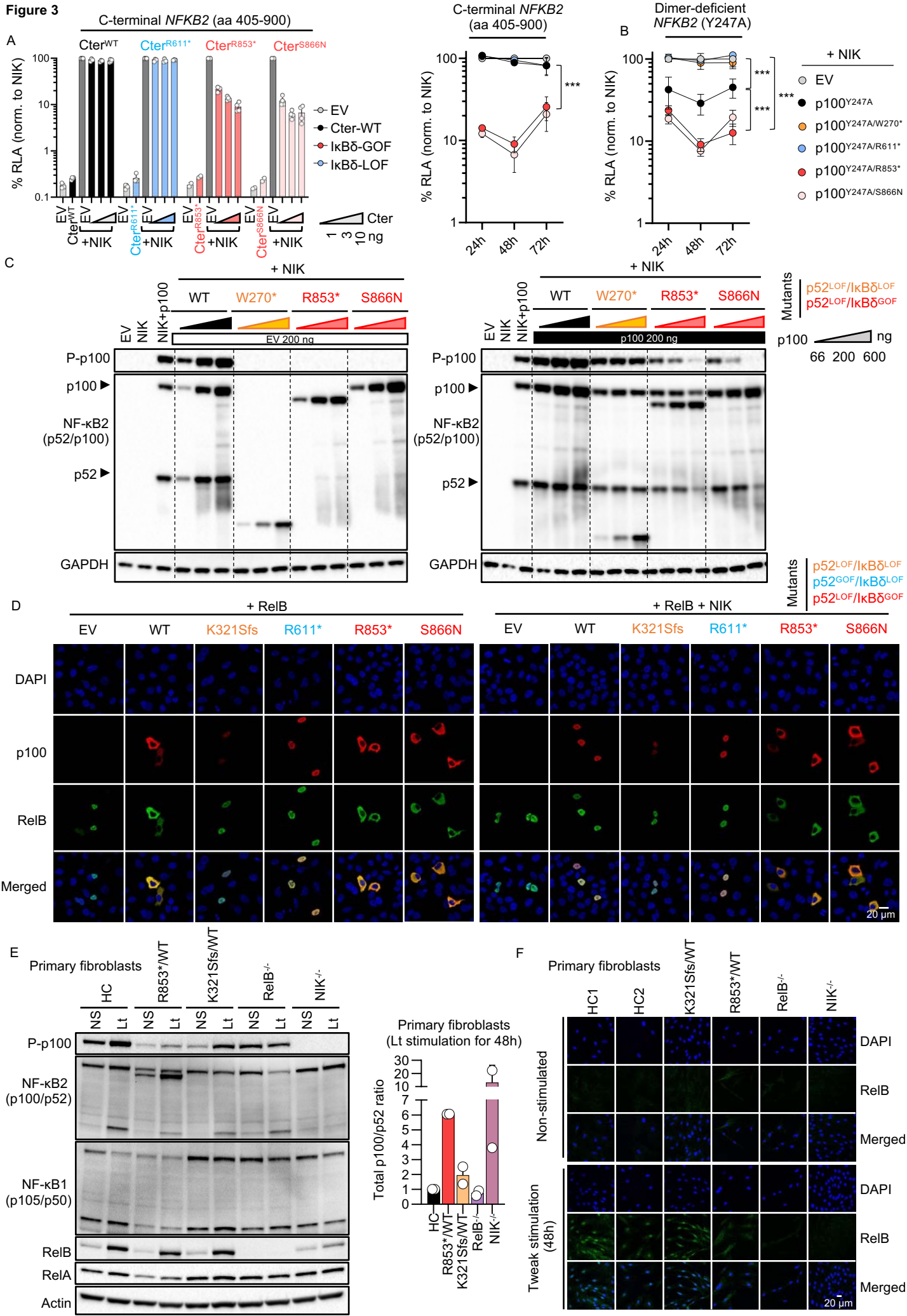
A
C-terminal NFKB2 (aa 405-900)
CterWT
CterR611*
CterR853*
CterS866N
% RLA (norm. to NIK)
EV
Cter-WT
IκBδ-GOF
IκBδ-LOF
+NIK
Cter
1 3 10 ng
C-terminal NFKB2 (aa 405-900)
B
Dimer-deficient NFKB2 (Y247A)
+ NIK
p100Y247A
p100Y247A/W270*
p100Y247A/R611*
p100Y247A/R853*
p100Y247A/S866N
24h
48h
72h
***
C
+ NIK
WT
W270*
R853*
S866N
EV
NIK
NIK+p100
EV 200 ng
p100 200 ng
Mutants
p52LOF/IκBδLOF
p52LOF/IκBδGOF
p52GOF/IκBδLOF
p100
ng
66 200 600
P-p100
p100
NF-κB2 (p52/p100)
p52
GAPDH
D
+ RelB
+ RelB + NIK
EV
WT
K321Sfs
R611*
R853*
S866N
DAPI
p100
RelB
Merged
20 µm
E
Primary fibroblasts
HC
R853*/WT
K321Sfs/WT
RelB-/-
NIK-/-
NS
Lt
P-p100
NF-κB2 (p100/p52)
NF-κB1 (p105/p50)
RelB
RelA
Actin
Primary fibroblasts (Lt stimulation for 48h)
Total p100/p52 ratio
F
Primary fibroblasts
HC1
HC2
K321Sfs/WT
R853*/WT
RelB-/-
NIK-/-
Non-stimulated
Tweak stimulation (48h)
DAPI
RelB
Merged
20 µm

Figure 4

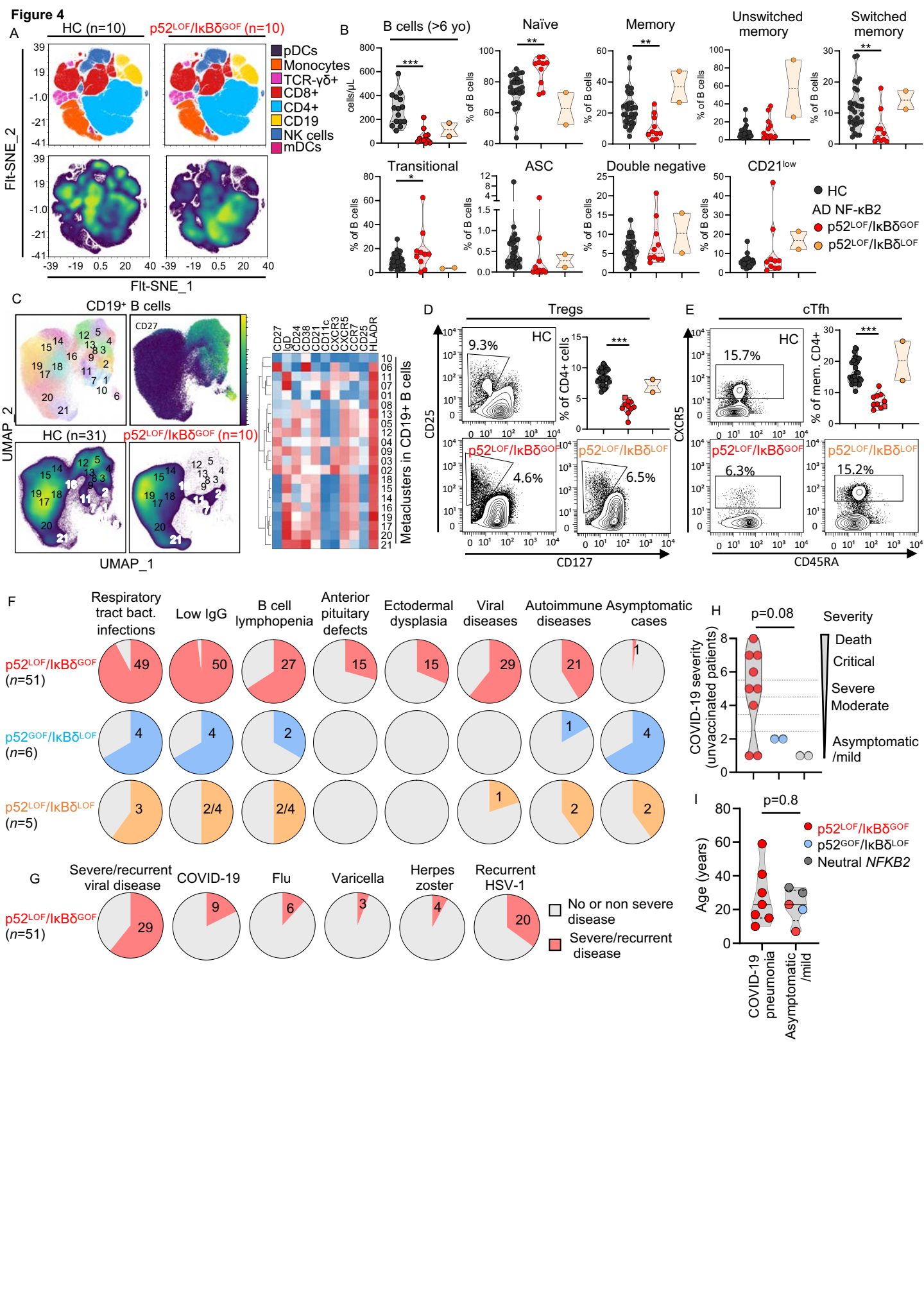
A
HC (n=10)
p52LOF/IκBδGOF (n=10)
pDCs
Monocytes
TCR-γδ+
CD8+
CD4+
CD19
NK cells
mDCs
Flt-SNE_2
Flt-SNE_1
B
B cells (>6 yo)
Naïve
Memory
Unswitched memory
Switched memory
Transitional
ASC
Double negative
CD21low
cells/μL
% of B cells
HC
AD NF-κB2
p52LOF/IκBδGOF
p52LOF/IκBδLOF
C
CD19+ B cells
CD27
UMAP_2
UMAP_1
HC (n=31)
p52LOF/IκBδGOF (n=10)
CD27
IgD
CD24
CD38
CD21
CD11c
CXCR3
CXCR5
CCR7
CD25
HLADR
Metaclusters in CD19+ B cells
D
Tregs
HC
9.3%
% of CD4+ cells
p52LOF/IκBδGOF
4.6%
p52LOF/IκBδLOF
6.5%
CD25
CD127
E
cTfh
HC
15.7%
% of mem. CD4+
p52LOF/IκBδGOF
6.3%
p52LOF/IκBδLOF
15.2%
CXCR5
CD45RA
F
Respiratory tract bact. infections
Low IgG
B cell lymphopenia
Anterior pituitary defects
Ectodermal dysplasia
Viral diseases
Autoimmune diseases
Asymptomatic cases
p52LOF/IκBδGOF (n=51)
49
50
27
15
15
29
21
1
p52GOF/IκBδLOF (n=6)
4
4
2
1
4
p52LOF/IκBδLOF (n=5)
3
2/4
2/4
1
2
2
G
Severe/recurrent viral disease
COVID-19
Flu
Varicella
Herpes zoster
Recurrent HSV-1
p52LOF/IκBδGOF (n=51)
29
9
6
3
4
20
No or non severe disease
Severe/recurrent disease
H
p=0.08
COVID-19 severity (unvaccinated patients)
Severity
Death
Critical
Severe
Moderate
Asymptomatic /mild
I
p=0.8
Age (years)
p52LOF/IκBδGOF
p52GOF/IκBδLOF
Neutral NFKB2
COVID-19 pneumonia
Asymptomatic /mild

Figure 5

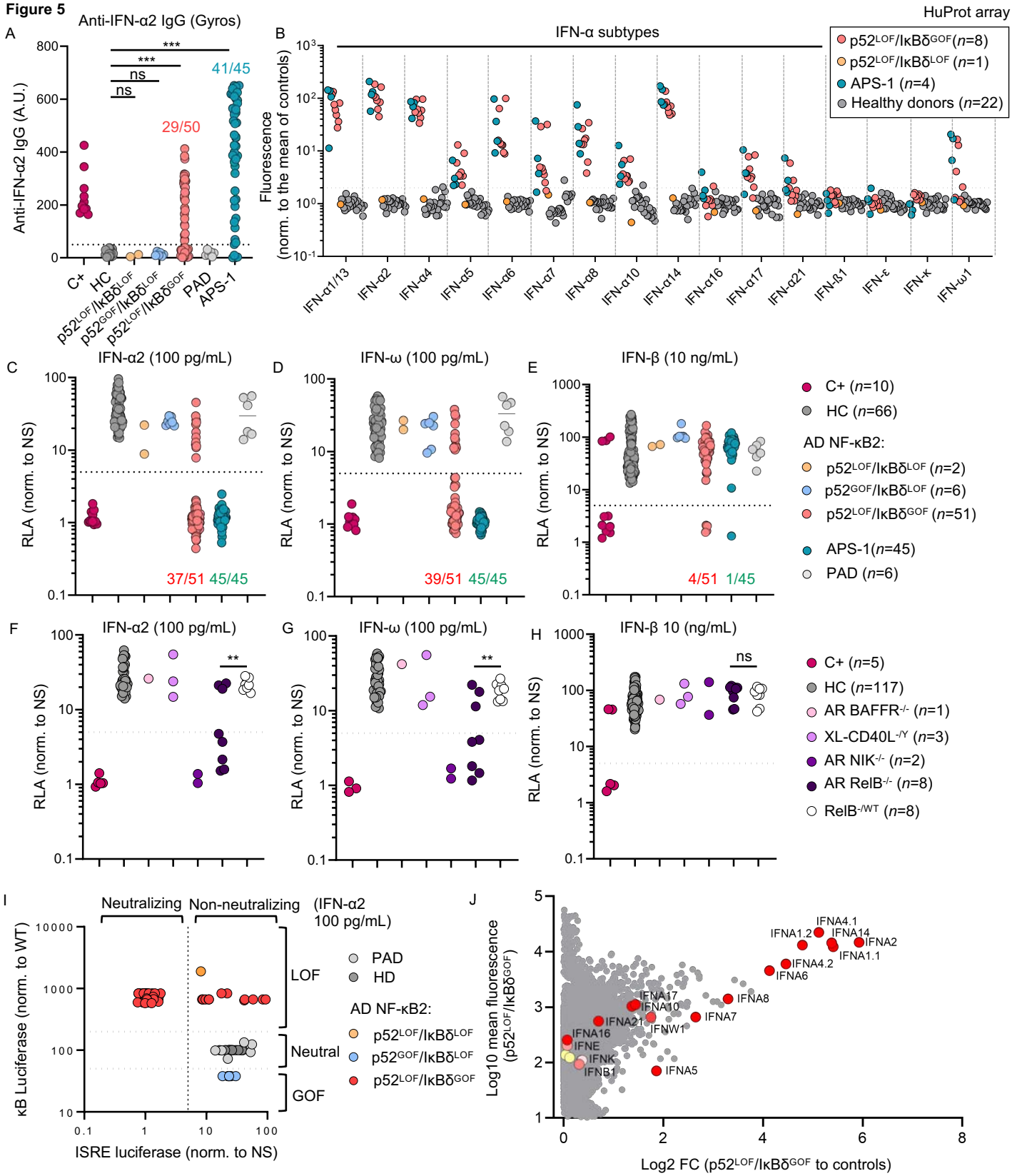
A
Anti-IFN-α2 IgG (Gyros)
Anti-IFN-α2 IgG (A.U.)
***
***
ns
ns
41/45
29/50
C+
HC
p52LOF/IκBδLOF
p52GOF/IκBδLOF
p52LOF/IκBδGOF
PAD
APS-1
B
IFN-α subtypes
HuProt array
Fluorescence (norm. to the mean of controls)
p52LOF/IκBδGOF (n=8)
p52LOF/IκBδLOF (n=1)
APS-1 (n=4)
Healthy donors (n=22)
IFN-α1/13
IFN-α2
IFN-α4
IFN-α5
IFN-α6
IFN-α7
IFN-α8
IFN-α10
IFN-α14
IFN-α16
IFN-α17
IFN-α21
IFN-β1
IFN-ε
IFN-κ
IFN-ω1
C
IFN-α2 (100 pg/mL)
RLA (norm. to NS)
37/51 45/45
D
IFN-ω (100 pg/mL)
39/51 45/45
E
IFN-β (10 ng/mL)
4/51 1/45
C+ (n=10)
HC (n=66)
AD NF-κB2:
p52LOF/IκBδLOF (n=2)
p52GOF/IκBδLOF (n=6)
p52LOF/IκBδGOF (n=51)
APS-1(n=45)
PAD (n=6)
F
IFN-α2 (100 pg/mL)
**
G
IFN-ω (100 pg/mL)
**
H
IFN-β 10 (ng/mL)
ns
C+ (n=5)
HC (n=117)
AR BAFFR-/- (n=1)
XL-CD40L-/Y (n=3)
AR NIK-/- (n=2)
AR RelB-/- (n=8)
RelB-/WT (n=8)
I
Neutralizing
Non-neutralizing
(IFN-α2 100 pg/mL)
κB Luciferase (norm. to WT)
ISRE luciferase (norm. to NS)
LOF
Neutral
GOF
PAD
HD
AD NF-κB2:
p52LOF/IκBδLOF
p52GOF/IκBδLOF
p52LOF/IκBδGOF
J
Log10 mean fluorescence (p52LOF/IκBδGOF)
Log2 FC (p52LOF/IκBδGOF to controls)
IFNA4.1
IFNA1.2
IFNA14
IFNA2
IFNA1.1
IFNA4.2
IFNA6
IFNA8
IFNA17
IFNA10
IFNA7
IFNA21
IFNW1
IFNA16
IFNE
IFNK
IFNB1
IFNA5

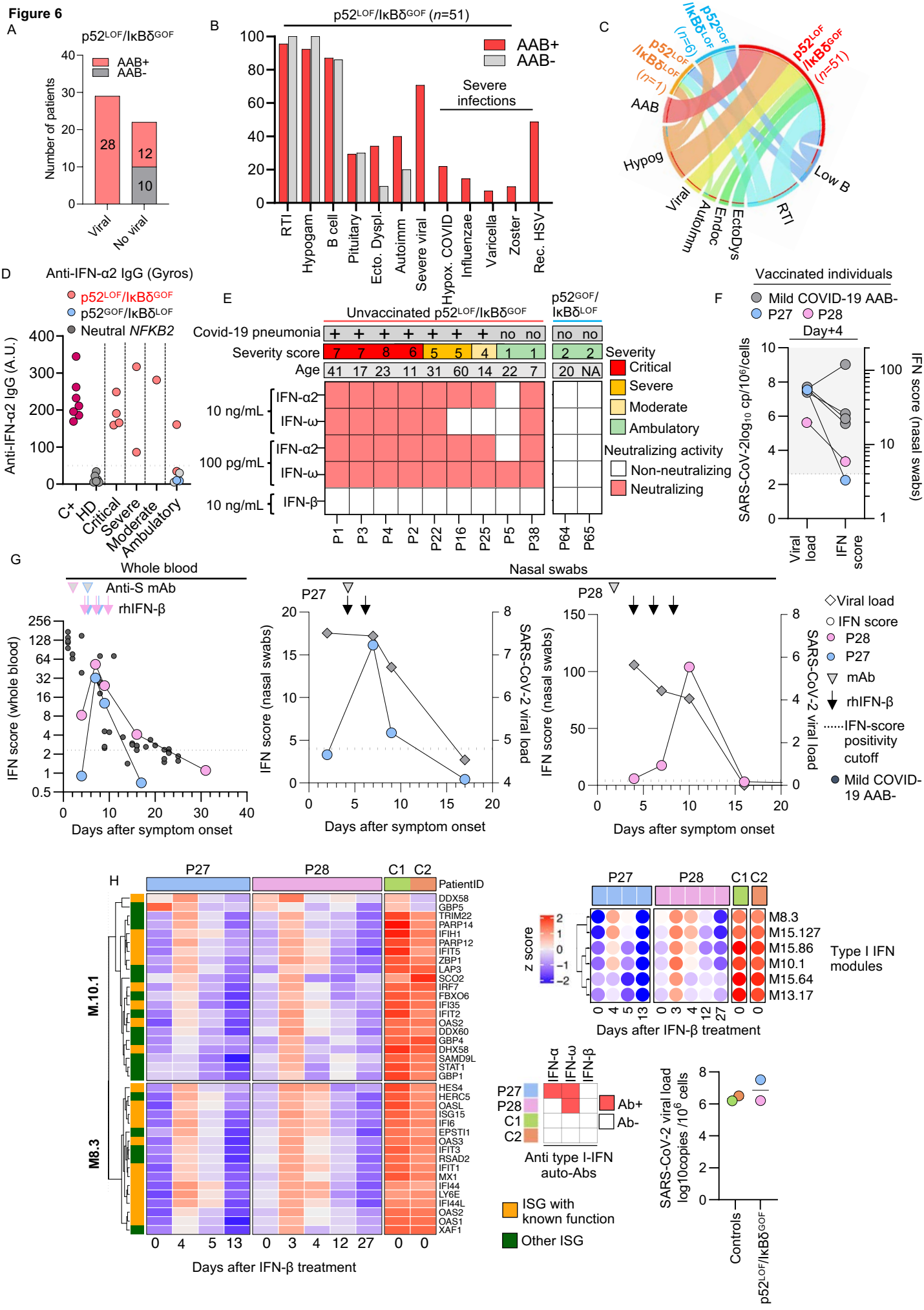
Figure 6
A
p52LOF/IκBδGOF
AAB+
AAB-
Number of patients
28
12
10
Viral
No viral
B
p52LOF/IκBδGOF (n=51)
AAB+
AAB-
Severe infections
RTI
Hypogam
B cell
Pituitary
Ecto. Dyspl.
Autoimm
Severe viral
Hypox. COVID
Influenzae
Varicella
Zoster
Rec. HSV
C
p52LOF/IκBδGOF (n=51)
p52GOF/IκBδLOF (n=6)
p52LOF/IκBδLOF (n=1)
AAB
Hypog
Viral
Autoimm
Endoc
EctoDys
RTI
Low B
D
Anti-IFN-α2 IgG (Gyros)
p52LOF/IκBδGOF
p52GOF/IκBδLOF
Neutral NFKB2
Anti-IFN-α2 IgG (A.U.)
C+
HD
Critical
Severe
Moderate
Ambulatory
E
Unvaccinated p52LOF/IκBδGOF
p52GOF/IκBδLOF
Covid-19 pneumonia
Severity score
Age
10 ng/mL
IFN-α2
IFN-ω
100 pg/mL
IFN-α2
IFN-ω
10 ng/mL
IFN-β
Severity
Critical
Severe
Moderate
Ambulatory
Neutralizing activity
Non-neutralizing
Neutralizing
P1
P3
P4
P2
P22
P16
P25
P5
P38
P64
P65
F
Vaccinated individuals
Mild COVID-19 AAB-
P27
P28
Day+4
SARS-CoV-2log10 cp/10^6/cells
IFN score (nasal swabs)
Viral load
IFN score
G
Whole blood
Anti-S mAb
rhIFN-β
IFN score (whole blood)
Days after symptom onset
Nasal swabs
P27
P28
IFN score (nasal swabs)
SARS-CoV-2 viral load
Days after symptom onset
Viral load
IFN score
P28
P27
mAb
rhIFN-β
IFN-score positivity cutoff
Mild COVID-19 AAB-
H
P27
P28
C1
C2
PatientID
M.10.1
M8.3
DDX58
GBP5
TRIM22
PARP14
IFIH1
PARP12
IFIT5
ZBP1
LAP3
SCO2
IRF7
FBXO6
IFI35
IFIT2
OAS2
DDX60
GBP4
DHX58
SAMD9L
STAT1
GBP1
HES4
HERC5
OASL
ISG15
IFI6
EPSTI1
OAS3
IFIT3
RSAD2
IFIT1
MX1
IFI44
LY6E
IFI44L
OAS2
OAS1
XAF1
Days after IFN-β treatment
z score
M8.3
M15.127
M15.86
M10.1
M15.64
M13.17
Type I IFN modules
Days after IFN-β treatment
IFN-α
IFN-ω
IFN-β
Ab+
Ab-
Anti type I-IFN auto-Abs
ISG with known function
Other ISG
SARS-CoV-2 viral load log10copies /10^6 cells
Controls
p52LOF/IκBδGOF

Figure 7

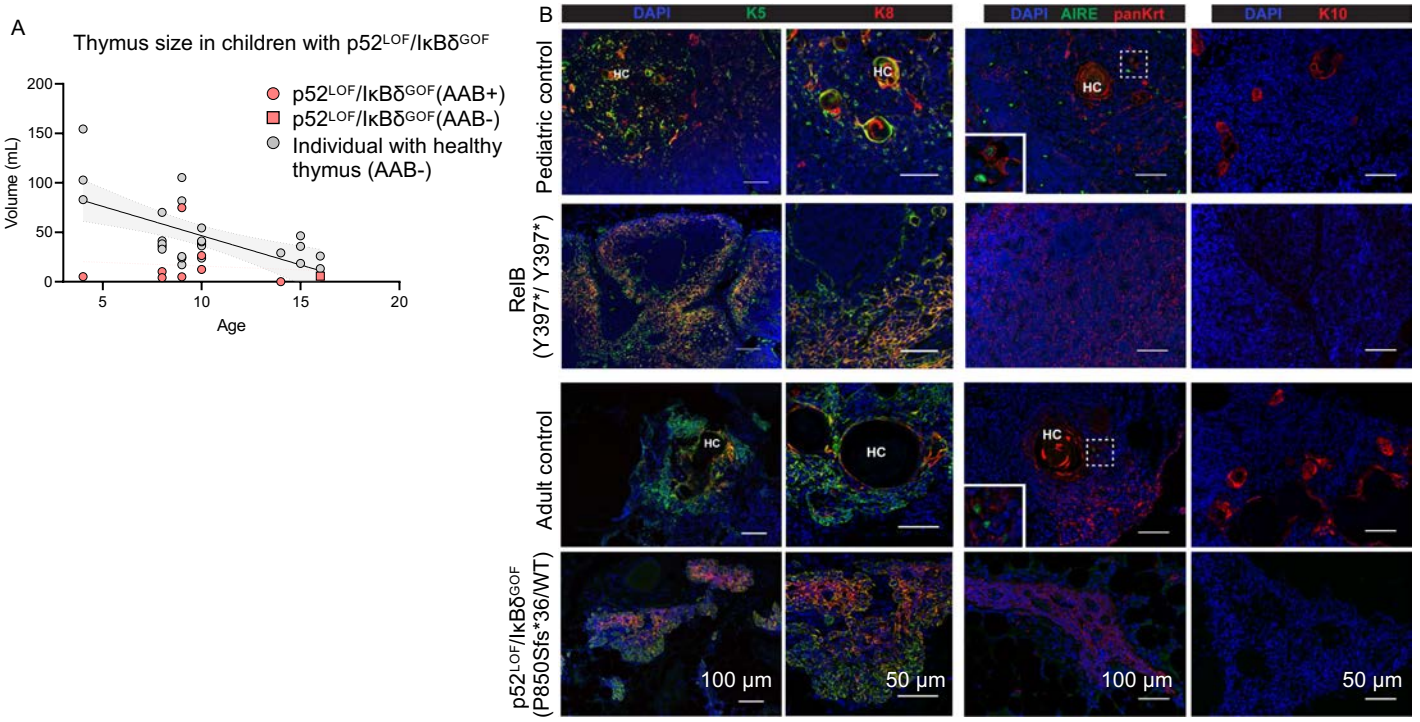
A
Thymus size in children with p52LOF/IκBδGOF
p52LOF/IκBδGOF(AAB+)
p52LOF/IκBδGOF(AAB-)
Individual with healthy thymus (AAB-)
Volume (mL)
Age
B
DAPI K5 K8
DAPI AIRE panKrt
DAPI K10
Pediatric control
RelB (Y397*/ Y397*)
Adult control
p52LOF/IκBδGOF (P850Sfs*36/WT)
HC
100 µm
50 µm